2-1-2018

On-chip optical sensors

Mohamed Elsayed

The American University in Cairo

School of Science and Engineering

On-chip Optical Sensors

A Thesis submitted to

Nanotechnology Program

In partial fulfillment of the requirements for

The Degree of Master of Science in Nanotechnology

By

Mohamed Elsayed

September 2017

The American University in Cairo
School of Sciences and Engineering

On Chip Optical Sensors

A thesis submitted by

Mohamed Elsayed

Submitted to Nanotechnology Program

In partial fulfillment of the requirements for

The Degree of Master of Science in Nanotechnology

Has been approved by

Dr. Mohamed A. Swillam _____
Thesis Supervisor
Affiliation: Associate Professor, Physics Department, American University in Cairo
Date _____

Dr. Yehea Ismail _____
Thesis Co-Supervisor
Affiliation: Professor and Director of Center of Nanoelectronics and Devices, American University in Cairo
Date _____

Dr. Karim Addas _____
Thesis first reader
Affiliation: Associate Professor, Physics Department, American University in Cairo
Date _____

Dr. Salah Obayya _____
Thesis second reader
Affiliation: Professor and Director of Center of Photonics and Smart Materials, Zewail City of Science and Technology
Date _____

_____
Department Chair
Date _____

_____
Dean of School of Sciences and Engineering
Date _____

ACKNOWLEDGEMENTS

First, I would like to thank Professors Mohamed Swillam and Yehea Ismail for their guidance and motivation and for having me a part of the nanophotonics research lab (NRL) and the center of nanoelectronics and devices (CND). They both have spent tremendous efforts in creating and maintaining a healthy research environment and for that I am deeply grateful. I would like to extend many thanks to members of the NRL and CND, for their help and friendship that will definitely continue for several years to come. Special thanks to my coauthors Aya Zaki and Abdelaziz Gouda. Special thanks to Raghi Samir for helping me learn the simulation tools in my first few weeks. Special thanks to Ahmad Bassam for help with scanning electron microscope images and Raman measurements and for helpful discussions. Special thanks to Hosam Mekawey and Hani Mostafa for their assistance in setting up the simulation environment.

I would like to thank the examiners, Dr. Salah Obayya and Dr. Karim Addas for their time and effort.

I would like to acknowledge the STRC team for their help. Thanks to Asmaa Gamal for training me to use the Raman. Thanks to Ahmed Nour, Ahmed Beltagy and Ahmed Ghazaly for their skills and dedication that definitely enhanced my learning experience. Thanks to Saleh for his continuous help.

The American University in Cairo is acknowledged for providing me a fellowship to fund this Master of Science degree. I would like to especially thank the course instructors: Dr. Mohamed Swillam, Dr. Tarek Ghanem, Dr. Nageh Allam, Dr. Wael Mamdouh, Dr. Yehea Ismail, Dr. Hassan Azzazy, Dr. Adham Ramadan, Dr. Mohab Anis. Every course I took was useful and helped shape this thesis and definitely enriched the educational experience at the AUC.

The Optical Society of America (OSA) is acknowledged for providing a travel grant to present at the international OSA network of students (IONS) conference 2016. AUC's Graduate Student Association is acknowledged for providing a grant to present at Photonics North conference 2016 through AUC's Office of Student Development (OSD). The AUC is acknowledged for providing a conference grant to present at META'16. The international society for optics and photonics (SPIE) is acknowledged for providing a travel grant to present at Photonics West 2017.

Lumerical is acknowledged for providing licenses for their software for some periods of time.

To my family, especially my father, mother and my closest friend, I say thank you for your endless unwavering support, patience and love during this period. Special thanks to my closest friend, Sara, my wife.

ABSTRACT

Adding more functionality to chips is an important trend in the advancement of technology. During the past couple of decades, integrated circuit developments have focused on keeping Moore's Law alive – "More of Moore". Moore's law predicts the doubling of the number of transistors on an integrated circuit every year. My research objectives revolve around "More than Moore", where different functionalities are sought to be integrated on chip. Sensing in particular is becoming of paramount importance in a variety of applications. Booming healthcare costs can be reduced with early diagnosis, which requires improved sensitivity and lower cost. To halt global warming, environmental monitoring requires miniature gas sensors that are cheap enough to be deployed at mass scale.

First, we explore a novel silicon waveguide platform that is expected to perform well as a sensor in comparison to the conventional 220 nm thick waveguide. 50 and 70 nm shallow silicon waveguides have the advantage of easier lithography than conventional 220 nm thick waveguides due to the large minimum feature size required of 1 µm. 1 µm wide waveguides in these shallow platforms are single mode. A multi-mode interference device is designed in this platform to function as the smallest MMI sensor, giving sensitivity of 427 nm / refractive index unit (RIU) at a length of 4 mm. The silicon photonic MMI sensor is based on detecting refractive index changes.

Refractometric techniques such as the MMI sensor require surface functionalization to achieve selectivity or specificity. Spectroscopic methods, usually reserved for material characterization in a research setting, can be adapted for highly specific label-free sensing. Chapter 4 explores the use of a highly doped III-V semiconductor for on chip infrared spectroscopy. Finite element method and finite different time domain were both used to design a plasmonic slot waveguide for gas sensing. On chip lasers and detectors have been designed using InAs. While InAs is still considered more expensive than silicon, the electronics industry expects to start incorporating more materials in standard fabrication processes, including III-V semiconductors for their superior properties including mobility. Thus, experimental realization of this sensor is feasible.

A drawback with infrared spectroscopy is that it is difficult to use with biological fluids. Chapter 5 explores the use of Raman spectroscopy as a sensing method. To adapt Raman spectroscopy for sensing, the most important task is to enhance the Raman signal. The way the Raman signal is generated means that the number of photons is generally very low and usually bulk material or concentrated fluids are used as

samples. To measure low concentrations of a probe molecule, the probe molecule is placed on a surface enhanced Raman spectroscopy (SERS) substrate. A typical SERS substrate is composed of metal nanostructures for their surface plasmon resonance property, which causes a large amplification in the electric field in particular hot spots. By decorated silicon nanowires with silver nanoparticles, an enhancement factor of 10^{11} was realized and picomolar concentrations of pyridine were detected using Raman spectroscopy.

In conclusion, this thesis provides new concepts and foundations in three directions that are all important for on chip optical sensing. First, silicon photonics is the technology of choice that is nearest to the market and a multi-mode interference sensor based on shallow silicon waveguides was designed. Further work can explore how to cascade such MMIs to increase sensitivity without sacrificing the free spectral range. Second, infrared plasmonics is a promising technology. Before semiconductor plasmonics, on chip devices operated in the visible or near IR and then microwave region of the electromagnetic spectrum. By using highly doped semiconductors, it is possible to bridge the gap and operate with mid-infrared wavelengths. The implications are highlighted by designing a waveguide platform that can be used for next generation on chip infrared spectroscopy. Third, Raman spectroscopy was exploited as a sensing technique by experimental realization of a SERS substrate using equipment-free fabrication methods.

TABLE OF CONTENTS

List of Figures

List of Equations

List of Tables

List of Publications

Journal papers

1. **Mohamed Elsayed**, Aya Zaki, Yehea Ismail, Mohamed A. Swillam, "Integrated lab-on-a-chip sensor using shallow silicon waveguide silicon-on-insulator (SOI) multimode interference (MMI) device" Submitted to Journal of Nanophotonics
2. **Mohamed Elsayed**, Abdelaziz Gouda, Yehea Ismail, Mohamed A. Swillam, "Silicon-based SERS substrates fabricated by Electroless etching" *Journal of Lightwave Technology* vol. 35, no. 14, pp. 3075-3081, July 15, 2017 DOI: 10.1109/JLT.2017.2707476
3. **Mohamed Elsayed**, Yehea Ismail, Mohamed A. Swillam, "Semiconductor Plasmonic Gas Sensor Using On-Chip Infrared Spectroscopy" *Applied Physics A* vol. 123, pp. 113-119, January 2017 DOI: 10.1007/s00339-016-0707-2

Conference papers

(= equal contribution) (underlined = presenter)*

1. **Mohamed Elsayed**, Aya Zaki, Yehea Ismail, Mohamed A. Swillam, "Integrated Lab-on-a-Chip Sensor using Shallow Silicon Waveguide Multimode Interference (MMI) Device", SPIE OPTO Photonics West, San Francisco, 28 Jan – 2 Feb 2017 (Oral)
2. **Mohamed Elsayed***, Abdelaziz Gouda*, Yehea Ismail, Mohamed A. Swillam, "Silver-decorated silicon nanowires array as Surface Enhanced Raman Scattering (SERS) substrate", SPIE OPTO Photonics West, San Francisco, 28 Jan – 2 Feb 2017 (Poster)
3. **Mohamed Elsayed**, Yehea Ismail, Mohamed A. Swillam, "Semiconductor Plasmonic Gas Sensor using on-chip Infrared Spectroscopy" , the 7th International Conference on Metamaterials, Photonics Crystals and Plasmonics (META'16), Malaga, Spain, 25-28 July, 2016 (Poster)
4. **Mohamed Elsayed**, Yehea Ismail, Mohamed A. Swillam, "Semiconductor Plasmonic Gas Sensor" Photonics North, Quebec City, 24-26 May, 2016 DOI: 10.1109/PN.2016.7537933 (Oral)
5. Abdelaziz Gouda, **Mohamed Elsayed**, Christen Tharwat, Mohamed Swillam, "Silicon-based Nanostructures as Surface Enhanced Raman Scattering Substrates", Photonics North, Quebec City, 24-26 May, 2016 DOI: 10.1109/PN.2016.7537981 (Poster)

CHAPTER 1. INTRODUCTION

1.1. Optical Sensors

Sensing is becoming more prevalent and ubiquitous in our daily lives. From the simple bimetallic strips in kettles to accelerometers in our cars, the widespread use of sensors is contributing to the safety and convenience of humankind. Table 1.1 compares different sensing technologies. For widespread use, sensors must be low cost, compact and easy to mass-produce. Thus the focus of this thesis is on-chip sensors. Regardless of the type of sensor, the end signal must always be converted to an electrical signal for further processing and incorporating in a feedback system when appropriate. Thus, a key feature for the sensor technology of choice is its ease of integration with electronics. The biggest advantage of optical sensors is that they have been used in a wide variety of applications and are seen as key enablers. For example, electrochemical methods alone are able to detect a certain subset of analytes with certain accuracy, but when adding optical sensors this subset becomes vastly expanded with much improved accuracy.

Table 1.1. Sensing techniques. Adapted from [1].

STIMULUS	QUANTITIES MEASURED	SIGNAL MEASURED
ACOUSTIC	Wave amplitude, phase	Acoustic → Electrical Acoustic → Optical → Electrical
BIOLOGICAL / CHEMICAL	Concentration, thickness of layer	Chemical → Electrical Chemical → Optical → Electrical
ELECTRIC	Conductivity, charge	Electrical
MAGNETIC	Magnetic field amplitude, phase, flux permeability	Magnetic → Electrical Magnetic → Optical → Electrical
OPTICAL	Refractive index, reflectivity, absorption	Optical → Electrical
THERMAL	Temperature, thermal conductivity,	Thermal → Electrical Thermal → Optical → Electrical
MECHANICAL	Pressure, position, velocity, force	Mechanical → Electrical Mechanical → Optical → Electrical

Early detection of the vast majority of cancers has been correlated with higher survival rates than late stage diagnosis. Ovarian cancer symptoms are very similar to non-serious health conditions such as bloating, lower back pain and loss of appetite leading to 80% of diagnosis occurring in late stages, where

chances of 5 year survival can be as low as 10% [2]. For early diagnosis, several biomarkers need to be measured simultaneously with high sensitivity and specificity [3, 4], and as many as 5 biomarkers have to be targeted, one of which is CA-125, considered a very rare molecule available in very low concentrations [5]. Cervical cancer has over 50% mortality rate % [6], the reason for high mortality rate is that the symptoms start to show when the disease has advanced to a very late stage that it is no longer responsive to treatment. A popular screening method is the Papanicolaou smear test (pap test), it is simple and inexpensive but suffers from a high false-negative rate [7, 8]. The human papillomavirus (HPV) itself can be detected by polymerase chain reaction (PCR) amplification followed by hybridization capture assay [9], but quantification can be difficult because the amplification step is very sensitive to the temperature, buffer composition and enzyme activity [10]. Thus, there is a strong need to be able to detect the virus without an amplification step, requiring detector sensitivities down to the femtomolar range and below.

1.2. Sensor Design considerations

Several standards have been proposed for design considerations for sensors, depending on the application. One application for example is diagnostics. By incorporating optical sensors on chip, it is possible to move from a centralized healthcare system, where blood samples are analyzed in highly specialized , to a decentralized healthcare system where the samples are analyzed at the location of the care provider or at home. This will bring about many benefits to both developed and developing countries: Patients will be more willing to take more frequent tests as it is more convenient for them, less chance sample fouling / contamination due to transporting in addition to the obvious cost advantages. For biosensors to find their way in the developing world, the ASSURED criteria were developed by the World Health Organization (WHO) [11]:

- Affordable by those at risk of infection
- Sensitive with very few false-negatives
- Specific with very few false-positives
- User-friendly tests that are simple to perform and require minimal training
- Rapid, to enable treatment at first visit, and Robust, for example not requiring refrigerated storage
- Equipment-free
- Delivered to those who need it

The WHO also identified the digitization and data-linking to be important for follow up visits and monitoring healthcare statistics of a large population [11]. Additionally, multiplexing is a useful feature. Multiplexing in the context of sensors refers to measuring several markers using one blood sample.

1.2.1. Cost

On chip sensors tackle the affordability criterion by operating on a small scale and requiring small sample and reagent volumes. In addition, as will be explained shortly, optical sensors can be designed to be label-free, thus reducing the amount of steps and reagents required. More importantly, on chip sensors can be integrated with microfluidics and electronics components to allow full automation. By reducing the user interaction required, no skilled worker is needed, and this obviously brings down the cost.

1.2.2. Sensitivity

As listed in the ASSURED criteria, improved sensitivity reduces false-negatives. A false negative happens when the sensor is not sensitive enough and cannot detect the biomarker. In general terms, a biomarker is some measurable quantity indicative of a disease or condition. For example, a person infected with Hepatitis C Virus (HCV) will have small concentrations of the virus in blood, so detecting this virus is indicative that the person has HCV. In practise however, it is sometimes easier to detect another marker, for example an antibody that is released by the body to fight the disease. So a biomarker may be the foreign body itself responsible for the disease or something else that is released by either the body or by the foreign body.

The immune system takes some time to detect a foreign body (antigen) and develop an antibody that is specific to that antigen. A patient just recently infected with HCV may test negative when an antibody test is used due to the antibody not being produced yet (the first few days after infection) or produced in quantities lower than the sensor detection limit. The virus itself is available in very small concentrations, and can be detected through the genetic material of the virus in the blood, ribonucleic acid (RNA). This is available in extremely small quantities and the detection methods are not sensitive enough to detect these small quantities. Expensive polymerase chain reaction (PCR) is required to amplify the genetic material before the actual detection. Despite the many disadvantages for using the antibody test as a diagnostic strategy, it is still used instead of the HCV RNA test. More sensitive solutions that can skip the PCR step are definitely needed.

It is important to stress that early detection is possible through detecting small concentrations of biomarkers. The current standard methods for detecting biomarkers are all labeled methods; the Enzyme-

Linked Immunosorbent Assay (ELISA) is the most popular. Suppose that a patient is infected with HCV. The body will try to fight HCV by producing antibodies that will act as a biomarker. A 96-well plate as shown in Figure 1.1 (a) is sold as part of a diagnostic kit for HCV [12]. It contains a capture antibody on the bottom of each well that binds specifically to the biomarker. A blood sample is inserted into one of these wells. The biomarkers will bind specifically to the capture antibodies and they will be "immobilized". The well is then washed, leaving behind only the immobilized biomarkers. Another antibody, called the detection antibody, is introduced and binds to the biomarker from the top side, creating a "sandwich" as shown in Figure 1.1 (b). A further enzyme-linked antibody, a "label", is added that causes a color change, the intensity of which is dependent on the amount of biomarker present [13]. A sensitive assay is one that undergoes an observable color change for very low concentrations. An insensitive assay is one that will only give an observable color change for high concentrations of the antibody being tested for. Thus, an insensitive assay is prone to giving false negative results. A diagnostic test based on a sensor with limited sensitivity will conclude that the patient does not have this biomarker although the patient may have very little concentrations of the biomarker that go undetected. This is quite problematic as it leads to late diagnosis of serious illnesses. In several diseases, symptoms appear only after the disease has progressed, by which time it is too late for successful intervention.

1.2.3. Selectivity

Selectivity refers to the test undergoing a color change due to the specific antibody that the assay is designed for. A non-selective test will undergo a color change due to molecules other than those being tested for, giving rise to false positives. In almost all ELISA tests, there is a trade-off between sensitivity and specificity; this is an important challenge that will be discussed in the next section. Continuing the HCV example, in many cases the body's immune response is able to fight the virus without symptoms. Thus, if a patient becomes infected with HCV, the body may release antibodies and successfully eradicate the virus, but the body continues producing the antibody for several years. A patient who has undergone this cycle (without even knowing it), may test false positive if the antibody test is used. Thus, HCV antibody test is not specific enough. As already mentioned in the previous section, one solution has been to opt for detection strategies involving the virus itself and not the antibody. However, these tests remain too expensive to be used ubiquitously.

In gas sensing application, optical sensors have been employed with high sensitivity, but selectivity remains a problem. Optical sensors have typically employed refractive index sensing. Gases have very

similar refractive indices around 1, with differences often in a fifth or sixth decimal place. Thus, a different mode of sensing for improved selectivity will be explored in this work.

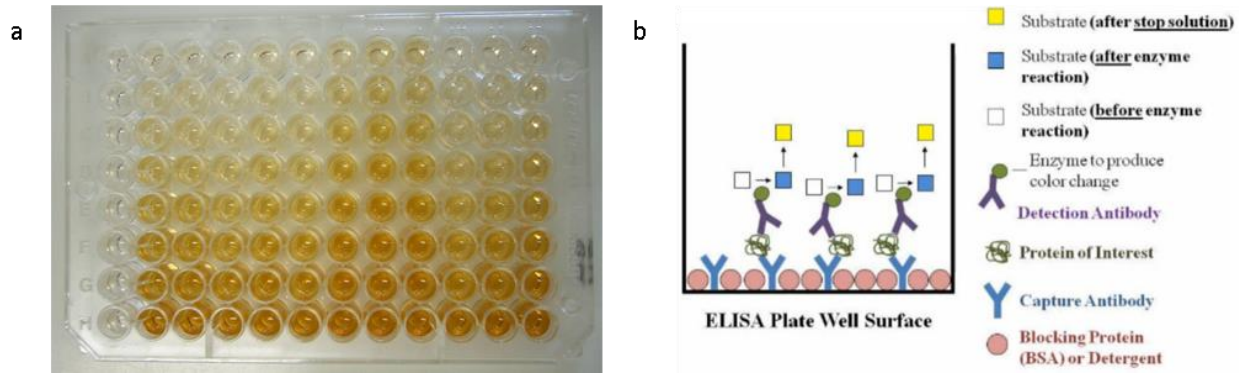

Figure 1.1. (a) 96-well plate used for ELISA [12]. (b). Schematic showing sandwich ELISA [13].

1.2.4. Multiplexing

In some cases, several biomarkers are used together to diagnose a specific condition, this is known as a panel of biomarkers. For example, inflammation of the heart would cause dying heart cells to release Troponin I (TnI) [14], so elevated levels of TnI indicate that there is something wrong with the heart. However, another biomarker would be needed to indicate the reason behind these dying heart cells. C-reactive protein (CRP) is released in any inflammatory response in the body (not just the heart). If both CRP and TnI are detected, this indicates that there is an inflammation of the heart, then doctors can take the correct course of action [15].

Many diseases require detecting a panel of biomarkers to help a physician reach a conclusive diagnosis [5]. In such cases, a single test that can detect several biomarkers would be beneficial over a method where several tests have to be conducted. On chip sensors allow multiplex ability. Due to their small size, several sensors, each sensitive to a different biomarker, can be placed on the same chip. A single sample can then be used for all the sensor in one experiment. Figure 1.2 shows an example of this approach. In this work, each region highlighted in a color contains 3 sensors that are sensitive to a particular antibody. Using a single sample injected using a syringe and a single laser input, all of the sensors' outputs are collected simultaneously using a single camera. Thus, this is a single experiment with measurements corresponding to several biomarkers.

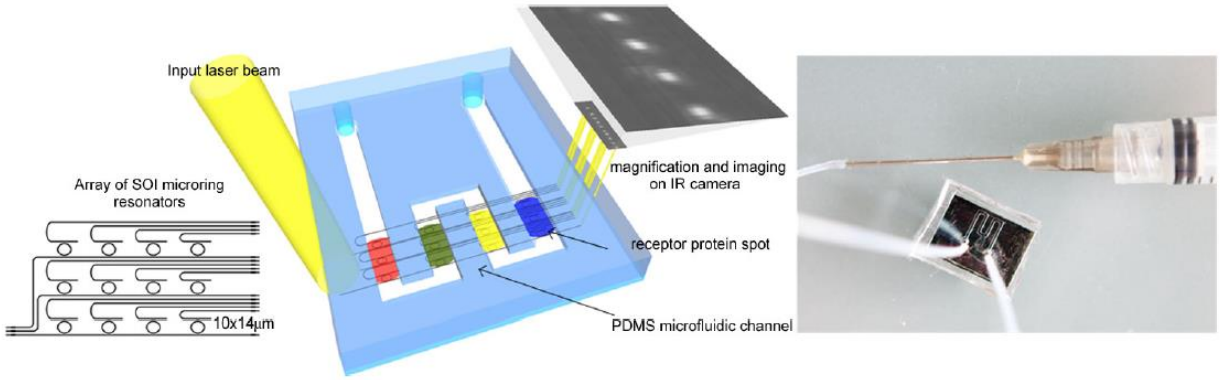

Figure 1.2. (Left) array of optical sensors on chip for multiplex sensing. (Middle) Single light excitation from input laser beam and single measurement using camera to capture fata from all 12 ring resonator sensors. Each 3 sensors are functionalized to be sensitive to a different material, as depicted by different colors. (Right) Optofluidic chip showing fluid manipulation. Reproduced from [16].

Similarly, in gas sensing, multiplex ability is very useful. Consider for example the application of environmental monitoring. Many gases should be monitored simultaneously, including carbon dioxide, carbon monoxide, ammonia, ethane, methane, hydrogen sulfide, methyl-phenol, benzyl alcohol [17].

1.3. Challenges

So far, sensors that have been used in diagnostic tests that meet the ASSURED criteria have been simple such as glucose measurements, blood pressure. Attempts to simplify more complicated diagnostic tests have not yet reached all the ASSURED criteria. For example, HIV tests either take too long time, require equipment or the simpler ones are not sensitive enough [11]. Another challenge is combining multiplex ability with the ASSURED criteria. Novel strategies in optical sensors can be employed to improve both sensitivity and selectivity, overcoming the conventional trade-off associated with conventional testing methods. Even with miniaturized on-chip sensors that still employ labeled methods, multiplexed sensors can be costly as each sensor needs to be functionalized for its specific test. As will be explained in the following chapter, using label-free optical methods can overcome this cost barrier. The same novel strategies can be used to measure the concentration of a number of markers without having to functionalize the surface. These novel strategies make use of characteristic spectroscopic signals of analytes instead of simple refractive index measurements.

1.4. Label-free sensing

So far in this thesis, there have been some mention of labeled and label-free methods. This section is dedicated to understand the differences between the two methods. As mentioned earlier, the current

standard testing methods used clinically use labeled methods. Labeled methods, such as the ELISA described above can be very sensitive, but their high running costs and complexity hamper their ubiquitous use. Label-free methods have traditionally had limitations in sensitivity and multiplexed sensing, but recent innovations in interferometers, plasmonic sensors and photonic crystals[18] have been game changers. Plasmonic sensors in particular have been demonstrated to sense even below the femtomolar range. However, selectivity remains an issue with label-free methods. For example, a label-free method would be used to measure the concentration of a particular known analyte, but its low specificity does not allow identifying the analyte. Infrared spectroscopy and Raman spectroscopy are two optical techniques that can be configured to operate as label-free detection tools. Infrared spectroscopy is well suited for a variety of analytes. However, the large absorption band of water requires that samples be completely dry for proper analysis. This would complicate sample preparation unnecessarily. For this reason, in this thesis, infrared spectroscopy is used in gas sensing. Raman spectroscopy on the other hand does not suffer from this issue and is well suited for biological fluids. The literature review section will discuss several examples of Raman spectroscopy used in biological applications.

1.5. References

[1] Y. B. Rashil Mehta, Harshit Mathur, Ankit Yadav, Anoop Kumar. (2014, 21 July 2017). *Sensors: The New Generation Technology*. Available: https://www.slideshare.net/nktydv/480-sensors-30751476

[2] A. Gentry-Maharaj and U. Menon, "Screening for ovarian cancer in the general population," *Best Practice and Research. Clinical Obstetrics and Gynaecology,* vol. 26, pp. 243-256, 2012.

[3] D. Badgwell and R. C. Bast, Jr., "Early detection of ovarian cancer," *Disease Markers,* vol. 23, pp. 397-410, 2007.

[4] R. C. Bast, Jr., M. Brewer, C. Zou, M. A. Hernandez, M. Daley, R. Ozols, K. Lu, Z. Lu, D. Badgwell, G. B. Mills, S. Skates, Z. Zhang, D. Chan, A. Lokshin, and Y. Yu, "Prevention and early detection of ovarian cancer: mission impossible?," *Recent Results in Cancer Research,* vol. 174, pp. 91-100, 2007.

[5] W. Jiang, R. Huang, C. Duan, L. Fu, Y. Xi, Y. Yang, W.-M. Yang, D. Yang, D.-H. Yang, and R.-P. Huang, "Identification of Five Serum Protein Markers for Detection of Ovarian Cancer by Antibody Arrays," *PLoS ONE,* vol. 8, p. e76795, 2013.

[6] L. A. Torre, F. Bray, R. L. Siegel, J. Ferlay, J. Lortet-Tieulent, and A. Jemal, "Global cancer statistics, 2012," *CA: A Cancer Journal for Clinicians,* vol. 65, pp. 87-108, 2015.

[7] N. S. Larsen, "Invasive Cervical Cancer Rising in Young White Females," *Journal of the National Cancer Institute,* vol. 86, pp. 6-7, January 5, 1994 1994.

[8] L. G. Koss, "The Papanicolaou test for cervical cancer detection. A triumph and a tragedy," *JAMA,* vol. 261, pp. 737-43, Feb 3 1989.

[9] C. J. L. M. Meijer, T. J. M. Helmerhorst, L. Rozendaal, J. C. van der Linden, F. J. Voorhorst, and J. M. M. Walboomers, "HPV typing and testing in gynaecological pathology: has the time come?," *Histopathology,* vol. 33, pp. 83-86, 1998.

[10] J. Li, J. Y. Lee, and E. S. Yeung, "Quantitative screening of single copies of human papilloma viral DNA without amplification," *Analytical Chemistry,* vol. 78, pp. 6490-6, Sep 15 2006.

[11] G. Wu and M. H. Zaman, "Low-cost tools for diagnosing and monitoring HIV infection in low-resource settings," *Bulletin of the World Health Organization,* vol. 90, pp. 914-920, 2012.

[12] BiotechMichael. *„Anti human IgG" Double Antibody Sandwich ELISA*. Available: https://commons.wikimedia.org/wiki/File:ELISA.jpg

[13] Y. Farhat. *Sandwich ELISA Protocol*. Available: http://protocol-place.com/assays/elisa/sandwich-elisa-protocol/

[14] F. Brunner, N. Schofer, M. Schlueter, F. Ojeda, T. Zeller, C. Bickel, T. Muenzel, T. Keller, S. Blankenberg, and B. Goldmann, "Diagnosis of acute myocardial infarction: super-sensitivity vs. high-sensitivity cardiac troponin I assay," *European Heart Journal,* vol. 34, 2015.

[15] M. E. Benford, M. Wang, J. Kameoka, and G. L. Coté, "Detection of cardiac biomarkers exploiting surface enhanced Raman scattering (SERS) using a nanofluidic channel based biosensor towards coronary point-of-care diagnostics," in *SPIE BiOS: Biomedical Optics*, 2009, pp. 719203-719203-6.

[16] K. De Vos, J. Girones, T. Claes, Y. De Koninck, S. Popelka, E. Schacht, R. Baets, and P. Bienstman, "Multiplexed antibody detection with an array of silicon-on-insulator microring resonators," *IEEE Photonics Journal,* vol. 1, pp. 225-235, 2009.

[17] P. Daukantas, "Air-Quality Monitoring in the Mid-Infrared," *Optics and Photonics News,* vol. 26, pp. 26-33, 2015.

[18] Q. Quan, D. L. Floyd, I. B. Burgess, P. B. Deotare, I. W. Frank, S. K. Y. Tang, R. Ilic, and M. Loncar, "Single particle detection in CMOS compatible photonic crystal nanobeam cavities," *Optics Express,* vol. 21, pp. 32225-32233, 2013/12/30 2013.

CHAPTER 2. BACKGROUND AND LITERATURE REVIEW

This chapter covers background related to the different aspects of this thesis. This background includes some historical perspective to appreciate how the technology is developing and some fundamental basics. It is best to discuss these basics in this chapter now before going through the actual devices designed as some of the explanations may be lengthy and such discussion would distract from the design objectives.

2.1. Optical sensing

Humans have always depended on their eyesight for almost all daily activities. It is therefore natural to turn to optical sensing methods. Since ancient times, doctors have used the color of skin, eye and bodily fluids as a means to assess patient health. The most common diagnostic tests make use of color change. Industrially, visual inspection has always been an integral part of quality assurance protocols and has recently been automated through the use of cameras and object recognition. Optical signals are always around us and detecting these signals has always been of strong interest.

Figure 2.1 shows electric and magnetic fields associated with an electromagnetic wave traveling in the z direction. Both fields are perpendicular to each other and to the direction of propagation. As we shall see shortly, optical devices often behave very differently depending on the light polarization. This particular wave is said to be vertically polarized because the electric field is in the vertical direction. Visible light spans only a small segment of the electromagnetic spectrum shown in Figure 2.2. Throughout this thesis, different sensing strategies make use of different parts of the electromagnetic spectrum. Equations 2.1 and 2.2 are fundamental properties of electromagnetic waves.

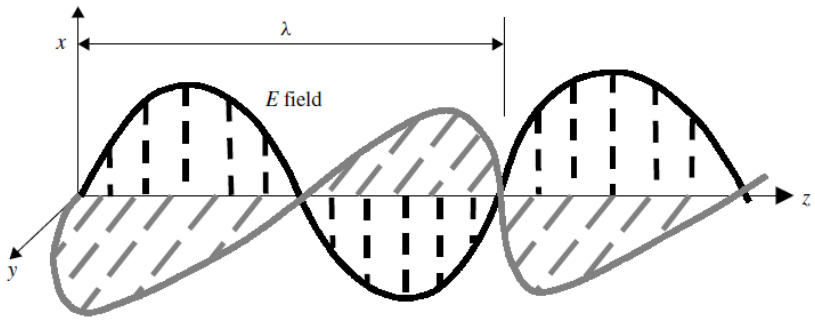

Figure 2.1. Propagation of plane-polarized light showing electric field component (black) and magnetic field component (grey). Reproduced from [1].

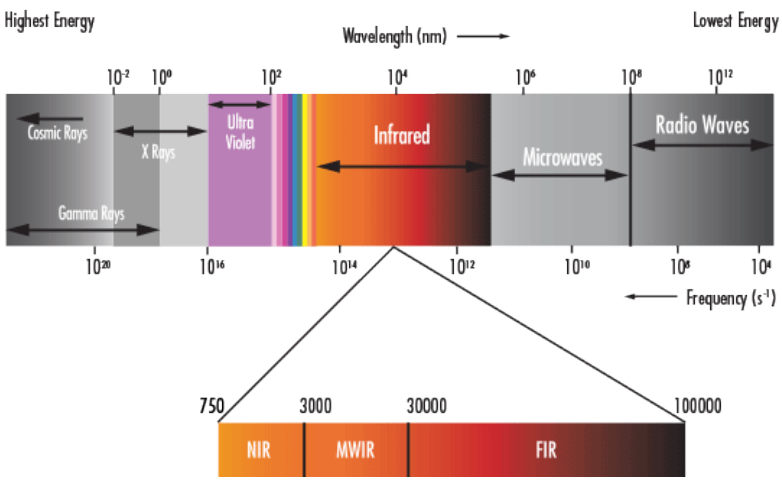

Figure 2.2. Electromagnetic spectrum. Reproduced from [2].

Equation 2.1 relates the wavelength λ and the frequency ν with the speed of light in a vacuum, c.

$$\lambda\nu = c \tag{2.1}$$

Equation 2.2 is known as Planck's equation and it describes the energy E of a photon using Planck's constant, h.

$$E = h\nu \tag{2.2}$$

The refractive index n of a material summarises some of its optical properties. First, it describes the speed of light in that medium through the phase velocity v as per equation 2.3.

$$n = \frac{c}{\mathrm{v}} \tag{2.3}$$

At the interface between two materials with different refractive indices, refraction occurs and this is described using Snell's law, shown diagrammatically in Figure 2.3 and in equation 2.4.

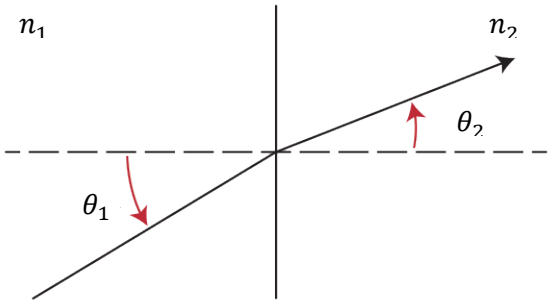

Figure 2.3. Refraction at the interface between materials of different refractive indices, n_1 and n_2. Adapted from [2].

$$n_1 \sin\theta_1 = n_2 \sin\theta_2 \tag{2.4}$$

To better understand how light as an electromagnetic wave behaves, Snell's law is obviously insufficient. and we have to resort to Maxwell's equations 2.5 and 2.6. As a simplification, the equations shown here assume a homogeneous and lossless dielectric medium.

$$\nabla \times \mathbf{E} = -\mu \frac{\partial \mathbf{H}}{\partial t} \quad 2.5$$

$$\nabla \times \mathbf{H} = \varepsilon \frac{\partial \mathbf{E}}{\partial t} \quad 2.6$$

Here, $\mathbf{E}$ is the electric field, $\mathbf{H}$ is the magnetic field strength, μ is the permeability of the medium and ε is the permittivity of the medium. Noting that ε and n are related as in equation 2.7, it becomes apparent how the refractive index has an effect on the electric field.

$$\varepsilon = \varepsilon_0 n^2 \quad 2.7$$

Light can be considered as a sinusoidally varying electromagnetic wave with angular frequency ω and propagation constant β propagating in the z direction, as described by equation 2.8 [3], where the x, y and z axes are as defined in Figure 2.1.

$$\tilde{\mathbf{E}} = \mathbf{E}(x, y) e^{i(\omega t - \beta z)} \quad 2.8$$

To exploit light in sensing, it is important to understand the fate of photons as they hit a material as summarised in Figure 2.4 and equations 2.9 and 2.10.

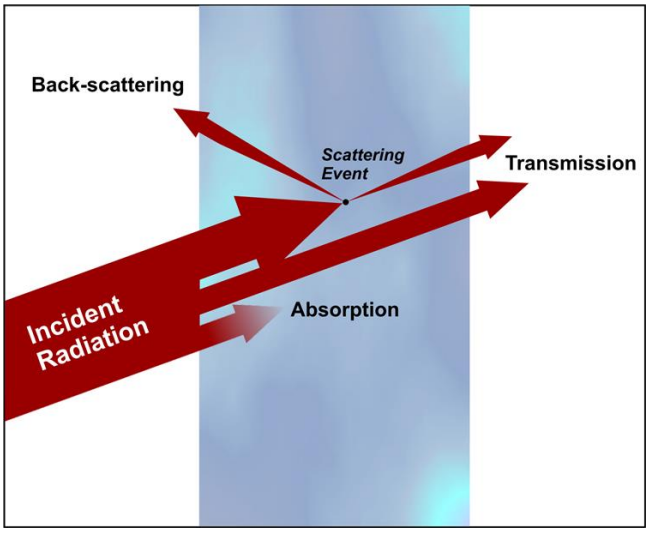

Figure 2.4. Fate of a photon, reproduced from [4].

$$\mathrm{T} = \frac{P}{P_0} \quad 2.9$$

$$\mathrm{A} = -\log T \quad 2.10$$

where T is the transmittance and A is the absorbance, P_0 is the power of the incident light, P is the power of the measured light.

The most common optical methods already used frequently in labs relies on the absorbance of labels as explained in the introduction. Figure 2.5 shows a typical tabletop ELISA plate reader. The optical system inside the plate reader often uses a broadband light source with a number of narrowband filters that are either manually or automatically changed depending on the particular experiment. For example, an ELISA plate reader configured for absorbance may have a broadband light source covering 400 to 750 nm wavelength. For a particular experiment that has the peak intensity at 407 nm, a 405 – 410 nm excitation filter is used that blocks all light and only allows light with 405 nm to 410 nm wavelength to pass. The measurement is based on the intensity of light that reaches the detector and a software calculates the absorbance of the sample.

Figure 2.5. ELISA Plate reader. Reproduced from [5].

While such measurement method is commonplace in the lab, fundamentally different approaches are required for true lab on a chip systems. The concept of a lab on a chip has been around for decades. Soon after the development of microelectronic integrated circuits in the 1950s, microelectromechanical systems (MEMS) were used to make pressure sensors in the 1960s. Fast forward to the first lab on chip system in 1979, a gas chromatograph [6]. Manz et al's visionary paper in 1990 reinvigorated the growth of the field by introducing the concept of a miniaturized total analysis system, integrating microfluidics, optics and electronics [7]. More importantly, they set solid theoretical insights highlighting the advantages of the miniaturization on chemical analysis: faster and more efficient separations, small sample volume and simultaneous measurements. Manz' vision for lab on a chip systems sees the sensing part occurring

real time and such approach has no room for time consuming and expensive labeled sensing approaches. This leads to studying alternative label-free on chip optical sensing strategies. Two approaches will be covered: refractometric techniques and spectroscopic techniques.

2.1.1. Refractometric sensing techniques

Refractometric sensing techniques rely on detecting the refractive index of a sample. Generally, a device is designed such that it has a particular response under a reference sample with known refractive index and the output changes in response to a change in the refractive index. A typical example is a ring resonator such as that shown in Figure 1.2. In a ring resonator, light of particular wavelengths only couple to the ring and stay "trapped" in the ring for a long time. This causes light of only this wavelength to reach the drop port. This resonance condition is very sensitive to the top cladding material. When the top clad is removed and different samples are introduced, the resonant wavelength of the ring resonator is sensitive to small refractive index changes. Therefore, a resonant wavelength shift $\Delta\lambda$ is observed for a refractive index change Δn. The sensitivity in refractive index units (RIU) can be defined as equation 2.11

$$S = \frac{\Delta\lambda}{\Delta n}\ (RIU) \qquad 2.11$$

The ring resonator was used as an example because it is one of the earliest and most common modulation and sensing method for photonic integrated circuits. However, the same performance characteristics hold for other refractometric sensing methods such as the interferometer, including the multi-mode interferometer (MMI) that will be studied at length in chapter 3.

Refractometric techniques can be designed to have very high sensitivity. However, such high sensitivity is only useful in determining the concentration of a known sample and selectivity is an issue. In gas sensing for example, the refractive index of many gases are very similar to each other to the 5th decimal place. In samples that contain a mixture of chemicals, such as blood samples, it may be difficult to know which chemical is causing the refractive index shift. Therefore, surface functionalization is often performed. This causes the surface of a sensor to be sensitive to particular chemicals only. This approach is practical and appropriate for several cases and a new sensor based on this approach will be designed in chapter 4. However, to be able to detect unknown analytes without pre-functionalized sensors, spectroscopic methods should be employed such as infrared spectroscopy and Raman spectroscopy.

2.1.2. Infrared Spectroscopy

At the atomic level, the atoms and molecules are normally not stationary. Figure 2.6 (a) shows atomic-level movements such as vibrations and rotations. Such movements have certain resonant frequencies

which match infrared frequencies. Thus, a photon with energy in the infrared regime can excite these resonant modes. When this happens, this photon is absorbed. Infrared spectroscopy exploits this phenomenon because the exact frequencies cause a signature spectroscopic response for a particular material such as the example in Figure 2.6 (b). Infrared spectroscopy has been used as a powerful characterization tool. However, the absorption peak corresponding to water it difficult to analyze biological samples due to the requirement to dry the samples. Nevertheless, it is a useful technique and will be employed in chapter 5 for the design of a gas sensor.

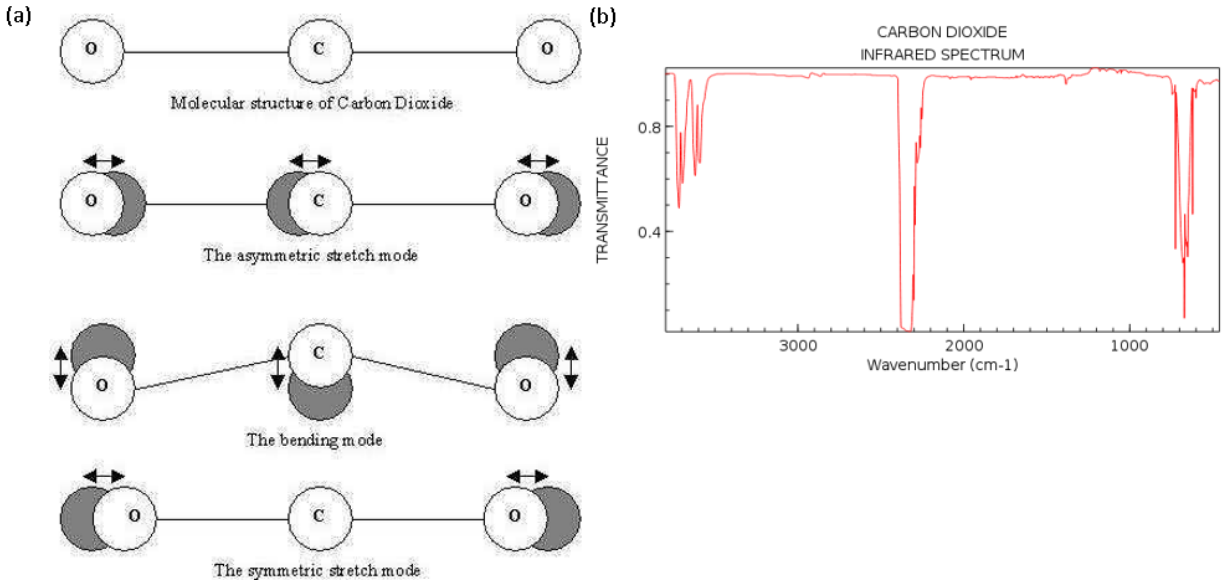

Figure 2.6. (a) Molecular vibrations in Carbon Dioxide. Reproduced from [8].(b) IR spectrum for CO_2 [9].

2.1.3. Raman Spectroscopy

Referring back to Figure 2.4, we note that the previously discussed sensing methods depend on just the transmission and absorption properties of the material. We can make use of the scattered signal. The way the light scatters can be more characteristic to a particular material than transmission or absorption properties. Raman spectroscopy is a label-free method that is able to deduce a wealth of information from a particular analyte in a single measurement. The mechanism is depicted in Figure 2.7. Briefly, incident light is scattered inelastically due to collisions with certain functional groups in a molecule or particular atoms. This inelastic scattering causes the reflected light to have different energies. More specifically, the intensity of light at different energies (frequencies) can be recorded as a spectrum and is found to be a characteristic fingerprint of the material. Usually, a high concentration of material is required to be able to accumulate enough signal-to-noise ratio and acquire a clear signal. However, for use in a sensor, a high

sensitivity is desirous and low concentrations must be detectable. Here comes the role of enhancing the Raman signal.

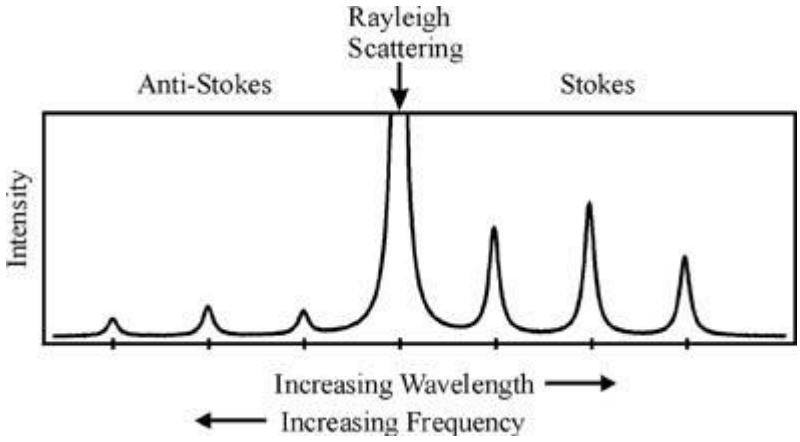

Figure 2.7. Elastic versus inelastic scattering. Incident photons have frequency v_0. The horizontal axis is the frequency of scattered photons and the vertical axis is the number of photons. Most scattered photons have the same frequency as the incident photons (Rayleigh scattering). Some photons scatter inelastically, either gaining energy (Anti-Stokes) or losing energy (Stokes). Reproduced from [10].

Many strategies have been used to enhance the Raman signal, the most famous of which is Surface Enhanced Raman Scattering (SERS), and most recently, Tip Enhanced Raman Scattering (TERS) and Interference Enhanced Raman Scattering (IERS). In the early days of investigating with SERS, there was much debate about the physical reason behind the phenomenon, eventually settling on the explanation that there are both chemical and electrical enhancement but the electrical enhancement due to plasmons is the dominant effect [11].

Plasmons, depicted in Figure 2.8 (a, b) were manipulated as early as the 4th century AD in the Lycargus cup shown in Figure 2.8 (c). The glass incorporated gold nanoparticles – being a metal, gold provided the required abundance of free electrons. When viewed using reflected light, it appears green. However, when lit from the inside, some wavelengths of light are absorbed and it appears red. The absorbed light excites plasmons on the gold nanoparticles [12]. This causes the color change that has made the Lycargus cup famous. Photography in the 18th and 19th century made use of silver nanoparticles, which was also based on surface plasmon resonance effects. The term plasmonics was coined in the early 2000s and refers to more controlled manipulation of plasmons and in particular propagating plasmons [13-18]. Therefore, while plasmons have been used since the ancient romans, they have not been fully understood until recently and the field of plasmonics is considered a relatively new field.

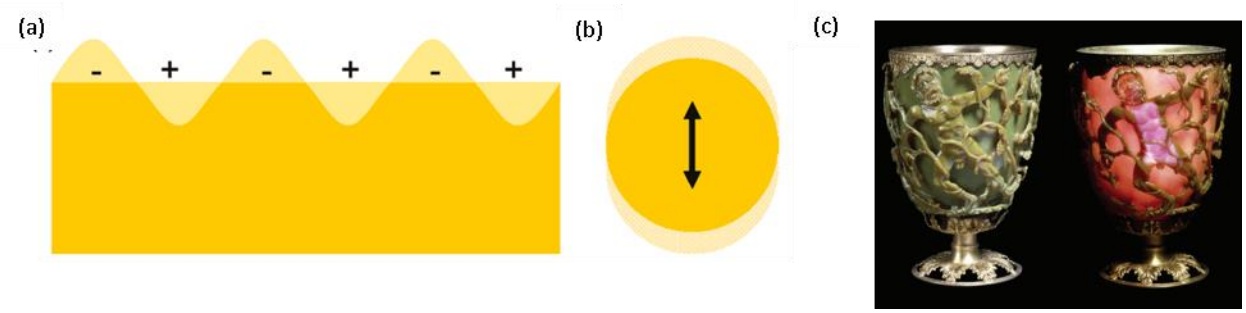

Figure 2.8. (a) Surface plasmons, (b) localized plasmon in surface plasmon resonance (SPR). Reproduced from [19]. (c) Lycargus cup changing color depending on lighting conditions, reproduced from [12].

Plasmonics involves manipulating plasmons, which are collective oscillations of electrons that are considered quasi-particles that behave in some ways similar to a photon, obeying Maxwell's equations [20]. Plasmons are excited due to incident light in specific conditions [20]. Plasmons manifest themselves in nano-scale materials with an abundant population of free electrons. The most typical use of plasmonics in biosensing applications involves the use of surface plasmon resonance (SPR) [19]. Briefly, a plasmon on a small nanoparticle will be localized and oscillate without propagating along the surface of the material [19] as demonstrated in Figure 2.8 (b). Resonance occurs when the frequency of incident electromagnetic field is equal to the frequency of oscillations, which themselves are a function of the material type, nanoparticle size and shape and more importantly, the surrounding material [19]. The electric field intensity due to a localized surface plasmon is greatly amplified and causes an enhancement of the Raman signal by a factor of E^4.

The earliest account of SERS was found almost 'by accident' in the late 1970s, and researchers were unable to fully explain the unusually high intensities they were getting in their Raman measurements [21]. Raman measurements usually have to be done on very smooth surfaces, but in the case of [21], applying a voltage caused the roughening of the electrode, and the Raman signal was found to be enhanced by a factor of 10^5. While surface plasmons were suggested as an explanation, no solid evidence was available at the time. A couple of years down the road, more research was underway regarding this phenomenon and the term 'surface enhanced Raman scattering' was coined [22, 23]. In addition to roughened metal films as in the first few experiments [21, 22], metal sol particles were also used due to their ease of preparation [23].

SERS remains the strongest candidate amongst Raman enhancement methods for ubiquitous use as a low cost sensing method. While conventionally, the setup had been quite complex, many advancements in nanotechnology have resulted in driving the cost of SERS substrates down drastically. In addition,

advancements in integrated optics have resulted in the idea of a fully integrated SERS-on-chip platform not too far-fetched (including on chip source and detectors).

Only in the past decade has SERS been suggested strongly as a biosensing mechanism, and there have been a plethora of strategies, from core/shell structures [24], bottom-up assembly of nanoparticles [25], achieving enhancements ranging from 10^3 to 10^7. The larger the enhancement, the larger the sensitivity. For single molecule detection, pushing the enhancement even further to 10^9 is needed [11] and this required a combination of strategies. Over the decades, after fully understanding the enhancement mechanism, it became clear that the best strategies involve either sharp nanoparticles such as cone or star shapes or to bring nanoparticles into very close proximity.

Metal nanoparticles or metal caps have been deposited onto nanowires in such a way so as to bring the nanoparticles in very close proximity to one another [26-30]. Highlighting one example, Schmidt et. al [27] deposited silver onto silicon nanowires and then managed to make the nanowires to lean towards each other as shown in Figure 2.9. This was done in a controllable manner without any complicated fabrication, just making use of a droplet's capillary forces as it dries up, pulling the nanowires closer together. The nanowires themselves were made using a maskless etching scheme without lithography, making the method amenable to low cost fabrication. The enhancement factor achieved varies depending on different calculation methods and assumptions, as previously outlined in [11], the enhancement factor is on the order of 10^6 to 10^{11} [27]. The reason for the large discrepancy is related to whether or not this enhancement factor is actually detectable experimentally.

The second method is to make sure that the nanoparticles have some sharp corners to have an antenna effect, such as crescent shaped silver [31] or nanocones. Ming et. al compared the performance of different shaped nanoparticles and concluded that the nanostar outperformed nanorods and nanopheres due to the sharp tips [32]. What's interesting about the work by Ming et. al is that the SERS was demonstrated for biosensing applications by monitoring DNA hybridization [32].

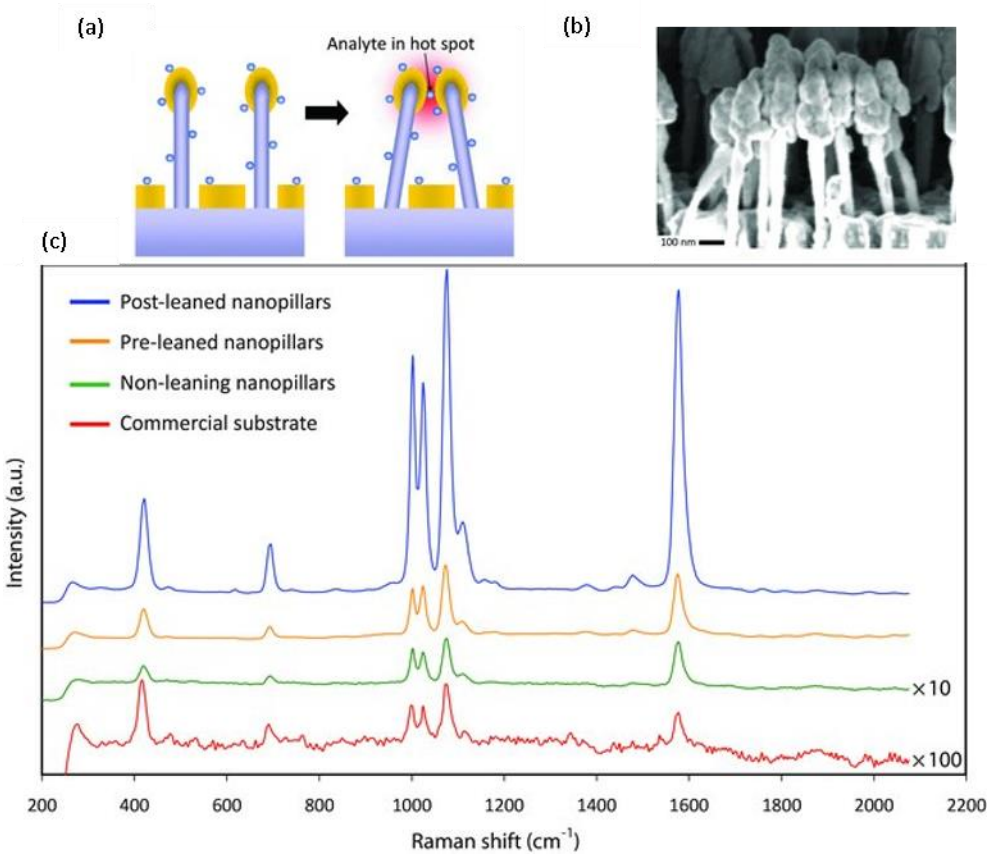

Figure 2.9. (a) leaning process. The region between the two gold nanoparticles is considered a 'hot spot' where the electric field is greatly amplified due to interaction between the plasmons on both nanoparticles, so the analyte's Raman signal is greatest when it is in this hot spot. (b) scanning electron microscope (SEM) image of leaned nanowires. (c) Raman signal obtained when using the optimally-leaned nanopillars (blue) greatly outperforms the non-leaning pillars (green) and those that leaned too much (yellow). Reproduced from [27].

An outstanding feat that deserves some attention was accomplished by Angelis et. al by patterning gratings onto a silver-coated nanocone [33]. These gratings cause surface propagating plasmons to move towards the tip of the nanocone to really strengthen the antenna effect as can be seen in Figure 2.10. What's more, with careful engineering, the surface was made to be superhydrophilic with the nanocone acting as a defect, causing the droplet to be pinned at this nanocone. A droplet of containing femotomolar concentrations of lysosome was made to evaporate in such a way so as to increase the concentration of the droplet while *delivering* the molecules to the nanocone. This way, it was possible to record the Raman signal of less than 5 molecules of lysosome [33].

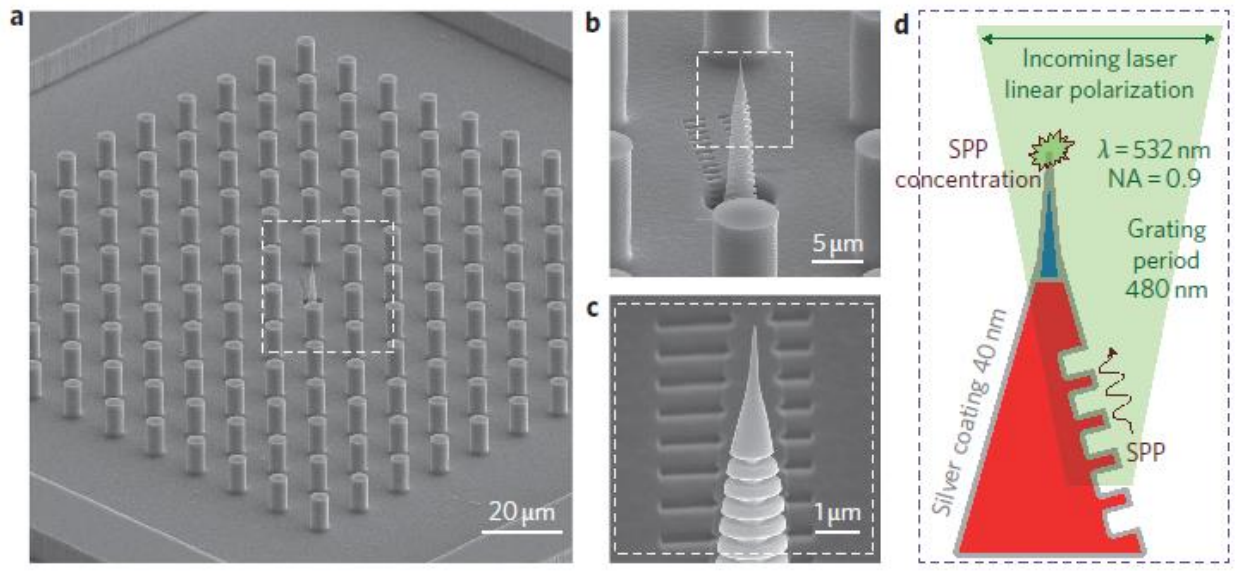

Figure 2.10. (a – c) SEM images of the plasmonic tip in the middle of the superhydrophobic surface. (d) schematic showing the operational principle of the plasmonic tip. Reproduced from [33].

2.2. Integrated Photonics

The first on chip optical sensor considered in this thesis is based on silicon photonics technology. This section covers how the silicon photonics industry emerged and introduces the reader to some basic photonics concepts.

2.2.1. History: From optical fibers to silicon photonics

The first optical fibers used in long-haul communications bought about a paradigm shift in not only technology, but indeed society at large [34]. Better communication infrastructure allowed the boom in internet usage and the subsequent changes in how people interact with each other [34]. Optical fibers are generally made using glass that is doped with different materials to create an inner core with a higher refractive index than the outer cladding, as depicted in Figure 2.11. The classical description of how light propagates in an optical fiber is using the concept of total internal reflection. That is, ideally, light reflects at the interface between the high index and low index materials and thus the light remains guided inside the high index region.

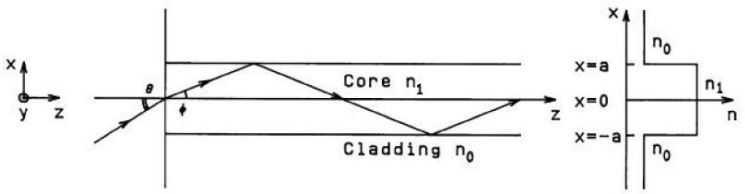

Figure 2.11 Guiding light in an optical fiber by total internal reflection. Reproduced from [3].

The 70s and 80s saw the start of research regarding planar on chip optical devices [35, 36] and integrated electro-optical systems were proposed since then. Despite silicon's use in electronics, its high index of refraction meant that nanoscale dimensions were required, which deterred its use. Commercial devices based on similar technology as optical fibers – that is doped glass – flourished, followed by III-V materials – Indium Phosphide (InP) in particular became a common standard for photonics chips [35, 37]. There are currently several foundries for InP Photonics with mature fabrication processes [37, 38]. InP chips are used to make optical switches and modulators for communications applications [37].

Integrating optics and electronics on the same chip has always been an elusive task. Such integration will allow reaping the benefits of optical communications along with the electronics. In particular, optical interconnects is a very important field [39]. Moore's law is endangered by the interconnect bottleneck [40, 41]. While smaller transistors generally bring about performance benefits, scaling down the size of metal interconnects brings about increased resistance and increased capacitance as the wiring gets denser, thus poorer performance [41, 42]. Therefore, there is an urgent need to consider other communication strategies for chip to chip and within the chip [39, 41, 43]. As optical communications has proved its reliability for decades in long distance communication, optical fibres have made their way in rack-to-rack communications, and is poised to go inside computers for chip to chip communications [44-48]. Silicon's higher refractive index than glass or InP meant that single mode operation requires geometries of a few hundred nanometers. Such resolution lithography started to be available in the late 80s and 1990s and silicon photonics has started since then [49-55]. Research in Silicon Photonics-electronics integration has accelerated strongly the past decade due to the impending interconnect bottleneck in addition to the new-found applications of silicon photonics in sensing applications [56-58]. In fact, many electronics companies have produced significant research on silicon photonics research including Intel , HP[59-61], Oracle [62-67] and IBM [68].

As elegantly quoted in an IBM paper "Interconnects of the future will be dominated by optics, as this offers the potential for a far better cost solution for all distances. As we look to exascale, even the

connections between processors on a common circuit card needs to be optical because of the amount of bandwidth needed. Silicon photonics represents a nearly ideal solution to the interconnect problem [69].” Figure 2.12 shows the evolution of the vision for future electro-optical chips. The 1974 vision did not even consider silicon but rather III-V materials.

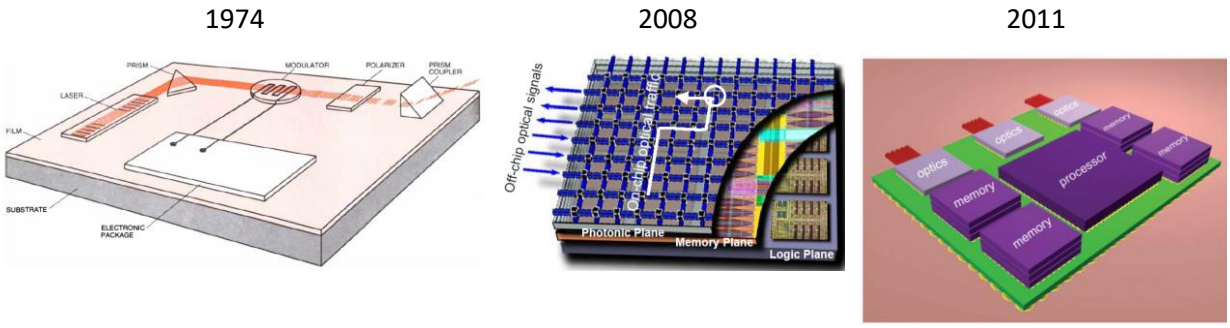

Figure 2.12. Vision of electro-optical integration over the years. Vision from 1974 by Bell Telephone Laboratories. Reproduced from [35]. Vision from 2008 for 2018 by IBM [70]. Vision from 2011 by IBM [69].

In silicon photonics, silicon is used as the core and silicon dioxide is used as the cladding. When on chip, it is possible to have the underclad different from the upperclad. A large refractive index contrast between silicon (n_{Si} = 3.4), and silicon dioxide (n_{SiO2} = 1.4) means that single-mode waveguides are smaller than was feasible using only glass or InP. Glass and InP single mode waveguides were usually around a few microns in width, while silicon waveguides are a few hundred nanometers in width. The high contrast means that light is well confined in the silicon and small bend radii of 5 µm are achievable with negligible loss. Thus, Silicon photonics allows highly dense integration of optical components on chip. Obviously, by using the same material as electronics, costs are much reduced. One drawback of purely silicon photonics is the difficulty to create on chip lasers as silicon is not a direct bandgap material, thus any attempts to produce light in silicon will inherently excite phonons. Thus, hybrid material systems incorporating silicon and InP devices are promising [57, 58]. Intel has already started commercial production of chips containing hybrid InP-silicon photonic interconnect systems reaching speeds of 100 gigabits per second [71]. In addition, Intel has been able to lead in Silicon photonics because they also accomplished automated testing platforms for silicon photonics, thus bringing true economies of scale to photonics from fabrication all the way to testing. The maturing technology has seen several foundries offering multi-project wafer (MPW) runs, making it possible to fabricate devices using state of the art capabilities and affordable cost [72].

2.2.2. Fundamentals of integrated photonics

Figure 2.13 (a) shows a slab waveguide with infinite width. Using the concept of total internal reflection, the index contrast causes the interface between two materials with high refractive index contrast to act

as a mirror. Light injected in the waveguide will remain trapped between these two mirrors. Consider the incident and reflected light at one of these mirrors. Constructive interference between these two causes the light intensity to be maximum at the center of the waveguide. This is known as the fundamental mode of the waveguide, as shown in Figure 2.13 (c). Higher order modes may exist which have different optical field profiles, such as the transverse magnetic mode shown in Figure 2.13 (d). A pulse of light injected along the z axis will propagate at different phase velocity v in each material with different refractive index n due to the relation in 2.3. Thus, light travels slower in regions with high refractive index. Light traveling in a certain mode along a waveguide will collectively travel with a certain group velocity n_g, and subsequently the whole waveguide can be considered as a material with effective refractive index n_{eff}. It suffices to note that each guided mode has an effective refractive index (sometimes simply referred to as "effective index") as in Figure 2.13 (b) and a group velocity. Figure 2.13 (b) is an example of how the thickness affects the number of guided modes and the effective refractive index of these modes. More detailed analysis and the equations that govern guided modes are out of the scope of this thesis and I refer the reader to [3] or [1].

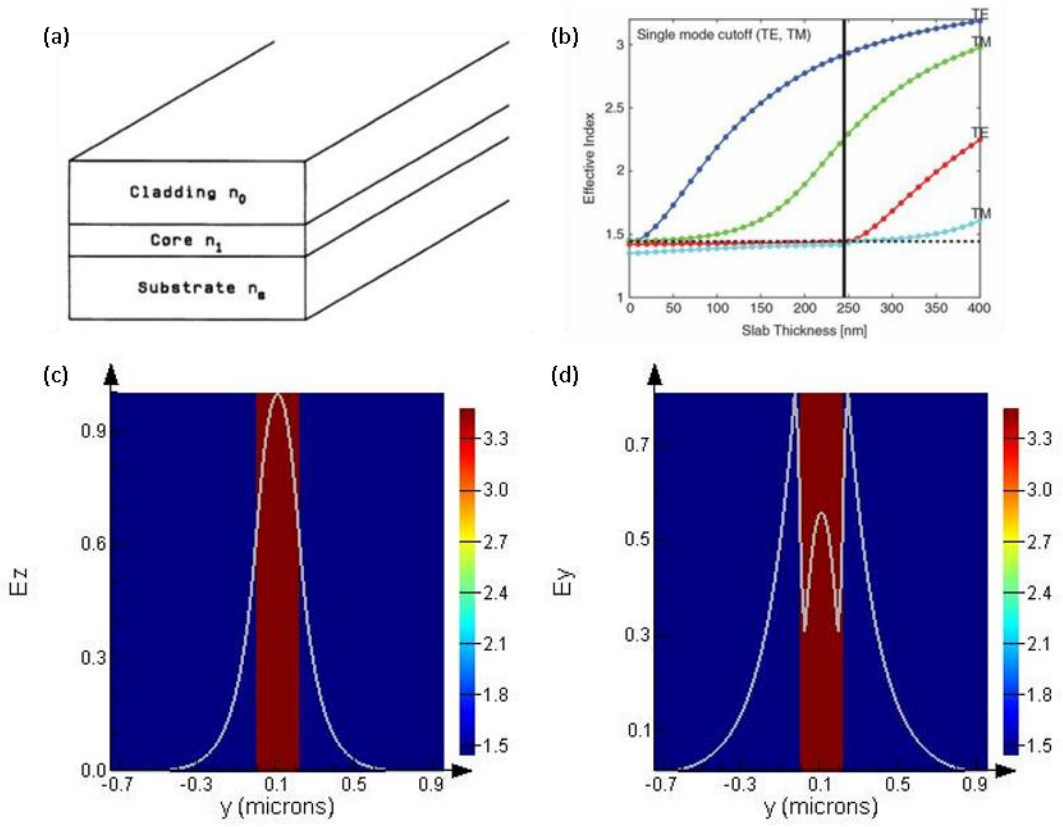

Figure 2.13. Slab waveguide analysis (a) schematic, (b) Effective index versus slab thickness for silicon core and oxide substrate and cladding, (c) TE mode, (d) TM mode for 220 nm thick slab waveguide with silicon core and oxide substrate and cladding. (a) reproduced from [3].

The previous discussion with slab waveguides were meant as an introduction because of the simple 1 dimensional analysis. However planar waveguides with finite width are more realistic. Figure 2.14 (a) shows the cross section of the two most common types of waveguides in silicon photonics, with light propagating into the page. Figure 2.14 (b, c) shows scanning electron microscope image of these waveguides. Figure 2.14 (d, e) show the mode profiles of a strip waveguide using silicon core with 220 nm height and 500 nm width and silicon dioxide bottom and top cladding. As mentioned earlier, the polarization of the light has a strong impact on how the light behaves in the waveguide. It is obvious for example that in the TM mode, more of the electric field is actually traveling in the cladding rather than in the core. Figure 2.14 (f) shows that the effective index of the mode changes for different waveguide widths. In addition, waveguides larger than 450 nm are no longer single mode and support two guided transverse electric (TE) modes.

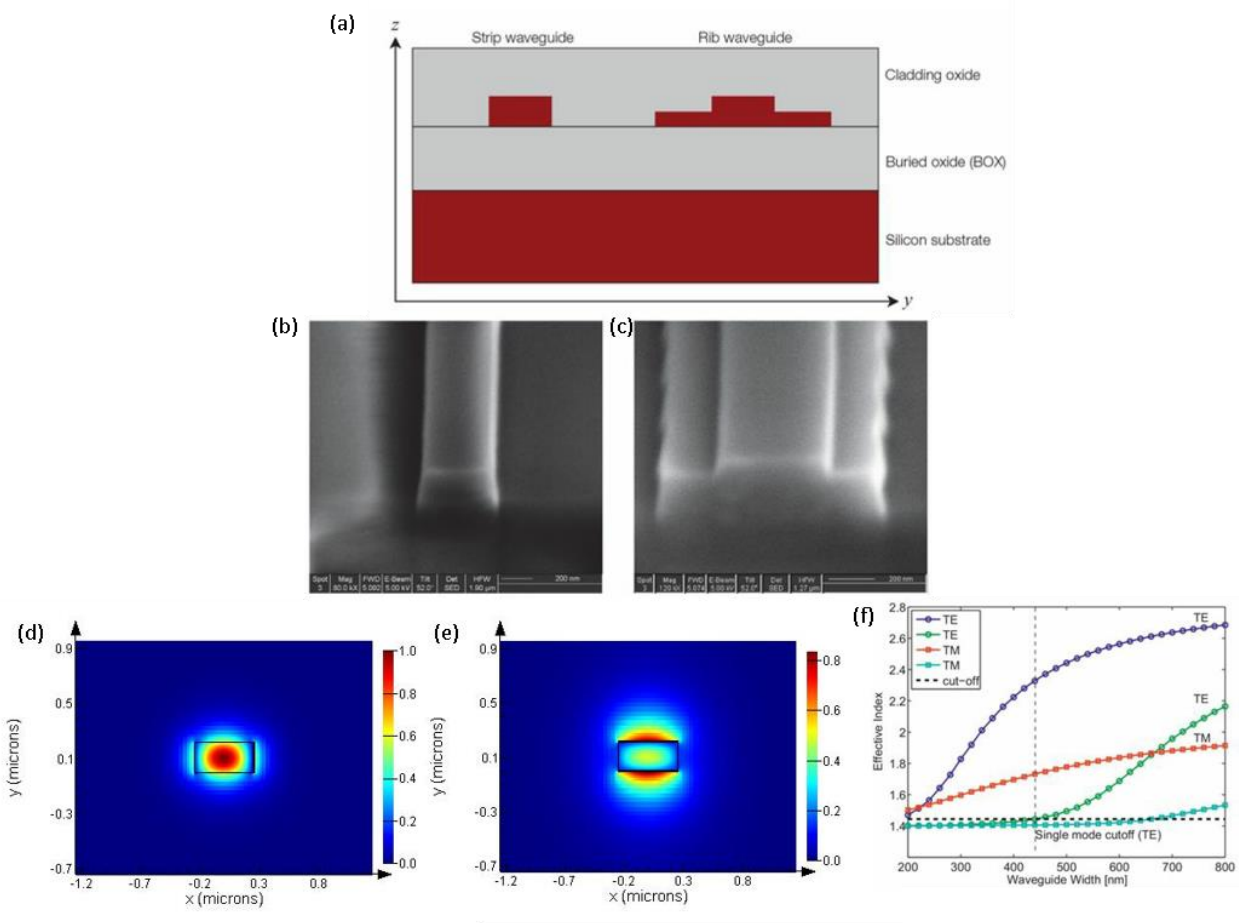

Figure 2.14. Silicon photonic waveguides. (a) cross section schemetic of the two common types of waveguides, strip and rib waveguides. (b, c) Scanning electron microscope images of strip and rib waveguides, respectively. (d) Transverse electric (TE) mode and (e) transverse magnetic (TM) mode of a strip waveguide with 500 nm width and 220 nm height, colorbar refers to intensity of the major component of the electric field. (f) Plot showing how effective index changes with waveguide width. Larger waveguides support higher number of modes. (a-c, f) reproduced from [72].

2.3. Plasmonics

Two on chip optical sensors in this thesis are based on plasmonics. This section covers how the field of plasmonics emerged and briefly goes through some fundamentals.

The previous section on silicon photonics mentioned how before silicon, optical waveguides measured a few microns in width. Silicon photonics managed to bring the size down to a few hundred nanometers in width. However, with ever-decreasing size of electronics, photonics components will be taking up much space on the chip even when using silicon photonics. Plasmonics offers the advantages of photonics such as high speed interconnects at a fraction of the size of photonics [73]. Plasmonics do not suffer the

diffraction limit that often is accompanied with photonics [74] and plasmonic-photonic couplers have emerged [75]. Plasmonic waveguides can actually have 90° bends unlike silicon photonics which required a bend radius of several microns, thus plasmonic circuits can be very dense [76]. In addition to the obvious size advantages, plasmonic circuits feature new phenomena that were difficult to achieve in the photonics regime. Due to the right-angle bends, 3D and multilevel plasmonic circuits are more realistic than 3D photonic circuits [77, 78]. Photonics in the mid-infrared is difficult due to material absorption. However, materials can be engineered to operate in the mid-infrared with plasmonics[73, 79, 80]. The mid-infrared is important in many applications and in sensing in particular [73]. The biggest challenge with plasmonics is that it uses materials that are often incompatible with electronics chips or that use expensive fabrication methods. Current research trends in plasmonics is to design plasmonic devices with semiconductor materials and using low cost fabrication methods.

2.3.1. Free electron gas model

The effect of plasmons on the optical properties of metals can be described using the free electron gas model. Plasmons are electrons with mass m and charge e that oscillate in response to an applied electric field $\mathbf{E}$, and the motion is subject to collisions as in Figure 2.15 at a frequency γ that dampen that motion [20]. Starting from the simple F = ma one can derive the model for the motion of a free electron subject to an electric field as in equation 2.12 [20].

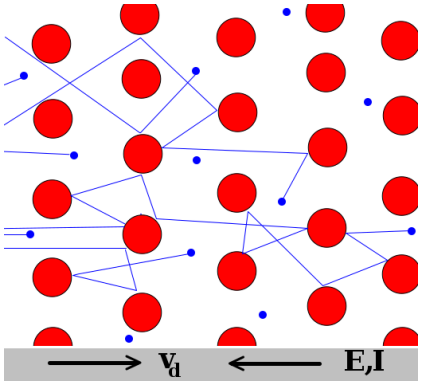

Figure 2.15. Free electrons (blue) in metal (atoms in red). Reproduced from [81].

$$m\ddot{\mathbf{x}} + m\gamma\dot{\mathbf{x}} = -e\mathbf{E} \qquad 2.12$$

Assuming a sinusoidal time-varying applied electric field as in the case of monochromatic light excitation, using Maxwell's equations, one can derive the dielectric function of metals as in 2.13, also known as the Drude model [20].

$$\varepsilon(\omega) = \left(1 - \frac{\omega_p^2}{\omega^2 + \gamma^2}\right) + i\frac{\gamma \cdot \omega_p^2}{\omega(\omega^2 + \gamma^2)}, \quad 2.13$$

Where $i = \sqrt{-1}$ and ω_p is the plasma frequency given by equation 2.14

$$\omega_p^2 = \frac{ne^2}{\varepsilon_0 m}, \quad 2.14$$

where n is the number of free carriers per cm^3. Readers interested in the full derivation can refer to [20]. Material effects manifest themselves by experimental verification of γ and the mass of the electron is replaced by the effective mass of the electron. Other material models have been developed such as Lorentz and Drude-Lorentz. While these more advanced models can be more accurate, they contain more parameters that require rigorous experimental verification.

2.3.2. Plasmonic waveguides

Figure 2.16 (a, b) compares between localized surface plasmon modes typically found in metal nanoparticles and propagating surface plasmon polariton modes required for plasmonic waveguides. When the metal-dielectric interface in Figure 2.16 (b) is bought close to another metal-dielectric interface, the SPPs couple to form plasmon slot waveguides as in Figure 2.16 (c, d).

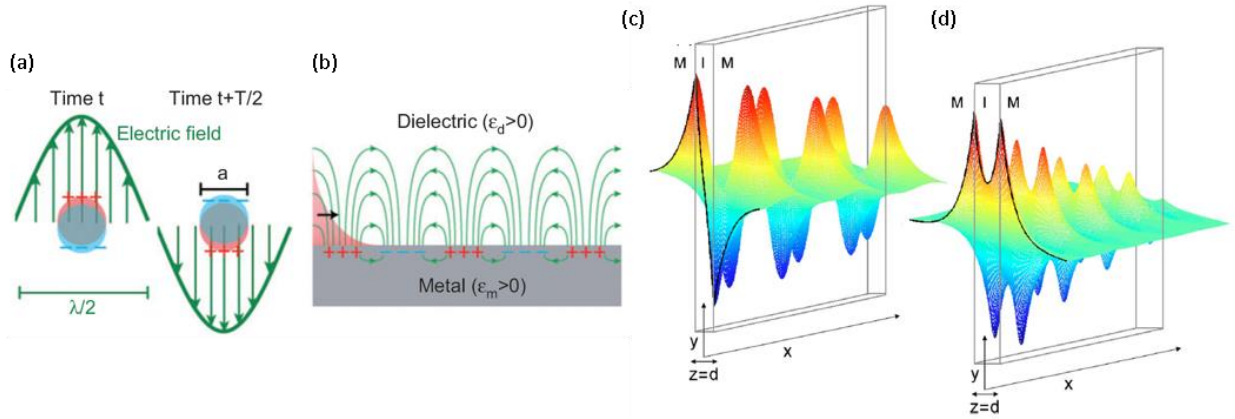

Figure 2.16. (a) localized surface plasmon mode and (b) propagating surface plasmon polariton mode. For both cases, metal is in grey, dielectric white background. Electric field shown by green arrows, red indicates the field intensity. (a, b) reproduced from [73]. When two metal-dielectric interfaces are bought near each other in a metal-insulator-metal (MIM) configuration, there exist coupled modes and can be (c) antisymmetric and (d) symmetric . (c, d) reproduced from [13].

2.4. References

[1] G. T. Reed and A. P. Knights, *Silicon photonics: an introduction*: John Wiley & Sons, 2004.

[2] E. Optics. *Optics 101: Level 1 Theoretical Foundations*. Available: https://www.edmundoptics.com/resources/application-notes/optics/optics-101-level-1-theoretical-foundations/

[3] K. Okamoto, *Fundamentals of optical waveguides*: Academic press, 2010.

[4] J. Brownson. (31/07/2017). *The "Life" of a Photon*. Available: https://www.e-education.psu.edu/eme810/sites/www.e-education.psu.edu.eme810/files/images/Lesson_03/radiationfates.png

[5] Pdcook. (2012, 31/07/2017). *BioTek microplate reader*. Available: https://commons.wikimedia.org/w/index.php?curid=19191924

[6] S. C. Terry, J. H. Jerman, and J. B. Angell, "A gas chromatographic air analyzer fabricated on a silicon wafer," *IEEE Transactions on Electron Devices,* vol. 26, pp. 1880-1886, 1979.

[7] A. Manz, N. Graber, and H. M. Widmer, "Miniaturized total chemical analysis systems: A novel concept for chemical sensing," *Sensors and Actuators B: Chemical,* vol. 1, pp. 244-248, 1990/01/01 1990.

[8] D. Kverno. *Oscillations and Resonance in a Carbon Dioxide Laser*. Available: http://www.phy.davidson.edu/StuHome/derekk/Resonance/pages/co2.htm

[9] I. Coblentz Society, "Evaluated Infrared Reference Spectra," in *NIST Chemistry WebBook, NIST Standard Reference Database Number 69*, P. J. L. a. W. G. Mallard, Ed., ed Gaithersburg MD, 20899: National Institute of Standards and Technology.

[10] O. Optical. *Raman Spectroscopy*. Available: http://www.omegafilters.com/applications/raman-spectroscopy/

[11] E. C. Le Ru, E. Blackie, M. Meyer, and P. G. Etchegoin, "Surface Enhanced Raman Scattering Enhancement Factors: A Comprehensive Study," *The Journal of Physical Chemistry C,* vol. 111, pp. 13794-13803, 2007/09/01 2007.

[12] U. Leonhardt, "Optical metamaterials: Invisibility cup," *Nature Photonics,* vol. 1, pp. 207-208, 2007.

[13] J. A. Dionne, L. A. Sweatlock, H. A. Atwater, and A. Polman, "Plasmon slot waveguides: Towards chip-scale propagation with subwavelength-scale localization," *Physical Review B,* vol. 73, 2006.

[14] K. Tanaka and M. Tanaka, "Simulations of nanometric optical circuits based on surface plasmon polariton gap waveguide," *Applied Physics Letters,* vol. 82, p. 1158, 2003.

[15] D. F. P. Pile, T. Ogawa, D. K. Gramotnev, Y. Matsuzaki, K. C. Vernon, K. Yamaguchi, T. Okamoto, M. Haraguchi, and M. Fukui, "Two-dimensionally localized modes of a nanoscale gap plasmon waveguide," *Applied Physics Letters,* vol. 87, p. 261114, 2005.

[16] S. A. Maier, P. G. Kik, H. A. Atwater, S. Meltzer, E. Harel, B. E. Koel, and A. A. Requicha, "Local detection of electromagnetic energy transport below the diffraction limit in metal nanoparticle plasmon waveguides," *Nature Materials,* vol. 2, p. 229, 2003.

[17] J. M. Steele, C. E. Moran, A. Lee, C. M. Aguirre, and N. J. Halas, "Metallodielectric gratings with subwavelength slots: Optical properties," *Physical Review B,* vol. 68, p. 205103, 2003.

[18] S. A. Maier and H. A. Atwater, "Plasmonics: Localization and guiding of electromagnetic energy in metal/dielectric structures," *Journal of Applied Physics,* vol. 98, p. 10, 2005.

[19] K. M. Mayer and J. H. Hafner, "Localized surface plasmon resonance sensors," *Chemical Reviews,* vol. 111, pp. 3828-57, Jun 8 2011.

[20] S. A. Maier, *Plasmonics: fundamentals and applications*: Springer US, 2007.

[21] M. G. Albrecht and J. A. Creighton, "Anomalously intense Raman spectra of pyridine at a silver electrode," *Journal of the American Chemical Society,* vol. 99, pp. 5215-5217, 1977/06/01 1977.

[22] U. Wenning, B. Pettinger, and H. Wetzel, "Anguler-resolved raman spectroscopy of pyridine on copper and gold electrodes," *Chemical Physics Letters,* vol. 70, pp. 49-54, 1980/02/15 1980.

[23] H. Wetzel and H. Gerischer, "Surface enhanced Raman scattering from pyridine and halide ions adsorbed on silver and gold sol particles," *Chemical Physics Letters,* vol. 76, pp. 460-464, 1980/12/15 1980.

[24] Z. Yang, Y. Li, Z. Li, D. Wu, J. Kang, H. Xu, and M. Sun, "Surface enhanced Raman scattering of pyridine adsorbed on Au@Pd core/shell nanoparticles," *The Journal of Chemical Physics,* vol. 130, p. 234705, 2009.

[25] F. Toderas, M. Baia, L. Baia, and S. Astilean, "Controlling gold nanoparticle assemblies for efficient surface-enhanced Raman scattering and localized surface plasmon resonance sensors," *Nanotechnology,* vol. 18, p. 255702, 2007.

[26] F. Bai, M. Li, P. Fu, R. Li, T. Gu, R. Huang, Z. Chen, B. Jiang, and Y. Li, "Silicon nanowire arrays coated with electroless Ag for increased surface-enhanced Raman scattering," *APL Materials,* vol. 3, p. 056101, 2015.

[27] M. S. Schmidt, J. Hübner, and A. Boisen, "Large area fabrication of leaning silicon nanopillars for surface enhanced Raman spectroscopy," *Advanced Materials,* vol. 24, 2012.

[28] L. Cao, B. Nabet, and J. E. Spanier, "Enhanced Raman scattering from individual semiconductor nanocones and nanowires," *Physical Review Letters,* vol. 96, p. 157402, 2006.

[29] S. Christiansen, M. Becker, S. Fahlbusch, J. Michler, V. Sivakov, G. Andrä, and R. Geiger, "Signal enhancement in nano-Raman spectroscopy by gold caps on silicon nanowires obtained by vapour–liquid–solid growth," *Nanotechnology,* vol. 18, p. 035503, 2007.

[30] Q. Hao, B. Wang, J. A. Bossard, B. Kiraly, Y. Zeng, I. K. Chiang, L. Jensen, D. H. Werner, and T. J. Huang, "Surface-Enhanced Raman Scattering Study on Graphene-Coated Metallic Nanostructure Substrates," *The Journal of Physical Chemistry C,* vol. 116, pp. 7249-7254, 2012/04/05 2012.

[31] M. Khorasaninejad, S. Raeis-Zadeh, S. Jafarlou, M. Wesolowski, C. Daley, J. Flannery, J. Forrest, S. Safavi-Naeini, and S. Saini, "Highly enhanced Raman scattering of graphene using plasmonic nano-structure," *Scientific reports,* vol. 3, 2013.

[32] M. Li, S. K. Cushing, J. Zhang, J. Lankford, Z. P. Aguilar, D. Ma, and N. Wu, "Shape-dependent surface-enhanced Raman scattering in gold–Raman-probe–silica sandwiched nanoparticles for biocompatible applications," *Nanotechnology,* vol. 23, p. 115501, 2012.

[33] F. De Angelis, F. Gentile, F. Mecarini, G. Das, M. Moretti, P. Candeloro, M. Coluccio, G. Cojoc, A. Accardo, and C. Liberale, "Breaking the diffusion limit with super-hydrophobic delivery of molecules to plasmonic nanofocusing SERS structures," *Nature Photonics,* vol. 5, pp. 682-687, 2011.

[34] A. Erik, K. Magnus, A. R. Chraplyvy, J. R. David, M. K. Peter, W. Peter, R. Kim, F. Johannes Karl, J. S. Seb, J. E. Benjamin, S. Marco, R. K. Frank, L. Andrew, P. Josep, T. Ioannis, E. B. John, S. Sudha, B.-P. Maïté, and G. Nicolas, "Roadmap of optical communications," *Journal of Optics,* vol. 18, p. 063002, 2016.

[35] P. Tien, "Integrated optics," *Scientific American,* vol. 230, pp. 28-35, 1974.

[36] R. Ulrich, "Self imaging system using a waveguide," ed: Google Patents, 1978.

[37] R. Nagarajan, M. Kato, J. Pleumeekers, P. Evans, S. Corzine, S. Hurtt, A. Dentai, S. Murthy, M. Missey, and R. Muthiah, "InP photonic integrated circuits," *IEEE Journal of Selected Topics in Quantum Electronics,* vol. 16, pp. 1113-1125, 2010.

[38] M. K. Smit, X. Leijtens, E. Bente, J. van der Tol, H. Ambrosius, D. Robbins, M. J. Wale, N. Grote, and M. Schell, "A generic foundry model for InP-based photonic ICs," in *Optical Fiber Communication Conference*, 2012, p. OM3E. 3.

[39] D. A. B. Miller, "Rationale and challenges for optical interconnects to electronic chips," *Proceedings of the IEEE,* vol. 88, pp. 728-749, 2000.

[40] D. Normile, "The End--Not Here Yet, But Coming Soon," *Science,* vol. 293, pp. 787-787, 2001-08-03 00:00:00 2001.

[41] R. Ho, K. W. Mai, and M. A. Horowitz, "The future of wires," *Proceedings of the IEEE,* vol. 89, pp. 490-504, 2001.

[42] R. Ho, M. Ken, and M. Horowitz, "Managing wire scaling: a circuit perspective," in *Interconnect Technology Conference, 2003. Proceedings of the IEEE 2003 International*, 2003, pp. 177-179.

[43] A. Karkar, T. Mak, K. F. Tong, and A. Yakovlev, "A Survey of Emerging Interconnects for On-Chip Efficient Multicast and Broadcast in Many-Cores," *IEEE Circuits and Systems Magazine,* vol. 16, pp. 58-72, 2016.

[44] M. Haurylau, C. Guoqing, C. Hui, Z. Jidong, N. A. Nelson, D. H. Albonesi, E. G. Friedman, and P. M. Fauchet, "On-Chip Optical Interconnect Roadmap: Challenges and Critical Directions," *Selected Topics in Quantum Electronics, IEEE Journal of,* vol. 12, pp. 1699-1705, 2006.

[45] G. T. Reed and A. P. Knights, "Silicon-On-Insulator (SOI) Photonics," in *Silicon Photonics*, ed: John Wiley & Sons, Ltd, 2005, pp. 57-110.

[46] C. Gunn, "CMOS Photonics for High-Speed Interconnects," *IEEE Micro,* vol. 26, pp. 58-66, 2006.

[47] R. Soref, "The Past, Present, and Future of Silicon Photonics," *IEEE Journal of Selected Topics in Quantum Electronics,* vol. 12, pp. 1678-1687, 2006.

[48] T. Barwicz, H. Byun, F. Gan, C. Holzwarth, M. Popovic, P. Rakich, M. Watts, E. Ippen, F. Kärtner, and H. Smith, "Silicon photonics for compact, energy-efficient interconnects [Invited]," *Journal of Optical Networking,* vol. 6, pp. 63-73, 2007.

[49] J. P. S. Lorenzo, R. A., "1.3 μm electro-optic silicon switch," *Appl. Phys. Lett.,* vol. 51, p. 3, 1987.

[50] R. Soref, Bennett, B., "Electrooptical effects in silicon," *EEE J. Quant. Electron,* vol. 23, p. 7, 1987.

[51] G. R. Cocorullo, I., "Thermo-optical modulation at 1.5 μm in silicon etalon," *Electron. Lett.,* vol. 28, p. 3, 1992.

[52] L. Friedman, Soref, R. A., Lorenzo, J. P., "Silicon double-injection electrooptic modulator with junction gate control," *J. Appl. Phys.,* vol. 63, p. 9, 1988.

[53] G. V. Treyz, "Silicon Mach–Zehnder waveguide interferometers operating at 1.3 μm," *Electron. Lett.,* vol. 27, p. 3, 1991.

[54] U. Fischer, Schuppert, B., Petermann, K., "Integrated optical switches in silicon based on SiGe-waveguides," *IEEE Photon. Tech. Lett.,* vol. 5, p. 3, 1993.

[55] P. D. Hewitt, Reed, G. T., "Multi micron dimension optical p-i-n modulators in silicon-on-insulator," in *SPIE*, 1999, pp. 237-243.

[56] C. Sun, M. T. Wade, Y. Lee, J. S. Orcutt, L. Alloatti, M. S. Georgas, A. S. Waterman, J. M. Shainline, R. R. Avizienis, S. Lin, B. R. Moss, R. Kumar, F. Pavanello, A. H. Atabaki, H. M. Cook, A. J. Ou, J. C. Leu, Y.-H. Chen, K. Asanović, R. J. Ram, M. A. Popović, and V. M. Stojanović, "Single-chip microprocessor that communicates directly using light," *Nature,* vol. 528, pp. 534-538, 2015.

[57] J. E. Bowers, T. Komljenovic, M. Davenport, J. Hulme, A. Y. Liu, C. T. Santis, A. Spott, S. Srinivasan, E. J. Stanton, and C. Zhang, "Recent advances in silicon photonic integrated circuits," 2016, pp. 977402-977402-18.

[58] T. David, Z. Aaron, E. B. John, K. Tin, T. R. Graham, V. Laurent, M.-M. Delphine, C. Eric, V. Léopold, F. Jean-Marc, H. Jean-Michel, H. S. Jens, X. Dan-Xia, B. Frédéric, O. B. Peter, Z. M. Goran, and M. Nedeljkovic, "Roadmap on silicon photonics," *Journal of Optics,* vol. 18, p. 073003, 2016.

[59] R. G. Beausoleil, P. J. Kuekes, G. S. Snider, S. Y. Wang, and R. S. Williams, "Nanoelectronic and Nanophotonic Interconnect," *Proceedings of the IEEE,* vol. 96, pp. 230-247, 2008.

[60] C. H. C. R. Wu, T. C. Huang, K. T. Cheng, R. Beausoleil, "20 Gb/s carrier-injection silicon microring modulator with SPICE-compatible dynamic model," presented at the Photonics in Switching, 2015.

[61] C. Zhang, D. Liang, C. Li, G. Kurczveil, J. E. Bowers, and R. G. Beausoleil, "High-speed Hybrid Silicon Microring Lasers," in *Circuits and Systems (MWSCAS), 2015 IEEE 58th International Midwest Symposium on*, 2015, pp. 1-4.

[62] J. E. Cunningham, I. Shubin, H. D. Thacker, J.-H. Lee, G. Li, X. Zheng, J. Lexau, R. Ho, J. G. Mitchell, and Y. Luo, "Scaling hybrid-integration of silicon photonics in freescale 130nm to TSMC 40nm-CMOS VLSI drivers for low power communications," in *2012 IEEE 62nd Electronic Components and Technology Conference*, 2012, pp. 1518-1525.

[63] Z. X. Li G, Thacker H, Yao J, Loo Y, Shubin I, Raj K, Cunningham JE, Krishnamoorthy AV., "40Gb/s Thermally Tunable CMOS ring Modulator," in *Group IV photonics*, San Diego, USA, 2012.

[64] X. Zheng, F. Liu, J. Lexau, D. Patil, G. Li, Y. Luo, H. Thacker, I. Shubin, J. Yao, K. Raj, R. Ho, J. E. Cunningham, and A. Krishnamoorthy, "Ultra-Low Power Arrayed CMOS Silicon Photonic Transceivers for an 80 Gbps WDM Optical Link," in *Optical Fiber Communication Conference/National Fiber Optic Engineers Conference 2011*, Los Angeles, California, 2011, p. PDPA1.

[65] F. Liu, D. Patil, J. Lexau, P. Amberg, M. Dayringer, J. Gainsley, H. F. Moghadam, X. Zheng, J. Cunningham, and A. Krishnamoorthy, "10 Gbps, 530 fJ/b optical transceiver circuits in 40 nm CMOS," in *IEEE Symp. VLSI circuits Dig. Tech. Papers*, 2011, pp. 290-291.

[66] X. Zheng, F. Liu, D. Patil, H. Thacker, Y. Luo, T. Pinguet, A. Mekis, J. Yao, G. Li, J. Shi, K. Raj, J. Lexau, E. Alon, R. Ho, J. E. Cunningham, and A. V. Krishnamoorthy, "A sub-picojoule-per-bit CMOS photonic receiver for densely integrated systems," *Optics Express,* vol. 18, pp. 204-211, 2010/01/04 2010.

[67] X. Z. A. V. Krishnamoorthy, D. Feng, J. Lexau, J. F. Buckwalter, H. D. Thacker, F. Liu, Y. Luo, E. Chang, P. Amberg, I. Shubin, S. S. Djordjevic, J. H. Lee, S. Lin, H. Liang, A. Abed, R. Shafiiha, K. Raj, R. Ho, M. Asghari, and J. E. Cunningham, "A low-power, high-speed, 9-channel germanium-silicon electro-absorption modulator array integrated with digital CMOS driver and wavelength multiplexer," *Optics Express,* vol. Vol. 22, p. 7, 2014.

[68] N. Dupuis, B. G. Lee, J. E. Proesel, A. Rylyakov, R. Rimolo-Donadio, C. W. Baks, C. L. Schow, A. Ramaswamy, J. E. Roth, R. S. Guzzon, B. Koch, D. K. Sparacin, and G. A. Fish, "30Gbps optical link utilizing heterogeneously integrated III-V/Si photonics and CMOS circuits," in *Optical Fiber Communications Conference and Exhibition (OFC), 2014*, 2014, pp. 1-3.

[69] P. W. Coteus, J. U. Knickerbocker, C. H. Lam, and Y. A. Vlasov, "Technologies for exascale systems," *IBM Journal of Research and Development,* vol. 55, pp. 14:1-14:12, 2011.

[70] Y. Vlasov, "Silicon photonics for next generation computing systems," in *34th European Conf. Optical Communications*, 2008.

[71] cnet. (2016, 17 July 2017). *Intel: Our laser chips will make sites like Google and Facebook faster*. Available: https://www.cnet.com/news/intel-our-laser-chips-will-make-sites-like-google-and-facebook-faster/

[72] L. Chrostowski and M. Hochberg, *Silicon photonics design: from devices to systems*: Cambridge University Press, 2015.

[73] S. Law, V. Podolskiy, and D. Wasserman, "Towards nano-scale photonics with micro-scale photons: the opportunities and challenges of mid-infrared plasmonics," *Nanophotonics,* vol. 2, 2013.

[74] D. K. Gramotnev and S. I. Bozhevolnyi, "Plasmonics beyond the diffraction limit," *Nat Photon,* vol. 4, pp. 83-91, 2010.

[75] B. Lau, M. A. Swillam, and A. S. Helmy, "Hybrid orthogonal junctions: wideband plasmonic slot-silicon waveguide couplers," *Optics Express,* vol. 18, pp. 27048-27059, 2010/12/20 2010.

[76] M. A. Swillam and A. S. Helmy, "Feedback effects in plasmonic slot waveguides examined using a closed form model," *IEEE Photonics Technology Letters,* vol. 24, p. 497, 2012.

[77] M. A. Swillam and A. S. Helmy, "Analysis and applications of 3D rectangular metallic waveguides," *Optics Express,* vol. 18, pp. 19831-19843, 2010/09/13 2010.

[78] M. H. El Sherif, O. S. Ahmed, M. H. Bakr, and M. A. Swillam, "Polarization-controlled excitation of multilevel plasmonic nano-circuits using single silicon nanowire," *Optics Express,* vol. 20, pp. 12473-12486, 2012/05/21 2012.

[79] S. Law, L. Yu, and D. Wasserman, "Epitaxial growth of engineered metals for mid-infrared plasmonics," *Journal of Vacuum Science & Technology B: Microelectronics and Nanometer Structures,* vol. 31, p. 03C121, 2013.

[80] S. Law, D. C. Adams, A. M. Taylor, and D. Wasserman, "Mid-infrared designer metals," *Opt Express,* vol. 20, pp. 12155-65, May 21 2012.

[81] Rafaelgarcia. (22 July 2017). *Electrona in crystallo fluentia*. Available: https://commons.wikimedia.org/w/index.php?curid=11926841

CHAPTER 3. INTEGRATED LAB-ON-A-CHIP SENSOR USING SHALLOW SILICON WAVEGUIDE SILICON-ON-INSULATOR (SOI) MULTIMODE INTERFERENCE (MMI) DEVICE

This chapter was submitted for publication in Journal of Nanophotonics with the following citation information and it will be reproduced here as is.

M. Y. Elsayed, Y. Ismail, and M. A. Swillam, "Integrated lab-on-a-chip sensor using shallow silicon waveguide silicon-on-insulator (SOI) multimode interference (MMI) device" Submitted to Journal of Nanophotonics.

ABSTRACT

Waveguides with sub-100 nm height offer a promising platform for sensors. After going through a thorough analysis of the guided modes in the 50 nm and 70 nm shallow waveguide platforms, the designs of MMI sensors based on these platforms have been optimized. A minimum feature size of 1 µm was used, thus any low cost photolithography can be used for fabrication. The effect of the sensor length on performance metrics were studied. At a length of 4 mm, the 50 nm silicon device layer platform provides a sensitivity of roughly 420 nm / RIU, FOM of 133 and a maximum Δn of 0.023. On the other hand, the 70 nm silicon device layer platform results in a more compact design: only 2.4 mm length was required to achieve similar FOM, 134 albeit having a lower sensitivity of 330 nm / RIU, while having maximum Δn of 0.018. The shallow SOI waveguide platform is promising in sensing applications using this simple MMI structure which can easily be integrated with microfluidics components.

3.1. Introduction

On chip sensing mechanisms include optical, electrical and mechanical methods [1]. Optical sensors are becoming more important for lab on a chip applications because they allow the analysis of a large variety of analytes and monitoring reactions real time with high temporal resolution [1]. Optical detection methods have been used extensively in the lab, such as detecting color changes and fluorescence and measuring the refractive index. Moving sensing on chip will allow using the same analysis techniques that researchers are already familiar with. Optical sensors based on refractive index change can be used as label-free detection methods for a variety of lab-on-a-chip applications. Ease of integration with

microfluidic and electronic components is a very important feature for a sensor to be considered a viable commercial solution.

An important parameter in sensors is having high light-matter interaction. One of the mostly used optical sensing methods is using resonance in a cavity such as fabry-perot cavity [2], ring resonator [3, 4], photonic crystal cavity [5] and plasmonic resonances [1, 6-10]. The objective is to cause the light to travel throughout the sensor several times. Spatial methods to increase the light-matter interaction include using nanowire wires [11] and slot waveguides. A simpler approach would be to use a shallow waveguide platform that leaks a lot of the light into the surrounding material. The performance of the waveguide will be strongly affected by the refractive index of the surrounding material and can thus be used as a sensor. Interference based methods are mach zhender interferometers (MZI) [12] and multimode interference (MMI) devices. MZI sensor have been employed for various lab on chip applications [13, 14] and this work employs an MMI as a sensor.

This work explores the shallow waveguide platform and assesses its possibility to use as a sensor. The shallow waveguide platform has many of the advantages of more conventional silicon platforms with the additional advantage of easy fabrication. The relatively larger minimum feature size required means that advanced lithographic techniques are not required [15]. Silicon nitride waveguides with 50 to 100 nm height were previously proposed [16]and ring resonators were designed using these shallow waveguides [17, 18]. For the silicon shallow waveguide proposed in this work, a grating coupler was previously designed to couple light to optical fibers with 50% efficiency [19].

A multimode interference device relies on the self-imaging concept. The different modes interfere constructively at specific lengths, causing the input field to be replicated. The underlying concepts and fundamentals are explained at length by Soldano and Pennings [20]. Multimode interference has been vastly employed in fibers for a variety of applications including sensing [21]. On-chip MMI devices have been mostly for signal processing applications such as waveguide division multiplexing and power splitting [22]. A few on chip MMI sensors were also proposed [23, 24] including a silicon-based MMI temperature sensor [25]. This work is the first silicon-on-insulator MMI sensor and it goes through the optimization of MMI sensors on various SOI platforms.

3.2. Analysis

Figure 3.1 (a) shows a 3 dimensional schematic of the proposed MMI sensor (not to scale). A commercial simulator eigenmode solver was used to perform the calculations [26]. Figure 3.1 (b) shows the electric

field profile for the single mode waveguide of the 50 nm height waveguide platform while Figure 3.1 (c) shows the electric field profile for a larger waveguide supporting 5 modes. In both cases, the shallow waveguide platform supports only transverse electric (TE) modes. For the 70 nm height case, the field profile is similar, also supporting only TE modes.

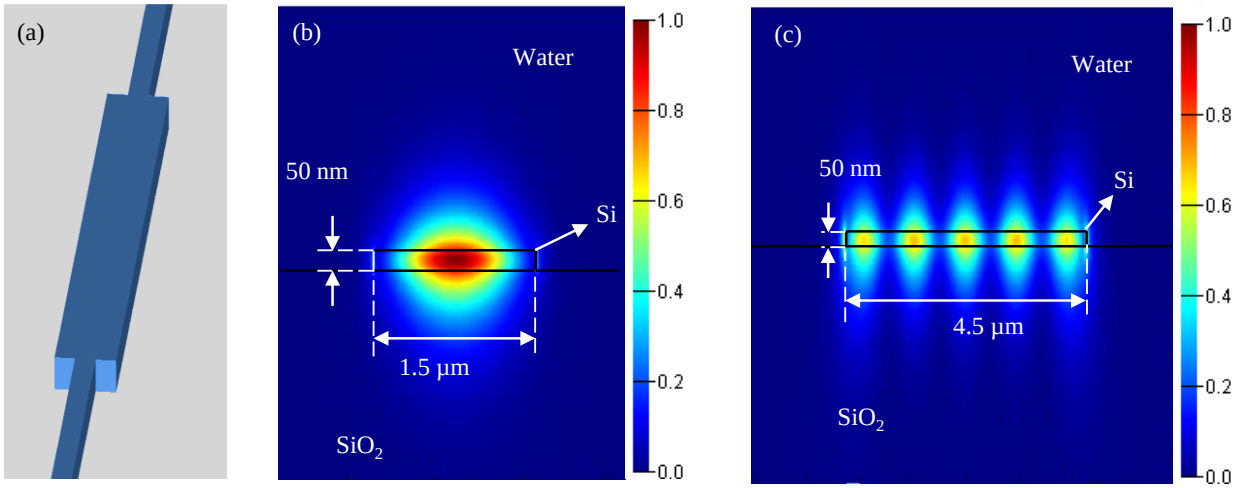

Figure 3.1. (a) 3D schematic of MMI sensor (not to scale), (b) mode profile of single mode waveguide, (c) mode profile of multimode section.

Figure 3.2 shows the dispersion analysis for both types of waveguides, the 50 nm height and the 70 nm height for different waveguide widths. It provides a good background for any further work with these platforms particularly those supporting multiple modes.

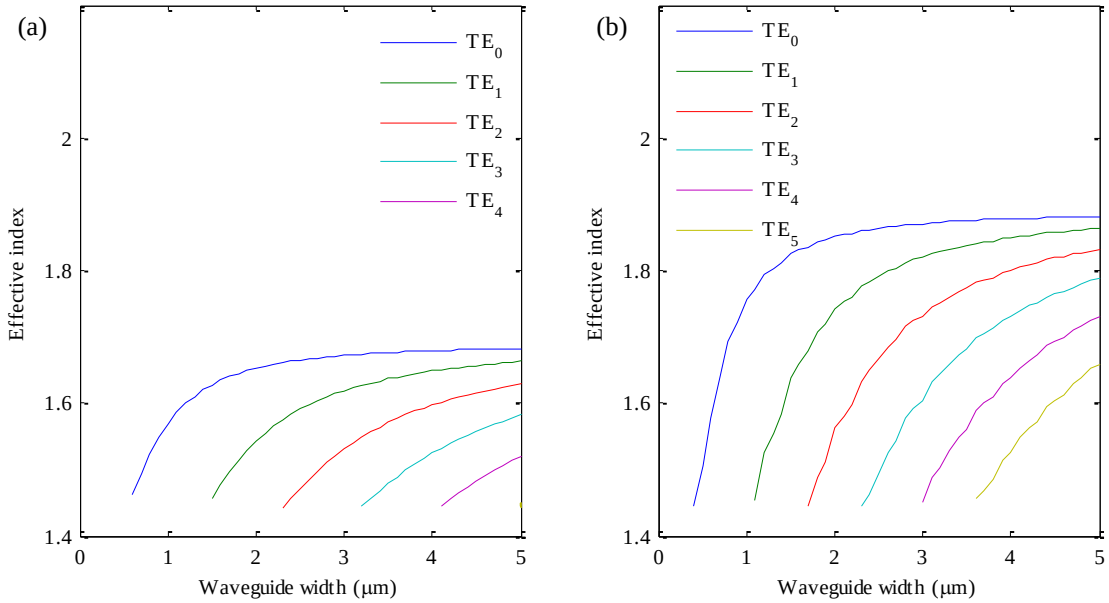

Figure 3.2. Effective indices of guided modes for various widths for (a) 50 nm height and (b) 70 nm height waveguides.

The shallow waveguide platform can be fabricated using a standard foundry process supporting partial etch. An example would be a silicon photonics process starting with SOI wafer with a thick BOX layer of several microns, 220 nm device layer and 150 nm partial etch, leaving behind 70 nm.

Sensing is based on the self-imaging principle of multi-mode interferometers. Each mode has a different effective index and thus a different phase velocity. Interference occurs between these modes after a certain distance, L. Figure 3.3 shows the field distribution in the multi-mode section, demonstrating that the input is replicated periodically.

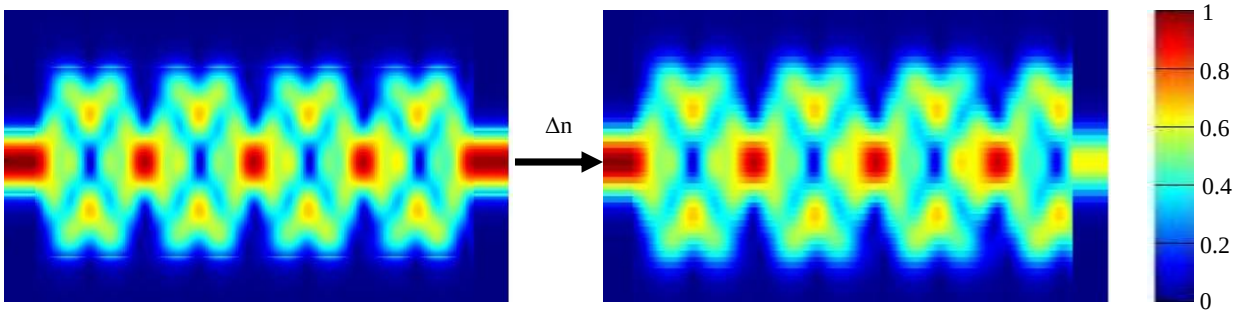

Figure 3.3. Visualizing the effect of Δn = 0.3. (Left) Background index 1.3. 4 self-images in a multi-mode section with length 94.1 µm for background refractive index 1.3. (Right) Background index 1.6. The beating length increased due to the increased n_eff and thus taking the output at the same distance 94.1 µm results in much lower transmission.

The beating length L_π is the where interference of the first two fundamental modes is maximum and is given by equation 3.1.

$$L_\pi = \frac{4 n_{eff} W_e^2}{3\lambda} \qquad 3.2$$

where n_{eff} is the effective index of the TE_0 mode, λ is the operating wavelength 1550nm, W_e is the effective width of the multi-mode section which was taken as the geometrical width in this work. Thus the refractive index of the superstrate affects the beating length directly through n_{eff}.

As explained previously [25], using a multi-mode section supporting more than 5 modes increases losses and has no benefit in sensitivity. Thus, for the 50 nm height waveguide, we fixed the multi-mode section width to 4.5 µm and for the 70 nm height waveguide, we fixed the multi-mode section width to 3 µm. The analysis in Figure 3.2 shows that these dimensions support 5 modes. Equation 3.3 describes the self-imaging length for symmetrical injection as in our case.

$$L = p\left(\frac{3 \cdot L_\pi}{4}\right) \qquad 3.4$$

3.3. Results

The design is a single input single output multi-mode interference (MMI) device with symmetric injection, where the input single mode waveguide is placed at the center of the multi-mode waveguide. The longer the MMI section, the more light-matter interaction there is. Therefore, several lengths corresponding to different multiples of the self-imaging length were analyzed for each of the 50 nm and 70 nm height waveguides. The performance of different length sensors is shown in Figure 3.4. Self-imaging occurs at these lengths at 1550 nm wavelength, and a wavelength sweep was performed. The spectral shift due to a change in refractive index is used as a performance indicator of the sensor as in equation 3.3.

$$Sensitivity = \frac{\Delta\lambda}{\Delta n} \quad \text{(nm/RIU)} \qquad 3.5$$

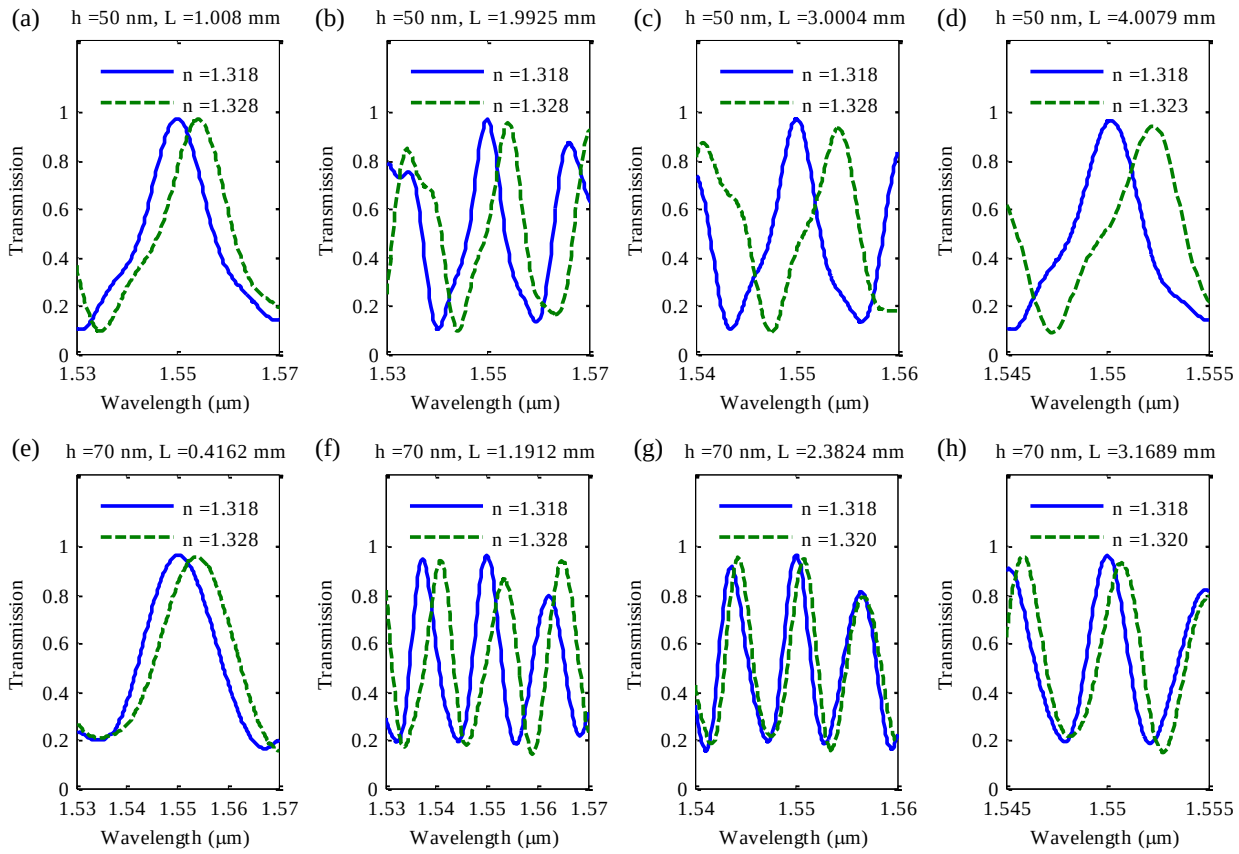

Figure 3.4. Spectral response of the sensor with reference (blue solid line) taken as water with n = 1.318 [27]. Peak transmission due to self-imaging is at 1550 nm wavelength. Green dashed line shows the red-shift due to a change in the refractive index. For (a) to (d), silicon device layer height is 50 nm, MMI section width is 4.5 μm and the MMI section length is about 1, 2, 3, 4 mm respectively. Δn is 0.01 for the shorter sensors and 0.05 for the 4 mm sensor. For (e) to (h), silicon device layer height is 70 nm, MMI section width is 3 μm and the MMI section length is about 0.4, 1.2, 2.4 and 3.2 mm respectively. Δn is 0.01 for the shorter sensors and 0.02 for the 2.4 and 3.2 mm sensors.

We found that the sensitivity as defined in equation 3.5 was not alone a good indicator of performance. In fact, the sensitivity was not affected strongly by the length. As expected, the shallower wavelength of 50 nm was more sensitive than the 70 nm one due to the mode leaking out of the core more in the shallower waveguide thus being more strongly affected by the surrounding medium. The 50 nm height MMI demonstrated a sensitivity of ~420 nm / RIU irrespective of the MMI section length while the 70 nm height MMI demonstrated a sensitivity of ~350 nm / RIU irrespective of the MMI section length. As is already evident from Figure 3.4, the full-width at half-maximum (FWHM) and free spectral range (FSR) respond strongly to the MMI section length. A figure of merit (FOM) can be defined as equation 3.6. A narrower FWHM makes it easier to extricate the spectral shift and thus this definition of the FOM is experimentally useful. The FSR's significance is in the maximum Δn that can be imposed. A Δn causing a $\Delta\lambda$ larger than the FSR will give an ambiguous spectral shift and the results will be difficult to interpret.

$$Figure\ of\ merit = \frac{Sensitivity}{FWHM} \qquad 3.6$$

Figure 3.5 (a) compares the FOM for the different sensor platforms. Despite the 50 nm height platform providing a better sensitivity than the 70 nm platform, the 70 nm platform provides sharper transmission peaks and thus outperforms the 50 nm platform using the FOM defined in equation 3.6. Figure 3.5 (b) shows that the longer MMI section length corresponds to narrower FSR and thus a smaller discernable Δn.

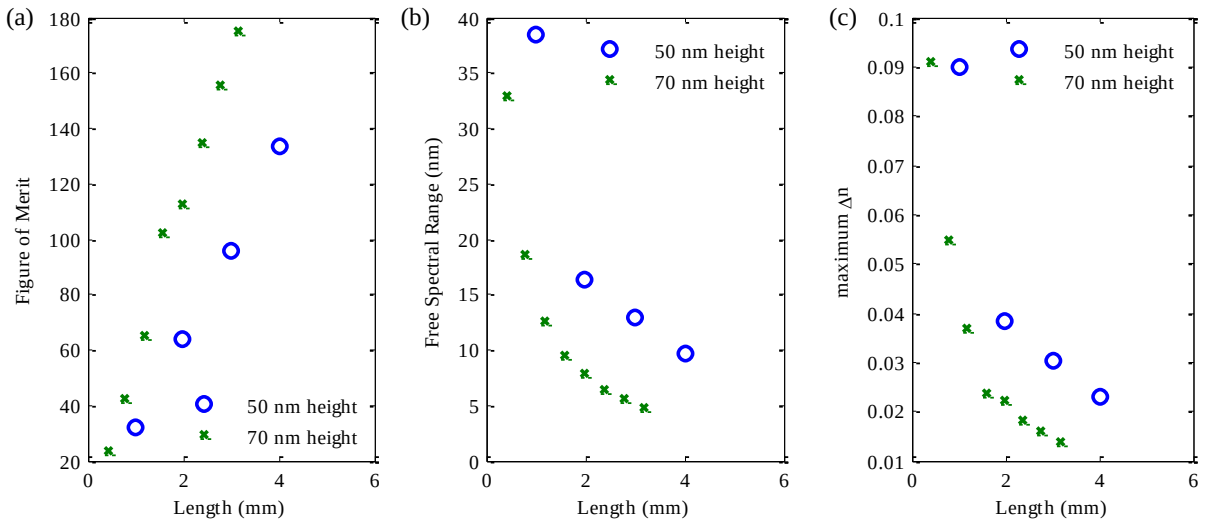

Figure 3.5. Performance metrics for the MMI sensor based on the shallow waveguide platforms: 50 nm (blue circles) and 70 nm (green crosses) silicon device layer. (a) Figure of merit as defined in equation 3.6 indicates the ease of which it is possible to measure a spectral shift. (b) Free spectral range is reduced with increasing length due causing a reduction in the maximum discernible Δn, (c).

3.4. Conclusions

The effects of waveguide width on the number of guided modes were presented for both the 50 nm height and 70 nm height waveguides. This analysis allowed the optimization of the design of MMI sensors based on these platforms. Such shallow silicon device layers are realizable in standard silicon photonics runs that include a partial etch step. Particular applications will require the designer to understand the tradeoffs. At a length of 4 mm, the 50 nm silicon device layer platform provides a sensitivity of roughly 420 nm / RIU, FOM of 133 and a maximum Δn of 0.023. On the other hand, the 70 nm silicon device layer platform results in a more compact design: only 2.4 mm length was required to achieve similar FOM, 134, while having maximum Δn of 0.018. The shallow SOI waveguide platform is promising in sensing applications using this simple MMI structure which can easily be integrated with microfluidics components.

3.5. References

[1] F. Vollmer and L. Yang, "Label-free detection with high-Q microcavities: a review of biosensing mechanisms for integrated devices," *Nanophotonics,* vol. 1, pp. 267-291, Dec 2012. doi: 10.1515/nanoph-2012-0021

[2] Y. Guo, H. Li, K. Reddy, H. S. Shelar, V. R. Nittoor, and X. Fan, "Optofluidic Fabry–Pérot cavity biosensor with integrated flow-through micro-/nanochannels," *Appl. Phys. Lett.,* vol. 98, p. 041104, 2011.

[3] K. De Vos, J. Girones, T. Claes, Y. De Koninck, S. Popelka, E. Schacht, R. Baets, and P. Bienstman, "Multiplexed antibody detection with an array of silicon-on-insulator microring resonators," *IEEE Photonics Journal,* vol. 1, pp. 225-235, 2009.

[4] C. Lerma Arce, D. Witters, R. Puers, J. Lammertyn, and P. Bienstman, "Silicon photonic sensors incorporated in a digital microfluidic system," *Anal. Bioanal. Chem.,* vol. 404, pp. 2887-94, Dec 2012. doi: 10.1007/s00216-012-6319-6

[5] M. Y. Azab, M. Hameed, A. Heikal, S. Obayya, and M. Swillam, "Surface plasmon photonic crystal fiber biosensor for glucose monitoring," in *Applied Computational Electromagnetics Society Symposium-Italy (ACES), 2017 International*, 2017, pp. 1-2.

[6] L. Guo, J. A. Jackman, H.-H. Yang, P. Chen, N.-J. Cho, and D.-H. Kim, "Strategies for enhancing the sensitivity of plasmonic nanosensors," *Nano Today,* vol. 10, pp. 213-239, 2015. doi: 10.1016/j.nantod.2015.02.007

[7] A. Zaki, K. Kirah, and M. Swillam, "High Sensitivity Hybrid Plasmonic Rectangular Resonator for Gas Sensing Applications," in *Frontiers in Optics 2015*, San Jose, California, 2015, p. JW2A.2. doi: 10.1364/fio.2015.jw2a.2

[8] S. M. Sherif and M. A. Swillam, "Metal-less silicon plasmonic mid-infrared gas sensor," *Journal of Nanophotonics,* vol. 10, pp. 026025-026025, 2016. doi: 10.1117/1.jnp.10.026025

[9] A. O. Zaki, K. Kirah, and M. A. Swillam, "Integrated optical sensor using hybrid plasmonics for lab on chip applications," *Journal of Optics,* vol. 18, p. 085803, 2016.

[10] R. Kotb, Y. Ismail, and M. A. Swillam, "Integrated coupled multi-stage plasmonic resonator for on-chip sensing," in *Proc. SPIE 9126, Nanophotonics V*, 2014, p. 91263M. doi: 10.1117/12.2057541

[11] R. Gamal, Y. Ismail, and M. A. Swillam, "Optical biosensor based on a silicon nanowire ridge waveguide for lab on chip applications," *Journal of Optics,* vol. 17, p. 045802, 2015.

[12] J. Zhou, Y. Wang, C. Liao, B. Sun, J. He, G. Yin, S. Liu, Z. Li, G. Wang, X. Zhong, and J. Zhao, "Intensity modulated refractive index sensor based on optical fiber Michelson interferometer," *Sens. Actuators, B,* vol. 208, pp. 315-319, 2015. doi: http://dx.doi.org/10.1016/j.snb.2014.11.014

[13] A. Densmore, M. Vachon, D.-X. Xu, S. Janz, R. Ma, Y.-H. Li, G. Lopinski, A. Delâge, J. Lapointe, and C. Luebbert, "Silicon photonic wire biosensor array for multiplexed real-time and label-free molecular detection," *Opt. Lett.,* vol. 34, pp. 3598-3600, 2009.

[14] A. B. Ayoub, A. E.-R. Nader, M. Saad, Q. Gan, and M. Swillam, "Fiber-optic-based interferometric sensor," in *Proc. of SPIE Vol*, 2017, pp. 101101G-1.

[15] P. Dong, W. Qian, S. Liao, H. Liang, C.-C. Kung, N.-N. Feng, R. Shafiiha, J. Fong, D. Feng, and A. V. Krishnamoorthy, "Low loss shallow-ridge silicon waveguides," *Opt. Express,* vol. 18, pp. 14474-14479, 2010.

[16] J. F. Bauters, M. J. R. Heck, D. John, D. Dai, M.-C. Tien, J. S. Barton, A. Leinse, R. G. Heideman, D. J. Blumenthal, and J. E. Bowers, "Ultra-low-loss high-aspect-ratio Si3N4 waveguides," *Opt. Express,* vol. 19, pp. 3163-3174, 2011/02/14 2011. doi: 10.1364/oe.19.003163

[17] M.-C. Tien, J. F. Bauters, M. J. R. Heck, D. T. Spencer, D. J. Blumenthal, and J. E. Bowers, "Ultra-high quality factor planar Si3N4 ring resonators on Si substrates," *Opt. Express,* vol. 19, pp. 13551-13556, 2011/07/04 2011. doi: 10.1364/oe.19.013551

[18] D. Ding, M. J. A. de Dood, J. F. Bauters, M. J. R. Heck, J. E. Bowers, and D. Bouwmeester, "Fano resonances in a multimode waveguide coupled to a high-Q silicon nitride ring resonator," *Opt. Express,* vol. 22, pp. 6778-6790, 2014/03/24 2014. doi: 10.1364/oe.22.006778

[19] A. S. Abdeen, A. B. Ayoub, A. M. Attiya, and M. A. Swillam, "High efficiency compact Bragg sensor," in *Photonics North (PN), 2016*, 2016, pp. 1-1.

[20] L. B. Soldano and E. C. Pennings, "Optical multi-mode interference devices based on self-imaging: principles and applications," *J. Lightwave Technol.,* vol. 13, pp. 615-627, 1995.

[21] C. Gouveia, G. Chesini, C. M. Cordeiro, J. Baptista, and P. A. Jorge, "Simultaneous measurement of refractive index and temperature using multimode interference inside a high birefringence fiber loop mirror," *Sens. Actuators, B,* vol. 177, pp. 717-723, 2013.

[22] M. Burla, B. Crockett, L. Chrostowski, and J. Azaña, "Ultra-high Q multimode waveguide ring resonators for microwave photonics signal processing," in *2015 International Topical Meeting on Microwave Photonics (MWP)*, 2015, pp. 1-4. doi: 10.1109/mwp.2015.7356707

[23] M. Kumar, R. Dwivedi, and A. Kumar, "Multimode Interference Based Planar Optical Waveguide Biosensor," in *International Conference on Fibre Optics and Photonics*, 2014, p. S5A. 8.

[24] R. A. Rodriguez, R. Dominguez-Cruz, D. A. May-Arrioja, I. Matias-Maestro, F. Arregui, and C. Ruiz-Zamarreno, "Fiber optic refractometer based in multimode interference effects (MMI) using Indium Tin Oxide (ITO) coating," in *SENSORS, 2015 IEEE*, 2015, pp. 1-3. doi: 10.1109/icsens.2015.7370600

[25] A. Irace and G. Breglio, "All-silicon optical temperature sensor based on Multi-Mode Interference," *Opt. Express,* vol. 11, pp. 2807-2812, 2003/11/03 2003. doi: 10.1364/oe.11.002807

[26] Lumerical Solutions Inc. Available: http://www.lumerical.com/tcad-products/mode/

[27] G. M. Hale and M. R. Querry, "Optical Constants of Water in the 200-nm to 200-µm Wavelength Region," *Appl. Opt.,* vol. 12, pp. 555-563, 1973/03/01 1973. doi: 10.1364/ao.12.000555

CHAPTER 4. SEMICONDUCTOR PLASMONIC GAS SENSOR USING ON-CHIP INFRARED SPECTROSCOPY

This chapter was published in Applied Physics A with the following citation information and it will be reproduced here as is.

M. Y. Elsayed, Y. Ismail, and M. A. Swillam, "Semiconductor plasmonic gas sensor using on-chip infrared spectroscopy," *Applied Physics A,* vol. 123, p. 113, 2017.

ABSTRACT

In this chapter, we take a novel approach in optical sensing of gases. Gases have conventionally been optically sensed using refractive index, which is a non-ideal method because of the difficulty in differentiating gases with very similar refractive indices. Infrared absorption spectra on the other hand have characteristic peaks in the fingerprint region that allow identifying the analyte. Highly doped n-type Indium Arsenide (InAs) was used to design a plasmonic slot waveguide and a dispersion analysis was carried out using the finite element method to study the effect of dopant concentration and waveguide geometry on the guided modes. Finite difference time domain was used to simulate the transmission spectrum of the waveguide with air, methane and octane and the characteristic peaks in the IR spectra showed up strongly. This is a very promising versatile method that can sense any IR active gas.

4.1. Introduction

Integrated optical sensors conventionally detect refractive index change of surrounding medium. This has served well in liquids whether in seawater monitoring or biosensing applications [1-3]. When sensing gases in particular, the sensor is required to be very sensitive, and there have been much progress in this area recently, particularly making use of plasmonic resonators [4, 5], nanowires [6] or photonic crystals [7] to achieve sensitive sensors with a small footprint. However, optical sensing methods are still limited with respect to selectivity; while detecting that the analyte is not air, even if the sensor is able to detect a minute change in refractive index, it is sometimes impossible to identify the gas responsible for the refractive index change. For example, at 1.68 μm, CO_2 and CH_4 have refractive indices of 1.0004372 and 1.0004365, respectively [8, 9]. So even while detecting that there is some pollutant, there is no way to identify the sample.

Selectivity has been highlighted as a problem for gas sensors in general, whether optical or not, as discussed in great detail in [10]. To improve selectivity for optical sensors, one method is to functionalize the surface of the sensor such that it will be sensitive to a specific gas. For example, nanoporous aluminosilicate was deposited on a ring resonator sensor, causing refractive index changes to be more pronounced for an alkali gas such as NH_3 in comparison to an acidic gas such as CO_2 [11]. While this improves selectivity, it is not specific as it is only selective in relative to a subset of gases. A sensor that takes selectivity a step further and achieve specificity is highly desirous. Furthermore, this method doesn't support real-time or label-free features, which are two of the most important advantages of optical sensing methods [10], dictating that a sensor with the correct functionalization has to be designed for each gas required.

The objective of this work is to design an integrated general purpose label-free sensor. The generality means that the sensor can be used for a wide range of gases with high specificity.

Infrared spectroscopy offers a rigorous label-free method to identify compounds based on the absorbance properties of specific bonds. IR spectroscopy is considered an elaborate method and is generally used in advanced research facilities. Miniaturizing IR spectroscopy to chip level will lead to more ubiquitous use of IR spectroscopy as one technique employable in a variety of applications, from environmental monitoring, investigating leaky oil and gas wells to diagnostics and quality control.

The wavelengths of interest are in the mid infrared, mostly around 3 to 10 μm. For example, an absorbance peak around 5.8 μm corresponds to a C=O bond stretching while absorbance peaks around 6.8 μm correspond to C-H bond bending. It is also possible to distinguish between different isomers of the same compound through the fingerprint region, generally from 6.5 μm to 10 μm. In this region, different bonds absorb the incoming energy through different mechanisms (e.g. stretching vs rotating). The sensing mechanism based on IR spectroscopy depends on characteristic peaks that collectively act as a signature for each gas.

Sensing in IR has been demonstrated using localized surface plasmon resonances (LSPR) [12, 13]. Localized surface plasmons are collective oscillations of electrons that remain localized on a small area on the interface between a metal and an insulator and they usually occur with particles smaller than the wavelength used for excitation. These nanoparticles can be designed such that the oscillations are strongest at specific wavelengths; i.e. they exhibit resonance. The resonant frequency is very sensitive to small changes in the refractive index of surrounding medium, and that is why LSPRs have been used in

sensing applications, with silver and gold being popular choices for the visible spectrum. More recently, doped semiconductors have been explored because of the potential to engineer the material properties to the application required; in particular extending the region of operation to the Infrared. Propagating surface plasmon polaritons (SPPs) have not yet been explored in the MIR.

Like LSPRs, SPPs are also collective oscillations of electrons but these oscillations propagate along the interface between the metal and insulator. Because they propagate, SPPs provide more possibilities with respect to light manipulation. SPPs can be exploited to direct light in MIR while staying at the submicron scale. The plasmonic slot waveguide fits well in this application because of the air gap, making it amenable to sensing applications due to the high overlap between the electric field and sensing medium. The plasmonic slot waveguide is easy to integrate with on-chip sources and detectors as coupling to and from the waveguide is feasible. In addition, sources and detectors working in the MIR are made from III-V semiconductors [14].

Silicon plasmonic slot waveguides have been previously explored for mid infrared applications [15], and while it has obvious advantages due to it being a standard material used in CMOS processing, there are limitations that can be overcome if other materials are explored. A very large doping concentration, exceeding 10^{21} cm^{-3} is required to achieve a plasma frequency in the mid infrared range [15]. More importantly, the transmission spectrum of silicon contains peaks over the range 5 to 10 μm, making it unsuitable for detection in this range [16]. Indium Arsenide (InAs) has been identified as a material that requires less doping concentration to function in the mid infrared [17] and it has a smooth transmission spectrum with no peaks in the mid infrared region [16].Indium Arsenide (InAs) detectors in particular have a high sensitivity in the MIR compared to other semiconductors[14]. InAs-based sources working in the mid infrared have been demonstrated [14, 18].

In this paper, we start by describing the material modeling approach then characterizing the plasmonic slot waveguide and studying the effect of changing the size of the gap and dopant concentration. In particular, we will highlight how the plasmonic slot waveguide can be engineered to work in different wavelength ranges. We then demonstrate the plasmonic slot waveguide as a gas sensor.

4.2. Methods

4.2.1. Numerical Simulations

Mode profiles for the plasmonic slot waveguide given in Figure 4.1 (a) were determined and dispersion analysis was performed using Finite Element Method using COMSOL Multiphysics with MATLAB. Perfectly

Matched Layer (PML) boundary conditions were used. Adaptive mesh refinement feature in COMSOL was used, and the mesh convergence test is shown in Figure 4.1 (b). The final used meshing used a mesh size of 1 nm in the gap as shown in Figure 4.1 (c, d). To ensure correct PML behavior, a large simulation region was used to ensure the boundaries are far from the slot. Due to working in infrared with wavelengths reaching 10 um, the Doped InAs arms extended 20 um to the left and right of the slot. Livelink was used between the two programs for semi-automated mode tracking during parametric sweeps. Finite Difference Time Domain (FDTD) using Lumerical was used to simulate the waveguide's transmission spectrum with different gases.

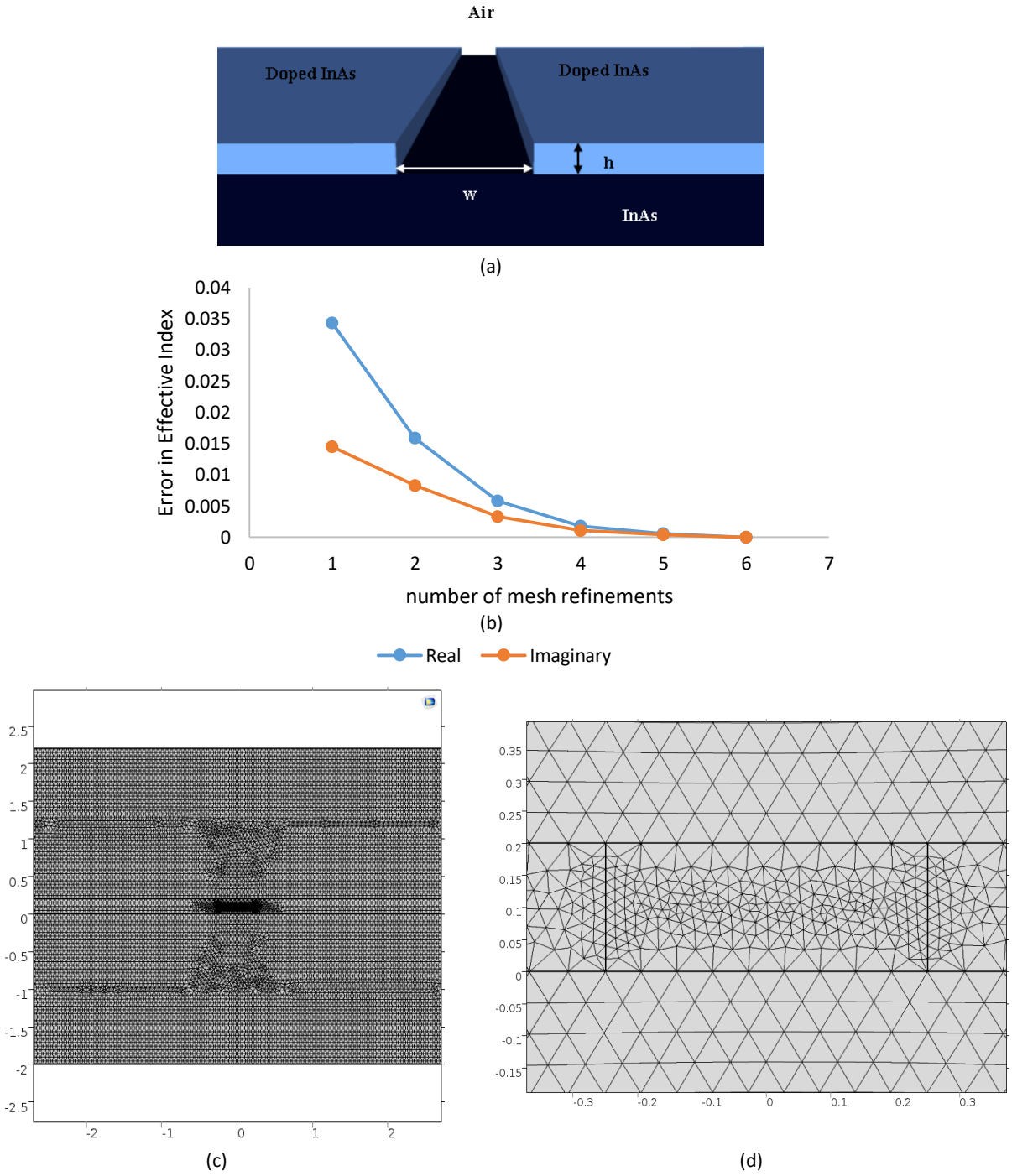

Figure 4.1. (a) n-type InAs plasmonic slot waveguide, (b) COMSOL Mesh convergence test using adaptive mesh refinement, (c) Meshing used for all the results, (d) zoom in the gap region showing minimum mesh element size 1 nm and maximum mesh element size 20 nm.

4.2.2. Material Modeling

4.2.2.1. Doped Indium Arsenide

For highly doped semi-conductor, we used the Drude model in equation 4.1 to obtain a relation between the permittivity ε and the angular frequency ω as a function of doping, as shown in Figure 4.2 (c). This model is for n-type InAs doped with Silicon.

$$\varepsilon(\omega) = \varepsilon_s\left(1 - \frac{\omega_p^2}{\omega^2 + \Gamma^2}\right) + i\varepsilon_s\frac{\Gamma \cdot \omega_p^2}{\omega\left(\omega^2 + \Gamma^2\right)}, \tag{4.1}$$

where ε_s is the relative permittivity of undoped InAs at low frequency, Γ is the scattering rate and ω_p is the plasma frequency, given by equation 4.2

$$\omega_p^2 = \frac{ne^2}{\varepsilon_s\varepsilon_0 m^*}, \tag{4.2}$$

where n is the carrier concentration, assumed to be equal to the dopant concentration N, e is the elementary charge, ε_0 is the permittivity of free space and $m^*$is the effective mass.

The work in this thesis uses novel materials for which the Lorentz and Drude-Lorentz models cannot be derived due to the lack of available information on InAs, and thus only the Drude model can be used. Furthermore, the study is a proof-of-concept one where we aim to understand the device behavior qualitatively and thus the limitations of the Drude model are not significant.

As demonstrated experimentally, Γ and m^* are both functions of N [12]. We exploited the fact that the semiconductor band gap changes as a function of dopant concentration using the empirical relation given in equation 4.3 [19]

$$\Delta \mathrm{E}_g = \mathrm{A} \cdot \mathrm{N}^{1/3} + \mathrm{B} \cdot \mathrm{N}^{1/4} + \mathrm{C} \cdot \mathrm{N}^{1/2}, \tag{4.3}$$

with A, B and C for InAs determined to be 14×10^{-9}, 1.97×10^{-7} and, 57.9×10^{-12} respectively [19]. This band gap is then related to the effective mass through the relation given in equation 4.4 [12], yielding Figure 4.2 (a).

$$\Delta \mathrm{E}_g = \left(\frac{h^2}{2m^*\mathrm{N}}\right)\left(\frac{3\mathrm{N}}{8\pi}\right)^{2/3}, \tag{4.4}$$

where *h* is Plank's constant.

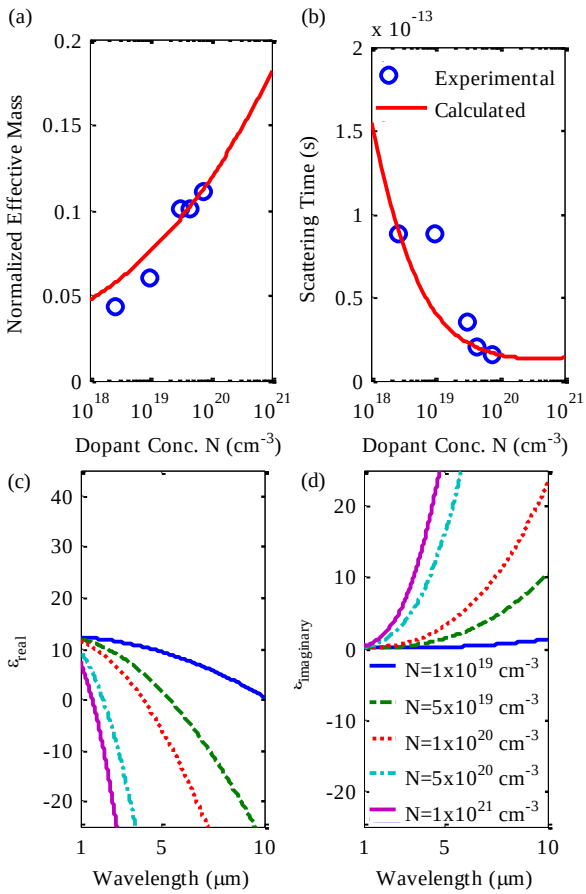

Figure 4.2.Empirical models of (a) effective mass versus dopant concentration, (b) scattering time versus dopant concentration. Experimental data for n-type InAs doped with Silicon [12]. Drude model shown in (c) and (d).

Scattering rate as a function of doping is shown in Figure 4.2 (b). We used the empirical model in equation 4.5 [20] to obtain the hall mobility as a function of doping while optimizing the parameters to fit the experimental data given in [12] as in Table 4.1. The hall factor [21] was found to be 1 in InAs for N>1x10^{19} cm^{-3}.

$$\mu(N) = \mu_{min} + \frac{\mu_{max}\left(\frac{300}{T}\right)^{\theta_1} - \mu_{min}}{1 + \left(\frac{N}{N_{eff}\left(\frac{T}{300}\right)^{\theta_2}}\right)^{\lambda}} \qquad 4.5$$

Finally, we can relate the drift mobility μ to the scattering time τ through $\mu = e\tau/m^*$. From those parameters, we have the Drude model for n-type InAs highly doped with Silicon as shown in Figure 4.2 (c).

We can deduce from Figure 4.2 (c) the advantages of working with InAs as the plasma wavelength is low in comparison with other semiconductors with the same dopant concentration, as already concluded in previous reports [17], giving access to plasmonic devices in the mid infrared range.

Table 4.1. Parameters for mobility model for doped InAs.

PARAMETER	VALUE
$\boldsymbol{\mu_{min}}$	80 $cm^2/V\ s$
$\boldsymbol{\mu_{max}}$	34500 $cm^2/V\ s$
$\boldsymbol{N_{eff}}$	$1.8x10^{17}\ cm^{-3}$
$\boldsymbol{\lambda}$	0.86
$\boldsymbol{\theta_1}$	1.57
$\boldsymbol{\theta_2}$	3.0

4.2.2.2. Analytes

Absorption data is readily available for many analytes of interest in the mid-infrared region. The complex refractive index can then be estimated as demonstrated in [22]. Absorption data for Methane and Octane were obtained from the NIST database [23]. The extinction coefficient, k, was obtained from absorption, α, through equation 4.6.

$$\alpha(\lambda) = \frac{4\pi k(\lambda)}{\lambda}. \qquad 4.6$$

Refractive index, n, was estimated for each wavelength λ_0 from k using the kramers-kronig relation in equation 4.7 following the implementation in [24], where $n(\lambda_1)$ is a known refractive index of the analyte at wavelength λ_1 and P is the Cauchy principal value of the integral.

$$n(\lambda_0) = n(\lambda_1) + P\left[\frac{2\left({\lambda_1}^2 - {\lambda_0}^2\right)}{\pi}\int_0^{\infty} \frac{\lambda k(\lambda)\, d\lambda}{\left({\lambda_0}^2 - \lambda^2\right)\left({\lambda_1}^2 - \lambda^2\right)}\right], \qquad 4.7$$

4.3. Results and Discussion

4.3.1. Dispersion Analysis

We studied the guided plasmonic modes supported by the plasmonic slot waveguide depicted in Figure 4.1. Figure 4.3 demonstrates that the operating bandwidth of the waveguide can be engineered by changing the dopant concentration; a dopant concentration of $N=1\times10^{20}\ cm^{-3}$ yields a plasmonic slot waveguide operating in the 6 to 10 µm wavelength window while a higher dopant concentration $N=1x10^{21}\ cm^{-3}$ gives a plasmonic slot waveguide operating at shorter wavelengths, from 2.7 to 6 µm. This is due to

the plasma frequency's dependence on carrier concentration as highlighted earlier in Figure 4.2 (c); at $N=1\times10^{20}$ cm^{-3}, the plasma wavelength is 4.24 µm while it is 1.65 µm at $N = 1\times10^{21}$ cm^{-3}, and it is well known that there is a forbidden region near the plasma frequency where the losses are too high to support guided modes [25].

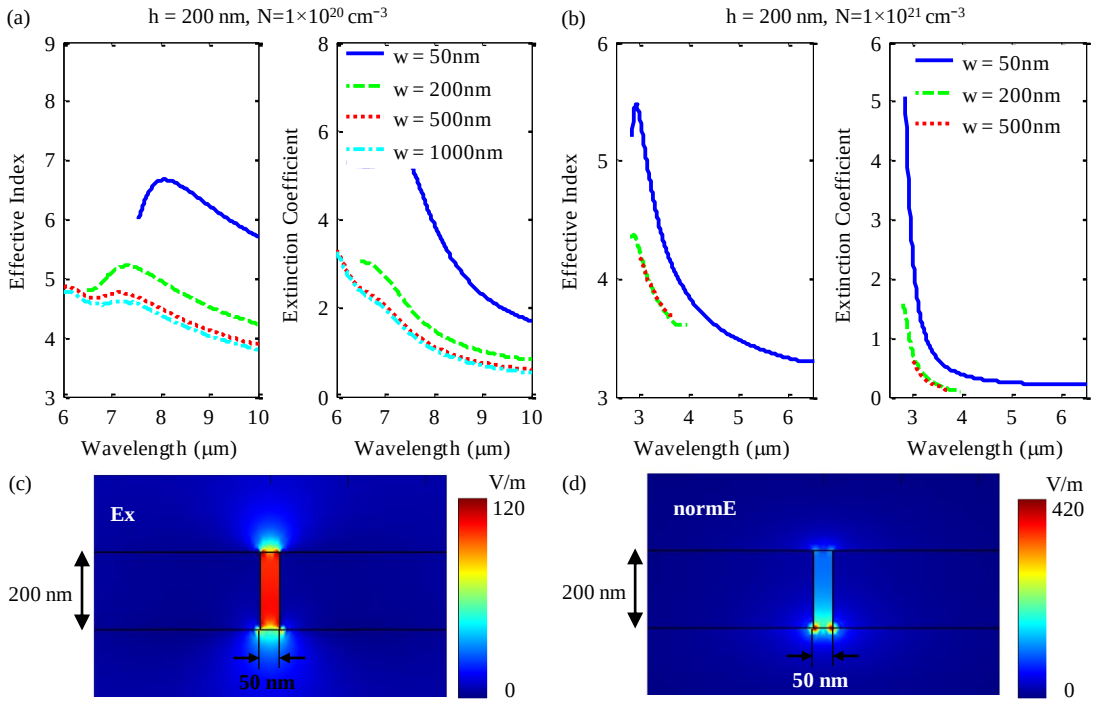

Figure 4.3. Dispersion relation for different slot widths for (a) $N=10^{20}$ cm^{-3}, (b) $N=10^{21}$ cm^{-3} (c) Mode profile for $N=10^{20}$ cm^{-3} at 8 µm, effective index = 6.6562+3.9123i, x component of electric field, (d) average electric field intensity (all directions).

The dispersion curves show that the effective index peaks at a specific wavelength, λ_{spp} [26]. The value and position of λ_{spp} is clearly affected by the slot gap width w. At wavelengths lower than λ_{spp} but higher than the plasma wavelength λ_{sp}, the modes have a negative group velocity. Also, that peak is much broader with lower dopant concentration (Figure 4.3 (a)) than with higher dopant concentration (Figure 4.3 (d)). Moreover, after a certain width, increasing the width further has no observable effect on the dispersion curve evident from the similarity in the dispersion curves for the 500 nm and 1000 nm widths.

We tuned the InAs dopant concentration to get a bandwidth around an interesting mode of operation for IR spectroscopy; Figure 4.4 shows the dispersion relation for the plasmonic slot waveguide with n-type InAs with $N=2.2\times10^{20}$ cm^{-3}. The dispersion curves don't change much when the gap width *w* is increased beyond 500 nm. Figure 4.4 (b) shows the effect of the height on the modes. Increasing the height of the

doped InAs layer *h* acts to decrease both real and imaginary curves down without any noticeable shift in λ_{spp}.

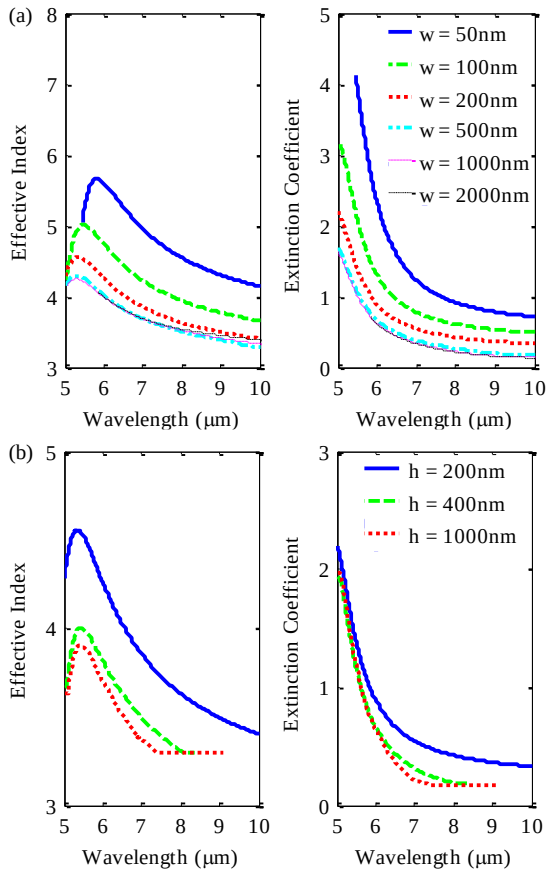

Figure 4.4. Dispersion relations for dopant concentration N = 2.2×10^{20} cm^{-3} (a) constant height 200 nm, changing width, (b) constant width 200 nm, changing height.

Figure 4.5 compares two slots with the same area but with different geometries. The effective index is strongly affected by the interface itself, which is obviously different whether the gap is wide or tall. The wide gap has an InAs/air interface of 200 nm + 200 nm for each side, for a total of 400 nm, while the tall gap has a total InAs/air interface of 2000 nm. Thus, the effective index is affected by the interface. On the other hand, the extinction coefficient remains the same for different geometries of the same cross sectional area.

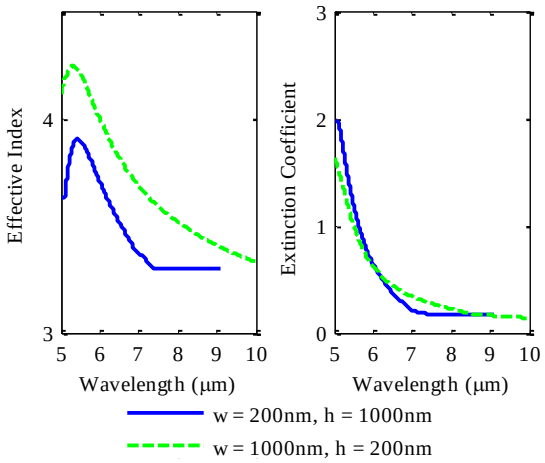

Figure 4.5. Dispersion analysis of different gap geometries for the same area. Blue solid line refers to InAs/air interface of 400 nm in total while the green dashed line refers to InAs/air interface of 2000 nm in total.

Dispersion analysis shows that the plasmonic slot waveguide range of operation can be engineered by controlling the dopant concentration in InAs. More accurately though, it is the carrier concentration responsible for modifying the range of operation. Thus, it is possible to design a single device whose range of operation is on-line tunable by controlling the carrier concentration through any of a variety of methods such as charge injection, p/n junction, optical pumping, etc.

4.3.2. Transmission Analysis and suitability as a sensor for hydrocarbons

Finite difference time domain (FDTD) method was used to study the transmission properties of the waveguide and how sensitive it is to the material in the gap. Figure 4.6 shows the transmission with a length of 1 μm (transmission time 5000 fs). For methane, the curve is easily distinguishable from that of air, but Octane's peaks are not too obvious. The sensitivity can easily be increased by increasing the waveguide length. In Figure 4.7, the signals are subtracted from that of air when used as a reference and normalized. In this case, the peaks that correspond to the IR absorption peaks are easy to identify and different materials can easily be distinguished using this method. FDTD analysis of a couple of gases was performed just as proof of concept, but the mode of operation that we described here is actually applicable to all IR-active materials.

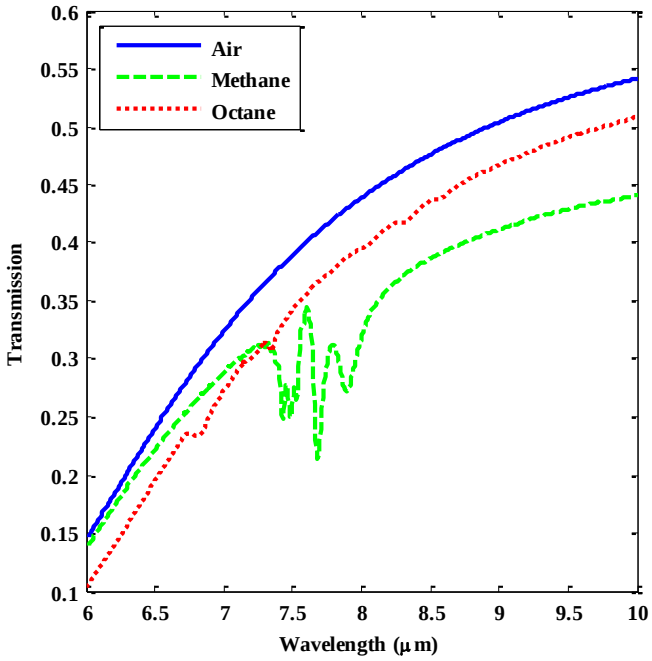

Figure 4.6. (a) Transmission spectrum for waveguide when filled with air (solid line), methane (dashed line) or octane (dotted line).

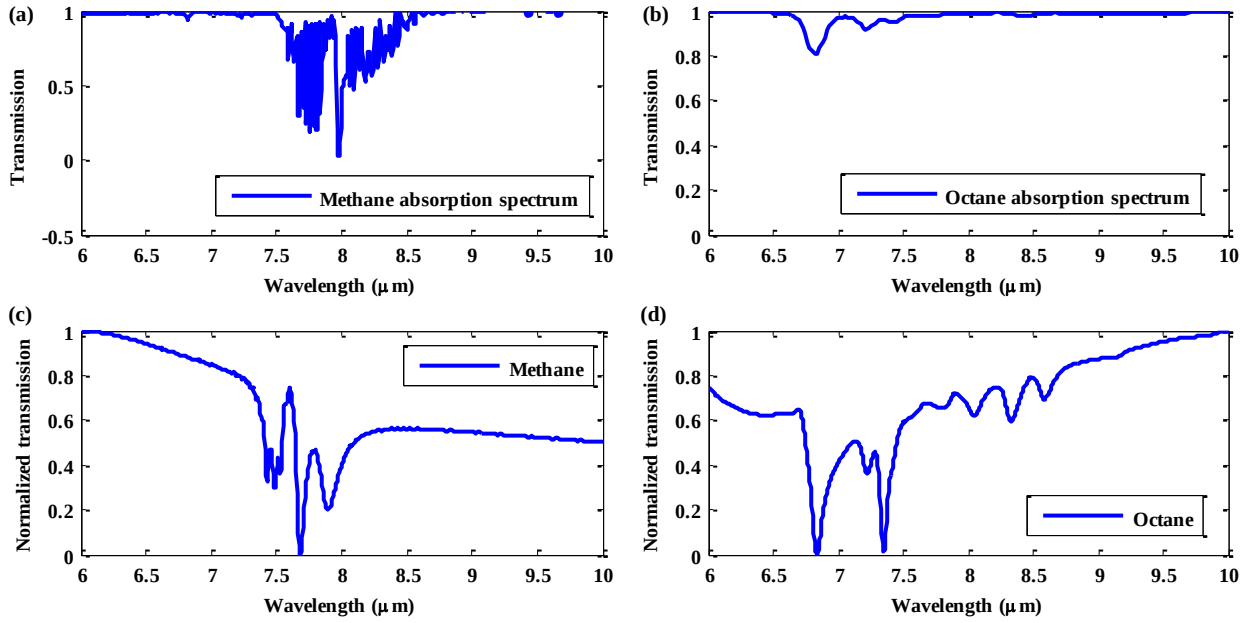

Figure 4.7. Absorption spectra as obtained from the NIST database [23] for (a) methane and (b) octane. The transmission spectra for methane (c) and octane (d) shown in Figure 4.6 was subtracted from that of air and normalized.

4.4. Conclusions

By engineering the plasmonic slot waveguide geometry and semiconductor dopant concentration, we were able to tune the response of the sensor to a wavelength range of interest, namely the mid infrared.

We have made use of characteristic infrared absorption peaks in the fingerprint region of the IR spectrum in methane and octane for integrated optical sensing using the plasmonic slot waveguide resulting in an ultracompact design. The plasmonic slot waveguide is designed using materials and processes that have been used to make on chip sources and detectors, so a fully integrated system is feasible. This approach can be easily adapted for a wide variety of IR-active materials.

4.5. References

[1] J. S. M. Rusby, "Measurements of the refractive index of sea water relative to copenhagen standard sea water," *Deep Sea Research and Oceanographic Abstracts,* vol. 14, pp. 427-IN14, 1967/08/01 1967.

[2] F. Hideki, A. Tomohiro, and T. Shuji, "High-sensitivity fiber-optic refractive index sensor based on multimode interference using small-core single-mode fiber for biosensing," *Japanese Journal of Applied Physics,* vol. 53, p. 04EL08, 2014.

[3] J. Zhou, Y. Wang, C. Liao, B. Sun, J. He, G. Yin, S. Liu, Z. Li, G. Wang, X. Zhong, and J. Zhao, "Intensity modulated refractive index sensor based on optical fiber Michelson interferometer," *Sensors and Actuators B: Chemical,* vol. 208, pp. 315-319, 2015.

[4] S. E. El-Zohary, A. Azzazi, H. Okamoto, T. Okamoto, M. Haraguchi, and M. A. Swillam, "Design optimization and fabrication of plasmonic nano sensor," 2014, pp. 89940V-89940V-6.

[5] R. Kotb, Y. Ismail, and M. A. Swillam, "Integrated coupled multi-stage plasmonic resonator for on-chip sensing," in *Proc. SPIE 9126, Nanophotonics V*, 2014, p. 91263M.

[6] R. Gamal, Y. Ismail, and M. A. Swillam, "Optical biosensor based on a silicon nanowire ridge waveguide for lab on chip applications," *Journal of Optics,* vol. 17, p. 045802, 2015.

[7] X. Wang, N. Lu, J. Zhu, and G. Jin, "An ultracompact refractive index gas-sensor based on photonic crystal microcavity," 2007, p. 68310D.

[8] A. Bideau-Mehu, Y. Guern, R. Abjean, and A. Johannin-Gilles, "Interferometric determination of the refractive index of carbon dioxide in the ultraviolet region," *Optics Communications,* vol. 9, pp. 432-434, 1973/12/01 1973.

[9] R. Rollefson and R. Havens, "Index of Refraction of Methane in the Infra-Red and the Dipole Moment of the CH Bond," *Physical Review,* vol. 57, pp. 710-717, 1940.

[10] X. Liu, S. Cheng, H. Liu, S. Hu, D. Zhang, and H. Ning, "A survey on gas sensing technology," *Sensors (Basel),* vol. 12, pp. 9635-65, 2012.

[11] N. A. Yebo, S. P. Sree, E. Levrau, C. Detavernier, Z. Hens, J. A. Martens, and R. Baets, "Selective and reversible ammonia gas detection with nanoporous film functionalized silicon photonic micro-ring resonator," *Optics Express,* vol. 20, pp. 11855-11862, 2012/05/21 2012.

[12] S. Law, D. C. Adams, A. M. Taylor, and D. Wasserman, "Mid-infrared designer metals," *Opt Express,* vol. 20, pp. 12155-65, May 21 2012.

[13] S. Law, L. Yu, A. Rosenberg, and D. Wasserman, "All-Semiconductor Plasmonic Nanoantennas for Infrared Sensing," *Nano Letters,* vol. 13, pp. 4569-4574, 2013/09/11 2013.

[14] A. G. Milnes and A. Y. Polyakov, "Indium arsenide: a semiconductor for high speed and electro-optical devices," *Materials Science and Engineering: B,* vol. 18, pp. 237-259, 1993/04/15 1993.

[15] R. Gamal, Y. Ismail, and M. A. Swillam, "Silicon Waveguides at the Mid-Infrared Range," *Journal of Lightwave Technology,* vol. 33, pp. 3207 - 3214, 2015.

[16] T. R. Harris, "Optical properties of Si, Ge, GaAs, GaSb, InAs, and InP at elevated temperatures," Master, Air Force Institute of Technology, 2010.

[17] D. Li and C. Z. Ning, "All-semiconductor active plasmonic system in mid-infrared wavelengths," *Optics Express,* vol. 19, pp. 14594-14603, 2011/07/18 2011.

[18] N. V. Zotova, N. D. Il'inskaya, S. A. Karandashev, B. A. Matveev, M. A. Remennyi, and N. M. Stus', "Sources of spontaneous emission based on indium arsenide," *Semiconductors (Translation of Fizika i Tekhnika Poluprovodnikov (Sankt-Peterburg)),* vol. 42, pp. 625-641, 2008.

[19] S. C. Jain, J. M. McGregor, and D. J. Roulston, "Band-gap narrowing in novel III-V semiconductors," *Journal of Applied Physics,* vol. 68, pp. 3747-3749, 1990.

[20] M. Sotoodeh, A. H. Khalid, and A. A. Rezazadeh, "Empirical low-field mobility model for III–V compounds applicable in device simulation codes," *Journal of Applied Physics,* vol. 87, pp. 2890-2900, 2000.

[21] R. S. Popovic, *Hall Effect Devices, Second Edition*: CRC Press, 2003.

[22] G. M. Hale and M. R. Querry, "Optical Constants of Water in the 200-nm to 200-µm Wavelength Region," *Applied Optics,* vol. 12, pp. 555-563, 1973/03/01 1973.

[23] I. Coblentz Society, "Evaluated Infrared Reference Spectra," in *NIST Chemistry WebBook, NIST Standard Reference Database Number 69*, P. J. L. a. W. G. Mallard, Ed., ed Gaithersburg MD, 20899: National Institute of Standards and Technology.

[24] J. J. S. V. Lucarini, K.-E. Peiponen, E.M. Vartiainen, *Kramers-Kronig Relations in Optical Materials Research* vol. 110. Berlin, Germany: Springer, 2005.

[25] F. Kong, B.-I. Wu, H. Chen, and J. A. Kong, "Surface plasmon mode analysis of nanoscale metallic rectangular waveguide," *Optics Express,* vol. 15, pp. 12331-12337, 2007/09/17 2007.

[26] M. A. Swillam and A. S. Helmy, "Analysis and applications of 3D rectangular metallic waveguides," *Optics Express,* vol. 18, pp. 19831-19843, 2010/09/13 2010.

CHAPTER 5. SILICON-BASED SERS SUBSTRATES FABRICATED BY ELECTROLESS ETCHING

This chapter was published in Journal of Lightwave Technology with the following citation information and it will be reproduced here as is.

M. Y. Elsayed, A. M. Gouda, Y. Ismail, and M. A. Swillam, "Silicon-Based SERS Substrates Fabricated by Electroless Etching," *J. Lightwave Technol.,* vol. 35, pp. 3075-3081, 2017. doi: 10.1109/jlt.2017.2707476

ABSTRACT

Surface enhanced Raman scattering has recently been proposed as a label free sensing method for diagnostic applications. Raman scattering is an excellent analysis tool because a wealth of information can be obtained using a single measurement, however the weak signal has made it unsuitable for detecting low concentrations of analytes. Using plasmonic nanostructures to create SERS substrates, the Raman signal can be amplified by several orders of magnitude, but SERS substrates have been complicated to fabricate. Here we report low cost silicon substrates based on simple fabrication method of silver nanoparticles and silicon nanowires decorated with these nanoparticles for use as a convenient practical platform for SERS-active substrates. In addition, the placement of silver nanoparticles on silicon nanowires allowed the auto-aligning of the hot spots such that low cost Raman systems with normal incident laser can be used. These substrates have the ability to detect wide range of concentrations of pyridine, as low as 10^{-11} M. An enhancement factor of around 6 to 8×10^5 was observed for silver nanoparticles alone. By depositing the same nanoparticles on silicon nanowires, the enhancement factor jumped by orders of magnitude to 10^{11}.

5.1. Introduction

Surface enhanced Raman scattering (SERS) allows using the optical signatures for label-free specific sensing by improving the sensitivity and allowing the detection of low concentrations. Surface enhanced Raman scattering (SERS) is caused by surface plasmons on metallic nanostructures enhancing the electric field [1].

The Raman signal is enhanced due to the amplified electric [1]. Since the discovery of the SERS effect, many SERS substrates were reported such as roughened silver electrodes, metal films [2] and silver and gold nanoparticles and sols[3]. SERS substrates can be classified into two main categories: metal nanoparticle colloids and nanostructures on planar substrates.

Metal nanoparticle colloids are easy to fabricate in a low cost method but it is unstable and the colloids can easily be contaminated if ultra-pure chemicals are not used in preparation [4]. Contaminants can

superimpose the SERS spectra of the analyte. Different shapes of metal nanostructures were reported experimentally such as nanotriangles [5], nanocubes [6, 7], grated nanocones [8], nanorods [6, 9], nanostars [9, 10] and nanodog-bone shape [6], and were able to reach enhancement factor on the order of 10^5 to 10^6 [8, 9] and even up to 10^9 [6]which is higher than metallic nanospheres because sharp nanostructures induce an antenna-like effect that amplifies the electric field greatly. However, reproducibility is an issue due to the difficulty in controlling the particle size and distribution [11]. Core/shell nanoparticles have also been explored with enhancement factors reaching 10^3 [12]. Nanostructures on planar substrates can further be categorized by bottom-up and top-down fabrication methods. SERS substrates prepared by bottom-up techniques have shown good stability and reproducibility by offering good control on size and demonstrated enhancement factors on the order of 10^5 to 10^7 [13-16]. Nanostructures prepared using lithographic techniques can prepare highly ordered metallic nanostructures with great accuracy in shape, size, and spacing between them. This fabrication method includes electron / ion beam lithography and nanoimprint lithography and were able to show enhancement factors on the order of 10^5 [17].

Despite these advancements in SERS substrates, we have yet to see ubiquitous use of SERS substrate for sensing applications due to the complicated fabrication methods with high cost and low yield. One solution is to metallize silicon nanostructures. Patterning silicon is very mature due to its extensive use in the electronics industry. In addition, silicon offers a strong and stable platform for metal nanoparticles fabrication as it acts as a reducing agent. The low zeta potential of metal nanoparticles formed on Silicon – less than -30 mV – decreases the interaction with molecules adsorbed on their surface for improved stability, robustness and reproducibility [18, 19]. Metallized Silicon nanostructures were previously used as effective SERS substrates in different applications [20-23]. The large surface area to volume ration allows exploiting surface modifications. In [20], the analyte is trapped in the hot spots and surface plasmons are confined if the spacing between the nanostructures is smaller than the excitation wavelength. High aspect ratio nanostructures enhances light scattering inside the material, increasing light-matter interaction due to the high surface area [22], improving SERS signal sensitivity.

Silicon nanowires (SiNW) in particular are gaining popularity in a variety of applications [24-27]. SiNW fabrication methods include Oxide assisted growth (OAG), vapor–liquid–solid (VLS)[28, 29], chemical vapor deposition (CVD) [24], molecular beam epitaxy[30], laser ablation[31], and thermal evaporation[32]. However, these methods are time consuming, costly and complicated for mass production. Top-down approaches are more common place in industry, in particular lithography and reactive ion etching [30, 33]. Nano-scale lithographic methods however are most suited for modest size of few mm^2 and cannot be used for large scale production. Electroless metal wet chemical etching

(EMWCE) is a solution-based process that is simple and low cost and has been demonstrated to quickly produce vertical highly dense crystalline SiNWs over a large area mostly for photovoltaic applications [34-41].

We report a simple low cost large area top-down fabrication approach with a good control over the dimensions. We start with single step etching and then decorate the SiNWs with silver nanoparticles using lithography-free and equipment-free method. Our fabrication method conveniently places the nanoparticles such that the hot spots are auto-aligned for best enhancement using normal incidence. As such, this substrate is useable with low cost Raman systems. We previously reported similar structures with modest enhancement factors of 20 to 40 with reduced graphene oxide [42]. With further optimizations, we report much stronger enhancement with pyridine, reaching 10^{11}.

5.2. Methods

5.2.1. Design Methodology

Finite Difference Time Domain (FDTD) simulations were used to predict the enhancement factor of different substrates. A 3D commercial FDTD Maxwell's equation solver [43] was used to study the electric field amplification at different locations. The material definitions of silicon and silver are based on curve fitting to the data of Palik [44] and Johnson and Christy [45], respectively. A simulation time of 40 fs was needed to observe the electric field amplification with dt = 0.00017 fs, i.e. over 200,000 time steps were required and the computation time using 4 cores typically took 18 to 24 hours. Due to the spherical shape, very fine meshing was needed and the mesh size was 0.1 nm at the hot spots. Source was total-field scattered-field which is a useful analytical tool in separating the scattered field from the incident field.

5.2.2. Fabrication

Silicon nanowires and silver nanoparticles can both be synthesized using electroless deposition. Silicon is a strong reducing reagent for metal ions, therefore it is possible to deposit nanoparticles directly on silicon substrate or silicon nanowires by redox displacement reaction using $AgNO_3$ and HF. $AgNO_3$ concentration and reaction temperature determine the redox reaction rate and the shape of silver structure. The role of HF is to remove the oxide layer which would otherwise inhibit the reaction by barricading charge transfer [36].

5.2.2.1. Silicon Nanowires

SiNWs were fabricated through single step catalytic electroless chemical etching using n-type Si (1 to 10 Ωcm resistivity, 650 to 700 µm thickness). The mechanism was discussed in details in our previous work involving solar cell applications [46]. For silicon nanowire formation, elevated temperature and

concentrations of $AgNO_3$ and HF are used, causing the formation of silver dendritic structures inside the silicon. Si squares were dipped in the etchant solution of $AgNO_3$ (5mM) and HF (3M) at 60 – 80°C using a water bath for 30 to 60 minutes. Silver dendritic structures formed during the etching process were removed using HNO_3 for 1 minute, leaving behind nanowires as shown in Figure 5.1 (a). Longer nanowires were found to bunch up due to capillary forces pulling them as the water between them is drying. In fact, this effect was previously exploited for SERS to reduce the spacing between metal nanoparticles on silicon nanowires [20]. We found that these capillary forces were very powerful for the longer nanowires prepared by dipping in the etchant solution for >45 minutes, causing aggregation and leading to effectively larger nanowires as shown in Figure 5.1 (d).

5.2.2.2. Silver Nanoparticles

For AgNP formation, moderately low concentration and temperature are used such that the silver structures remain superficial and do not penetrate deep into the silicon. Si squares were dipped in the deposition solution of $AgNO_3$ (0.5mM) and HF (0.14M) at 11°C for 2 to 5 minutes, yielding the silver nanoparticles (AgNPs) shown in Figure 5.1 (b).

5.2.2.3. Silicon nanowires decorated with silver nanoparticles

Figure 5.1 (c) shows the SiNWs that were decorated with AgNPs by dipping them in $AgNO_3$ and HF using the same conditions for AgNPs.

The size distributions of the different nanostructures are shown in Figure 5.1 (d) – (f) and are summarized in Table 5.1, where incubation time refers to either etching time (when forming SiNWs) or deposition time (when forming AgNPs). An interesting observation is the different nanoparticle diameter when grown on bare silicon compared with those grown on silicon nanowires. On a bare surface, there are a multitude of nucleation sites, so many particles form and then grow with time. On silicon nanowires, only the tip of the nanowire acts as a nucleation site, so there are a small number of nucleation sites. The number of nanoparticles produced is therefore much less. However, the same amount of reactants is present in solution, so the same amount of silver is produced in the synthesis process, thus the particles are larger. Additionally, nanoparticle growth rate is different on nanowire as compared to on bare silicon. On bare silicon, reactants reach the nucleation site from the top only, so the rate of particle growth is low. In nanowire, reactants can reach the nanoparticle from all direction, so the rate of particle growth is higher.

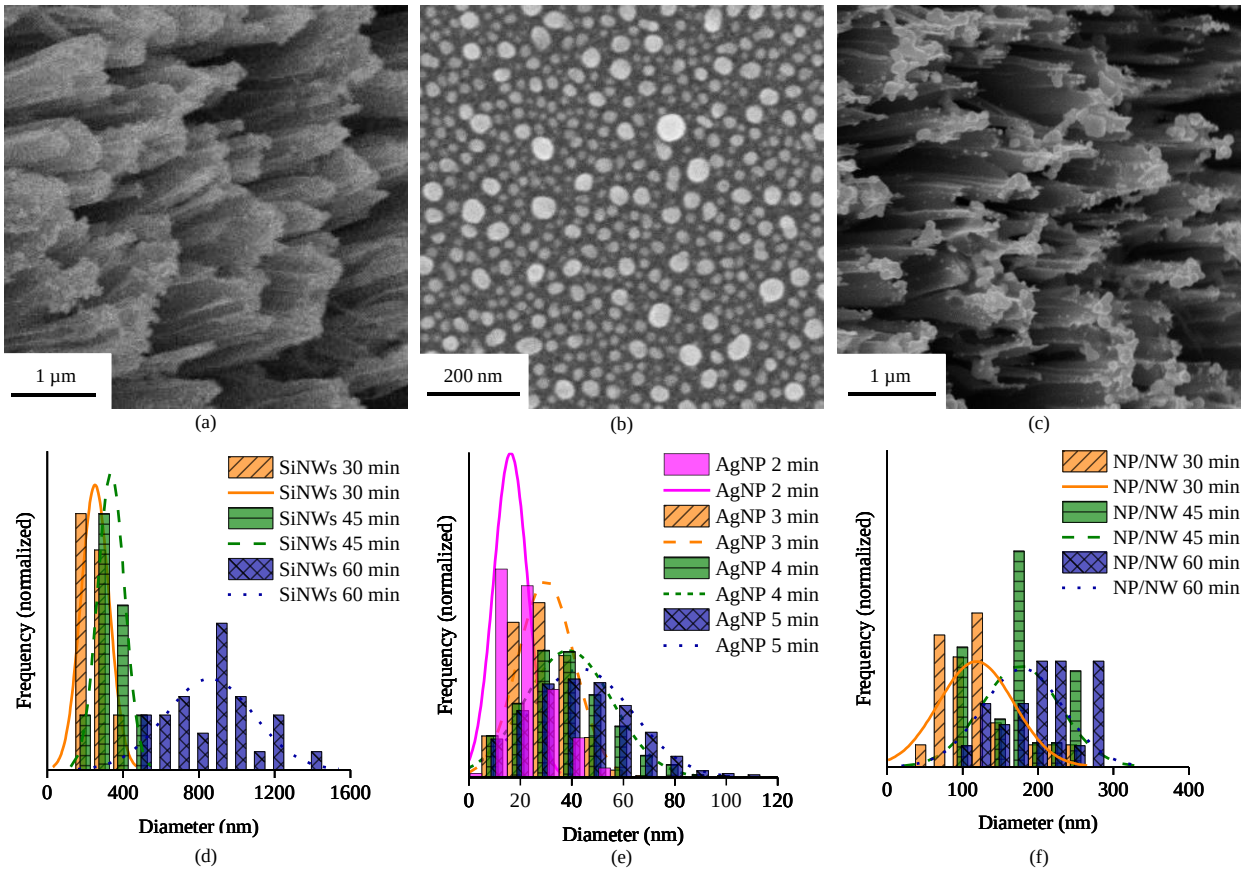

Figure 5.1. Fabricated nanostructures. (a) 45° tilted SEM image of silicon nanowires prepared with 45 minutes incubation time. (b) Top view SEM image of silver nanoparticles prepared with 2 minutes incubation time (c) 45° tilted SEM image of silver nanoparticle-decorated silicon nanowires prepared with 30 minutes incubation time for silicon nanowires followed by 5 minutes incubation time for silver nanoparticles. Size distribution of (d) silicon nanowires diameters, (e) silver nanoparticles, and (f) diameters of silver nanoparticles that are decorating the silicon nanowires. For (f), silver nanoparticles were prepared by incubating for 5 minutes. Bars show histograms while lines show normal distribution.

5.2.3. Raman Scattering measurements

Serial dilutions were performed to prepare aqueous solutions of pyridine with different concentrations from 0.01 M to 10^{-11} M. A droplet of known volume and concentration of pyridine was deposited on different SERS substrates and left covered for 1 hour for the pyridine to adsorb on the substrate. Measurements were performed using a ProRaman-L analyzer comprising a 532 nm wavelength 66 mW laser diode with 2.0 cm^{-1} linewidth. The laser power was measured using, a Newport 1918-R power meter, the linewidth was measured using Ocean Optics USB4000 spectrometer and the spot size was measured using Newport LBP-3-USB mode profiler. The detector is a CCD camera that is thermoelectrically cooled to -50°C. The laser is fiber coupled to a 0.22 NA objective lens which is mounted adjacent to the detector. The sample is placed flat underneath (and perpendicular to) this assembly at a spacing of 7 mm. The spot was Gaussian with 0.7 mm diameter.

Table 5.1. Nanostructure diameters versus incubation time

SiNW	**SiNW Diameter**	
Etching time	**Mean**	**S.D.**
30 minutes	252 nm	74 nm
45 minutes	336 nm	71 nm
60 minutes	857 nm	232 nm
AgNP	**AgNP Diameter**	
Deposition time	**Mean**	**S.D.**
2 minutes	16 nm	7 nm
3 minutes	30 nm	11 nm
4 minutes	39 nm	17 nm
5 minutes	43 nm	20 nm
AgNP on SiNW	**AgNP Diameter**	
Etching time[a]	**Mean**	**S.D.**
30 minutes	118 nm	50 nm
45 minutes	177 nm	52 nm
60 minutes	180 nm	54 nm

[a]AgNP deposition time on all SiNW was 5 minutes

5.3. Results

Figure 5.2 shows the simulation results. Figure 5.2 (a) and (b) show the electric field enhancement between the AgNP and Si. There is a drastic amplification of the electric field due to surface plasmons. Raman enhancement factor is given by equation 5.1.

$$Enhancement\ factor\ =\ {E_{excitation}}^2 \cdot {E_{emission}}^2 \qquad 5.1$$

where $E_{excitation}$ is the electric field at the excitation wavelength (532 nm) and $E_{emission}$ is the electric field at the emission wavelength at v1 peak of pyridine around 1050 cm^{-1} (563 nm).

Simulations suggested that increasing the nanoparticle size increases the enhancement factor, Figure 5.2 (d) because the electromagnetic field is more strongly localized in the gap. Figure 5.2 (b) shows the electric field amplification in SiNWs decorated with AgNPs and it explains the large enhancement factor in the metallized nanowires. This is strongly related to the direction of light propagation in relation to the hot spot, the spacing between the SiNW and AgNP. The hot spot is vertically aligned and is thus oriented with the direction of light polarization. Figure 5.2 (e) shows that by depositing these nanoparticles on silicon nanowires, enhancement factors around 10^7 to 10^8 and as high as 10^9 is possible. Coupling between nanoparticles can also occur when the nanowires bring the

nanoparticles very close to one another. Figure 5.2 (c) shows the electric field amplification caused by coupling two silver nanoparticles with 1 nm gap in between. Figure 5.2 (f) highlights the effect that the coupled nanoparticles have; enhancement factor increased by an order of 2.

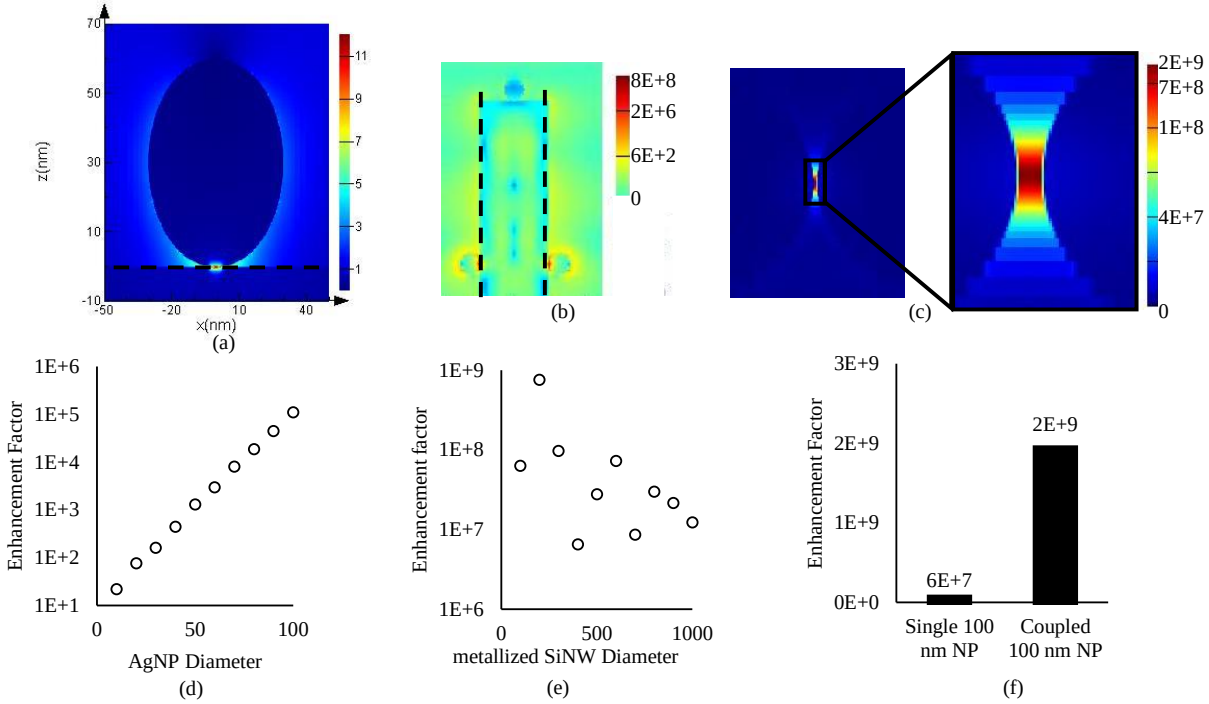

Figure 5.2. Simulation results showing electric field distribution with 532 nm wavelength incident laser for (a) 60 nm diameter silver nanoparticle. Linear scale, E^4 plotted at 532 nm. (b) 200 nm diameter silicon nanowire decorated with 60 nm diameter silver nanoparticles. Log scale, E^4 plotted at 532 nm. (c) Coupled 100 nm diameter silver nanoparticles each on 100 nm diameter nanowires with 1 nm gap in between. Linear scale, E^4 plotted at 532 nm. Simulated enhancement factors for (d) different diameters of silver nanoparticles on silicon substrate, (e) different diameter silicon nanowires decorated with 60 nm diameter silver nanoparticles, and (f) Coupling between metallized silicon nanowires. The dashed lines define the boundaries of Si.

Figure 5.3 shows the experimental Raman spectra obtained for low concentration pyridine on AgNP prepared with different times. The scale bars for the Raman spectra are equivalent. Thus, it is easy to see the increased enhancement effect of depositing the nanoparticles on the nanowires for those prepared with 30 minutes incubation time in comparison to the nanoparticles deposited on bare silicon. When the nanoparticles were deposited on the nanowires prepared with 45 and 60 minutes incubation time, the Raman spectra obtained are actually degraded compared to the nanoparticles alone.

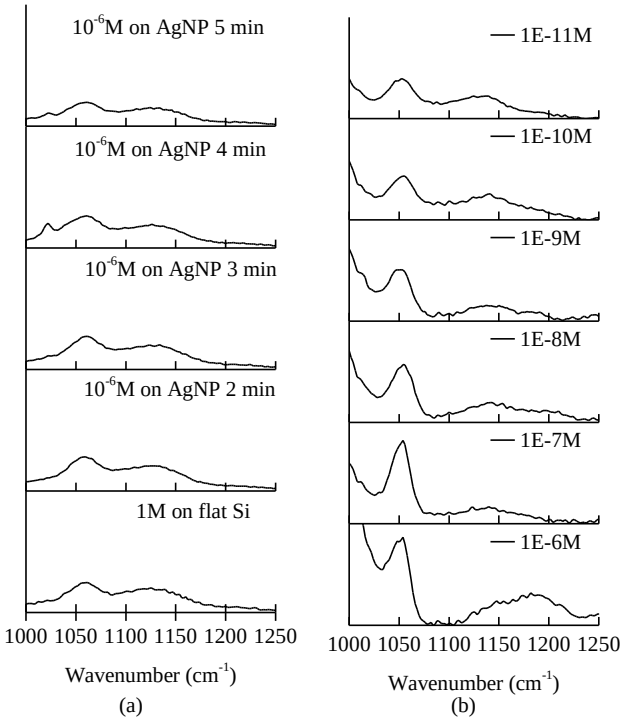

Figure 5.3. Experimental Raman spectra of pyridine for different substrates, (a) low concentration pyridine on silver nanoparticles compared with 1M pyridine in vial. (b) low concentrations pyridine on silicon nanowires that are decorated with silver nanoparticles.

As discussed earlier, these long times etching produced longer nanowires than those prepared with 30 minutes incubation, causing the nanowires to be prone to collapse. Figure 5.3 (b) shows the Raman spectra obtained for pyridine as low as 10^{-11}M on the SiNW / AgNP prepared using 30 minutes etching time and 5 minutes deposition time. The 1050 cm^{-1} peak was visible in all cases.

Enhancement factor was calculated as in equation 5.2 below

$$E.F. = \frac{I_{SERS}}{I_{REF}} \cdot \frac{N_{REF}}{N_{SERS}} \qquad 5.2$$

where I refers to intensity, N is the number of pyridine molecules adsorbed on the surface. The reference was taken to be 1 M pyridine on bare silicon or $N_{REF} = 1 \times 10^{18}$. For 10^{-6} M pyridine, N_{SERS} was estimated to be between 6×10^{11} and 3×10^{12} as not all experiments used the same droplet volume. For the lower concentrations, N_{SERS} was as low as 6×10^{6}.

Figure 5.4 (a) shows the intensity versus Pyridine concentration to assess the substrate's usability as a quantitative sensor. Large changes in concentration are associated with large changes in intensity only until 10^{-9} M. For 10^{-10} M and 10^{-11} M, the change in intensity is too low to confidently use the measurement as a quantitative one. Nevertheless, this SERS substrate is useful for detecting a very small concentration of the probe molecule. Figure 5.4 (b) shows the calculated enhancement factors from the measured intensity values at the lowest concentration detected for each SERS substrate.

With an observed experimental enhancement factor around 6×10^5 to 8×10^5 for nanoparticles with diameters 40 to 60 nm, we see a good match between simulations and experiments. The experiments slightly outperform the simulations due to some aggregation of nanoparticles that cause effectively larger diameter nanoparticles. We chose the densest and largest nanoparticle preparation conditions to metallize nanowires. For metallized nanowires, we observed an experimental enhancement factor of 3×10^{11}.

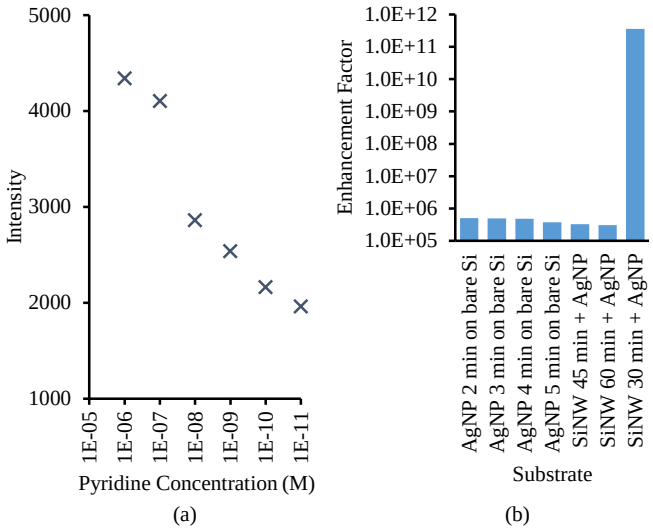

Figure 5.4. (a) Intensity of the v1 peak around 1050 cm^{-1} for different pyridine concentrations left to incubate of silicon nanowires prepared by 30 minutes etching time and decorated with silver nanoparticles prepared by 5 minutes deposition time. (b) Experimental enhancement factors for different SERS substrates.

Figure 5.5 assesses the reproducibility of the SERS substrate using 10^{-9}M pyridine on the SiNW prepared using 30 minutes etching time decorated with AgNP prepared using 5 minutes deposition time. Spot to spot variation was 16.9%, sample to sample variation was 16.8% and batch to batch variation was 22.9%. Figure 5.6 shows its robustness, using the sample experimental conditions. After 8 days, the signal has degraded by 9%. Overall, the SERS substrate is able to give a qualitative signal for the presence of the probe molecule at extremely low concentrations.

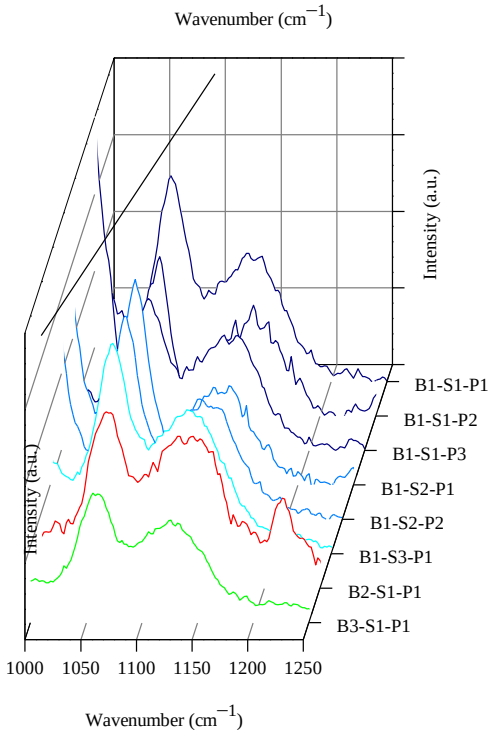

Figure 5.5. Results of repeatability experiment. The dark blue spectra are different positions on the same sample (P1 – P3). Different shades of blue are different samples prepared in the same batch (S1-S3) while different colors refer to different batches.

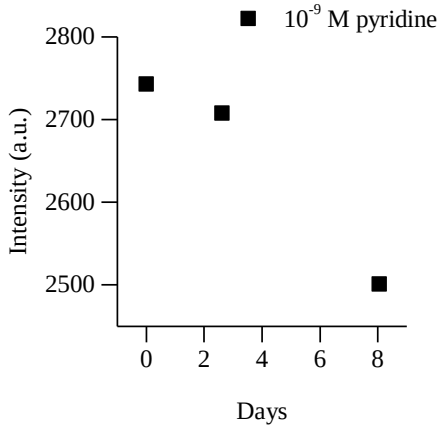

Figure 5.6. Robustness. After 8 days, the intensity of the signal was 8% lower than the initial measurement.

Table 5.2 compares our results with recently published results using decorated SiNWs as active SERS substrates [47, 48]. We fabricated our SERS substrates in low cost simple fabrication method and detected a very low concentration with high E.F compared to [47, 48].

Table 5.2. Comparison of this work with the state of the art

FABRICATION METHOD	PROBE MOLECULE	MIN. CONC.	E.F
MACE, ELECTROLESS DEPOSITION (THIS WORK)	Pyridine	10^{-11}M	3.5×10^{11}

LITHOGRAPHY / MACE [22]	4-methylbenzenethiol	10 mM	Not reported
WET TEXTURING – THERMAL EVAPORATION [49, 50]	Rhodamine 6G	10^{-8}M	9.5×10^{6} [49] 1.2×10^{9} [50]
E-BEAM EVAPORATION, CVD, SPUTTERING [51]	Rhodamine 6G	10^{-10}M	1.5×10^{7}
MACE, ELECTROLESS DEPOSITION [23]	Rhodamine 6G	10^{-15}M	Not reported
SAM, ICP [47]	4,4'-Bipyridine	1 mM	Not reported
METAL CLAD WAVEGUIDE [48]	1,4-BDT	Not reported	39

The state of art of our work is the fabrication of our SERS substrates in one step low cost and low energy required method and also tuning the dimensions of our nanostructures till we reach the best E.F. In case of using SiNWs as SERS substrates we studied the E.F with increasing diameter and length of SINWs we found that the increasing diameter and length inhibits enhancement. This could be resulted from that the longer and larger diameter SiNWs trapped more light than the shorter one so the signal remained in the structure and didn't reach Raman detector [47].

The ProRaman-L analyzer used in this work is a low-cost compact system. SERS have traditionally required the use of more complex systems for accurate tuning of resonant wavelength and incident angle. The silver nanoparticles are orientated such that the incident angle excites the resonant modes on the nanoparticle without requiring accurate tuning of angle. This work greatly increases the accessibility of SERS experiments by using a substrate that is easy to prepare and a low cost measurement system.

5.4. Conclusions

Metal assisted chemical etching is a simple method that was used to fabricate surface enhanced Raman scattering (SERS) substrates based on silver nanoparticles-decorated silicon nanowires. Simulations showed that the enhancement factor of nanoparticles increased from 20 to 10^{5} as the nanoparticle size increased. By depositing these silver nanoparticles on silicon nanowires, we observed a drastic increase in the enhancement factor reaching 10^{11} experimentally and enabling the detection of picomolar concentrations of pyridine.

5.5. References

[1] A. Campion and P. Kambhampati, "Surface-enhanced Raman scattering," *Chem. Soc. Rev.,* vol. 27, pp. 241-250, 1998.

[2] A. Brolo, D. Irish, and J. Lipkowski, "Surface-enhanced Raman spectra of pyridine and pyrazine adsorbed on a Au (210) single-crystal electrode," *The Journal of Physical Chemistry B,* vol. 101, pp. 3906-3909, 1997.

[3] H. Wetzel and H. Gerischer, "Surface enhanced Raman scattering from pyridine and halide ions adsorbed on silver and gold sol particles," *Chem. Phys. Lett.,* vol. 76, pp. 460-464, 1980/12/15 1980. doi: http://dx.doi.org/10.1016/0009-2614(80)80647-6

[4] A. Fojtik and A. Henglein, "Laser ablation of films and suspended particles in a solvent: formation of cluster and colloid solutions," *Berichte der Bunsen-Gesellschaft,* vol. 97, pp. 252-254, 1993.

[5] S. Chen and D. L. Carroll, "Synthesis and characterization of truncated triangular silver nanoplates," *Nano Lett.,* vol. 2, pp. 1003-1007, 2002. doi: 10.1021/nl025674h

[6] C. J. Orendorff, A. Gole, T. K. Sau, and C. J. Murphy, "Surface-enhanced Raman spectroscopy of self-assembled monolayers: sandwich architecture and nanoparticle shape dependence," *Anal. Chem.,* vol. 77, pp. 3261-3266, 2005. doi: 10.1021/ac048176x

[7] Y. Sun and Y. Xia, "Shape-controlled synthesis of gold and silver nanoparticles," *Science,* vol. 298, pp. 2176-2179, 2002.

[8] F. De Angelis, F. Gentile, F. Mecarini, G. Das, M. Moretti, P. Candeloro, M. Coluccio, G. Cojoc, A. Accardo, and C. Liberale, "Breaking the diffusion limit with super-hydrophobic delivery of molecules to plasmonic nanofocusing SERS structures," *Nat. Photonics,* vol. 5, pp. 682-687, 2011. doi: 10.1038/nphoton.2011.222

[9] M. Li, S. K. Cushing, J. Zhang, J. Lankford, Z. P. Aguilar, D. Ma, and N. Wu, "Shape-dependent surface-enhanced Raman scattering in gold–Raman-probe–silica sandwiched nanoparticles for biocompatible applications," *Nanotechnology,* vol. 23, p. 115501, 2012. doi: 10.1088/0957-4484/23/11/115501

[10] P. S. Kumar, I. Pastoriza-Santos, B. Rodríguez-González, F. J. G. De Abajo, and L. M. Liz-Marzan, "High-yield synthesis and optical response of gold nanostars," *Nanotechnology,* vol. 19, p. 015606, 2007. doi: 10.1088/0957-4484/19/01/015606

[11] M. Procházka, *Surface-Enhanced Raman Spectroscopy: Bioanalytical, Biomolecular and Medical Applications*: Springer, 2015.

[12] Z. Yang, Y. Li, Z. Li, D. Wu, J. Kang, H. Xu, and M. Sun, "Surface enhanced Raman scattering of pyridine adsorbed on Au@Pd core/shell nanoparticles," *The Journal of Chemical Physics,* vol. 130, p. 234705, 2009. doi: doi:http://dx.doi.org/10.1063/1.3153917

[13] L. G. Olson, Y.-S. Lo, T. P. Beebe Jr, and J. M. Harris, "Characterization of silane-modified immobilized gold colloids as a substrate for surface-enhanced Raman spectroscopy," *Anal. Chem.,* vol. 73, pp. 4268-4276, 2001.

[14] F. Toderas, M. Baia, L. Baia, and S. Astilean, "Controlling gold nanoparticle assemblies for efficient surface-enhanced Raman scattering and localized surface plasmon resonance sensors," *Nanotechnology,* vol. 18, p. 255702, 2007.

[15] M. Procházka, P. Šimáková, and N. Hajduková-Šmídová, "SE (R) RS microspectroscopy of porphyrins on immobilized Au nanoparticles: Testing spectral sensitivity and reproducibility," *Colloids Surf., A,* vol. 402, pp. 24-28, 2012.

[16] M. Fan, G. F. S. Andrade, and A. G. Brolo, "A review on the fabrication of substrates for surface enhanced Raman spectroscopy and their applications in analytical chemistry," *Anal. Chim. Acta,* vol. 693, pp. 7-25, 2011. doi: http://dx.doi.org/10.1016/j.aca.2011.03.002

[17] G. Das, M. Chirumamilla, A. Toma, A. Gopalakrishnan, R. P. Zaccaria, A. Alabastri, M. Leoncini, and E. Di Fabrizio, "Plasmon based biosensor for distinguishing different peptides mutation states," *Sci. Rep.,* vol. 3, p. 1792, 2013.

[18] D. Weitz, M. Lin, and C. Sandroff, "Colloidal aggregation revisited: new insights based on fractal structure and surface-enhanced Raman scattering," *Surf. Sci.,* vol. 158, pp. 147-164, 1985.

[19] E. Le Ru and P. Etchegoin, *Principles of Surface-Enhanced Raman Spectroscopy: and related plasmonic effects*: Elsevier, 2008.

[20] M. S. Schmidt, J. Hübner, and A. Boisen, "Large area fabrication of leaning silicon nanopillars for surface enhanced Raman spectroscopy," *Adv. Mater.,* vol. 24, 2012.

[21] M. Becker, V. Sivakov, U. Gösele, T. Stelzner, G. Andrä, H. J. Reich, S. Hoffmann, J. Michler, and S. H. Christiansen, "Nanowires Enabling Signal-Enhanced Nanoscale Raman Spectroscopy," *Small,* vol. 4, pp. 398-404, 2008.

[22] J. Yang, J. Li, Q. Gong, J. Teng, and M. Hong, "High aspect ratio SiNW arrays with Ag nanoparticles decoration for strong SERS detection," *Nanotechnology,* vol. 25, p. 465707, 2014.

[23] F. Bai, M. Li, P. Fu, R. Li, T. Gu, R. Huang, Z. Chen, B. Jiang, and Y. Li, "Silicon nanowire arrays coated with electroless Ag for increased surface-enhanced Raman scattering," *APL Materials,* vol. 3, p. 056101, 2015.

[24] F. M. Hassan, A. R. Elsayed, V. Chabot, R. Batmaz, X. Xiao, and Z. Chen, "Subeutectic Growth of Single-Crystal Silicon Nanowires Grown on and Wrapped with Graphene Nanosheets: High-

Performance Anode Material for Lithium-Ion Battery," *Acs Applied Materials & Interfaces,* vol. 6, pp. 13757-13764, 2014/08/27 2014. doi: 10.1021/am5032067

[25] L. J. Chen, "Silicon nanowires: the key building block for future electronic devices," *J. Mater. Chem.,* vol. 17, pp. 4639-4643, 2007.

[26] B. Tian, X. Zheng, T. J. Kempa, Y. Fang, N. Yu, G. Yu, J. Huang, and C. M. Lieber, "Coaxial silicon nanowires as solar cells and nanoelectronic power sources," *Nature,* vol. 449, pp. 885-889, 2007.

[27] R. Gamal, Y. Ismail, and M. A. Swillam, "Optical biosensor based on a silicon nanowire ridge waveguide for lab on chip applications," *Journal of Optics,* vol. 17, p. 045802, 2015.

[28] L. Latu-Romain, C. Mouchet, C. Cayron, E. Rouviere, and J.-P. Simonato, "Growth parameters and shape specific synthesis of silicon nanowires by the VLS method," *Journal of Nanoparticle Research,* vol. 10, pp. 1287-1291, 2008.

[29] R. Wagner and W. Ellis, "Vapor-liquid-solid mechanism of single crystal growth," *Appl. Phys. Lett.,* vol. 4, pp. 89-90, 1964.

[30] B. Fuhrmann, H. S. Leipner, H.-R. Höche, L. Schubert, P. Werner, and U. Gösele, "Ordered arrays of silicon nanowires produced by nanosphere lithography and molecular beam epitaxy," *Nano Lett.,* vol. 5, pp. 2524-2527, 2005.

[31] Y.-H. Yang, S.-J. Wu, H.-S. Chiu, P.-I. Lin, and Y.-T. Chen, "Catalytic growth of silicon nanowires assisted by laser ablation," *The Journal of Physical Chemistry B,* vol. 108, pp. 846-852, 2004.

[32] H. Pan, S. Lim, C. Poh, H. Sun, X. Wu, Y. Feng, and J. Lin, "Growth of Si nanowires by thermal evaporation," *Nanotechnology,* vol. 16, p. 417, 2005.

[33] Y. Fu, A. Colli, A. Fasoli, J. Luo, A. Flewitt, A. Ferrari, and W. Milne, "Deep reactive ion etching as a tool for nanostructure fabrication," *Journal of Vacuum Science & Technology B,* vol. 27, pp. 1520-1526, 2009.

[34] R. Das, S. S. Nath, D. Chakdar, G. Gope, and R. Bhattacharjee, "Synthesis of silver nanoparticles and their optical properties," *Journal of Experimental Nanoscience,* vol. 5, pp. 357-362, 2010.

[35] A. M. Gouda, M. Elsayed, N. K. Allam, and M. A. Swillam, "Black silicon based on simple fabrication of mesoporous silicon nanowires for solar energy harvesting," in *2016 IEEE 43rd Photovoltaic Specialists Conference (PVSC)*, 2016, pp. 2893-2895. doi: 10.1109/pvsc.2016.7750185

[36] S. K. Srivastava, D. Kumar, S. Schmitt, K. Sood, S. Christiansen, and P. Singh, "Large area fabrication of vertical silicon nanowire arrays by silver-assisted single-step chemical etching and their formation kinetics," *Nanotechnology,* vol. 25, p. 175601, 2014.

[37] H. Han, Z. Huang, and W. Lee, "Metal-assisted chemical etching of silicon and nanotechnology applications," *Nano Today,* vol. 9, pp. 271-304, 2014.

[38] S. A. Razek, M. A. Swillam, and N. K. Allam, "Vertically aligned crystalline silicon nanowires with controlled diameters for energy conversion applications: Experimental and theoretical insights," *J. Appl. Phys.,* vol. 115, p. 194305, 2014. doi: doi:http://dx.doi.org/10.1063/1.4876477

[39] D. Kumar, S. K. Srivastava, P. Singh, K. Sood, V. Singh, N. Dilawar, and M. Husain, "Room temperature growth of wafer-scale silicon nanowire arrays and their Raman characteristics," *Journal of Nanoparticle Research,* vol. 12, pp. 2267-2276, 2010.

[40] A. G. Nassiopoulou, V. Gianneta, and C. Katsogridakis, "Si nanowires by a single-step metal-assisted chemical etching process on lithographically defined areas: formation kinetics," *Nanoscale Research Letters,* vol. 6, pp. 1-8, 2011.

[41] K. Peng, J. Hu, Y. Yan, Y. Wu, H. Fang, Y. Xu, S. Lee, and J. Zhu, "Fabrication of single-crystalline silicon nanowires by scratching a silicon surface with catalytic metal particles," *Adv. Funct. Mater.,* vol. 16, pp. 387-394, 2006.

[42] A. M. Gouda, M. Y. Elsayed, C. Tharwat, and M. A. Swillam, "Silicon-based nanostructures as surface enhanced Raman scattering substrates," in *2016 Photonics North (PN)*, 2016, pp. 1-1. doi: 10.1109/pn.2016.7537981

[43] Lumerical Solutions Inc. Available: http://www.lumerical.com/tcad-products/fdtd/

[44] E. D. Palik, *Handbook of Optical Constants of Solids*: Elsevier Science, 2012.

[45] P. B. Johnson and R.-W. Christy, "Optical constants of the noble metals," *Physical Review B,* vol. 6, p. 4370, 1972.

[46] A. M. Gouda, N. K. Allam, and M. A. Swillam, "Facile omnidirectional black silicon based on porous and nonporous silicon nanowires for energy applications," in *2016 Photonics North (PN)*, 2016, pp. 1-1. doi: 10.1109/pn.2016.7537973

[47] Y. Li, L. Zhou, L. Tang, M. Li, and J. J. He, "Improved Surface Enhanced Raman Scattering Based on Hybrid Au Nanostructures for Biomolecule Detection," *IEEE Photonics Journal,* vol. 8, pp. 1-7, 2016. doi: 10.1109/jphot.2016.2619063

[48] Y. Wang, M. Huang, K. Wang, X. Liu, Y. Zou, B. Song, and J. Chen, "Raman Enhancement in Metal-Cladding Waveguide and the Influence of the Metal Film Surface Roughness," *J. Lightwave Technol.,* vol. 34, pp. 3616-3621, 2016. doi: 10.1109/jlt.2016.2571618

[49] S. Jiang, J. Guo, C. Zhang, C. Li, M. Wang, Z. Li, S. Gao, P. Chen, H. Si, and S. Xu, "A sensitive, uniform, reproducible and stable SERS substrate has been presented based on MoS2@Ag

nanoparticles@pyramidal silicon," *RSC Advances,* vol. 7, pp. 5764-5773, 2017. doi: 10.1039/c6ra26879j

[50] C. Zhang, S. Z. Jiang, C. Yang, C. H. Li, Y. Y. Huo, X. Y. Liu, A. H. Liu, Q. Wei, S. S. Gao, X. G. Gao, and B. Y. Man, "Gold@silver bimetal nanoparticles/pyramidal silicon 3D substrate with high reproducibility for high-performance SERS," *Sci. Rep.,* vol. 6, p. 25243, 2016. doi: 10.1038/srep25243

[51] L. He, C. Ai, W. Wang, N. Gao, X. Yao, C. Tian, and K. Zhang, "An effective three-dimensional surface-enhanced Raman scattering substrate based on oblique Si nanowire arrays decorated with Ag nanoparticles," *J. Mater. Sci.,* vol. 51, pp. 3854-3860, 2016. doi: 10.1007/s10853-015-9704-7

CHAPTER 6. CONCLUSIONS

On-chip optical sensing is highly versatile for lab on a chip applications. The cost of healthcare is increasing at an alarming rate and accurate, early and low cost diagnosis is the best way to reach a more sustainable healthcare system, and this requires the use of lab on a chip systems. This thesis focused on three different sensing concepts: measuring the refractive index, infrared spectroscopy, Raman spectroscopy.

We designed a multimode interference (MMI) sensor using shallow waveguide silicon photonics platform. The advantage of silicon photonics is that it is already being commercialized and many of the fabrication and characterization expertise gained in the mature electronics industry can be transferred easily to silicon photonics. In this work we opted for a shallow platform of only 50 to 70 nm height. This has not been explored extensively because the major applications of silicon photonics has been in communications, where high density is a necessity, and the shallow waveguide platform exhibits high losses with small band radius, thus it is not suitable for dense photonic integrated circuits. However, in sensing applications, the shallow waveguide provides increased light-matter interaction due to low confinement. The MMI sensor designed has a sensitivity around 420 nm / RIU. This work was designed to be able to fabricate it using the facilities at the Science and Technology Research Center at the AUC. Further work would be to carry out this fabrication and perform experimental verification. In addition, it would also be interesting to fabricate the MMI sensors designed here using commercial foundry services and see how the performance of the in-house sensors compare with those fabricated using a standard process. It would be of utmost importance to study the fabrication tolerance of the MMI sensors and see how much variation between devices and explore ways to overcome these variations.

Next, I designed a plasmonic slot waveguide gas sensor using on chip infrared spectroscopy. Gas sensing using refractive index is not effective as different gases have very similar refractive indices up to the 6^{th} decimal place. Infrared spectroscopy has been suggested as a more specific gas sensing technique. However, for large scale deployment, on chip solutions are necessary. Metals provide good plasmonic response only in the visible range of wavelengths. By doping semiconductors, we can “engineer” materials with desired plasmonic properties. In this work, Indium Arsenide was chosen as the semiconductor requiring the least amount of n-type dopant to enable supporting surface plasmon polaritons (SPP) in the mid infrared. With a dopant concentration of 2.2×10^{20} cm^{-3}, the plasmonic slot waveguide was designed to support modes from 5 to 10 µm wavelengths, corresponding to the fingerprint region of infrared spectroscopy. The fingerprint region is highly characteristic of the sample being measured. The geometry

of the plasmonic slot waveguide uses a slot with cross section 200 nm by 200 nm and using a length of just 1 μm, the transmission of the waveguide matches the infrared spectrum of the gas inside the slot. Future work would be to design a plasmonic resonant structure to enable detecting the concentration of the analyte in addition to identifying the analyte, i.e. study the sensitivity of a sensor based on this plasmonic slot waveguide.

Finally, a surface enhanced Raman spectroscopy (SERS) substrate based on silicon nanowires decorated with silver nanoparticles was designed. In this work, a low cost, equipment free fabrication method was used to pattern silicon into silicon nanowires using metal assisted chemical etching. Silver nanoparticles were deposited on the silicon nanowires using electroless deposition. Different etching and deposition conditions were used to arrive at a SERS substrate that boasts an enhancement factor on the order of 10^{11}. The substrate is able to detect pyridine with a signal intensity that is correlated with the pyridine intensity in micro- and nanomolar concentrations. Picomolar concentrations of pyridine were also successfully detected. It would be interested for extending this work to explore different shape nanoparticles, in particular those with sharp corners such as squares, triangles and stars as they are expected to exhibit high electric field amplification due to an antenna effect. Such nanoparticles have been fabricated using exquisite fabrication methods, a low cost fabrication of cubical nanoparticles would be beneficial extension of this work. Experimental verification using other probe molecules and biologically relevant samples would be useful.

The connecting theme for the different sensors presented here is that they are all on chip and realizable. Full systems on chip are possible for all three sensor configurations, for complete lab on chip applications that provide sample-to-answer functionality. Silicon photonics is already commercially used. III-V semiconductors including InAs are planned to be introduced in the electronics industry within the next five years due to their superior mobility over silicon to continue performance improvements. Lastly, the silicon nanowire platform is already experimentally verified. This work demonstrated several solutions for on chip optical sensing.

Bibliography

The numbering used in this bibliography does not correspond to the in-text citations. The thesis was written such that each chapter is a standalone document with its own references section where the references listed correctly correspond to the numbered citations. This bibliography merely combines all the references used in all the chapters.

[1] Y. B. Rashil Mehta, Harshit Mathur, Ankit Yadav, Anoop Kumar. (2014, 21 July 2017). Sensors: The New Generation Technology. Available: https://www.slideshare.net/nktydv/480-sensors-30751476

[2] A. Gentry-Maharaj and U. Menon, "Screening for ovarian cancer in the general population," Best Pract. Res. Clin. Obstet. Gynaecol., vol. 26, pp. 243-256, 2012. doi: http://dx.doi.org/10.1016/j.bpobgyn.2011.11.006

[3] D. Badgwell and R. C. Bast, Jr., "Early detection of ovarian cancer," Dis. Markers, vol. 23, pp. 397-410, 2007.

[4] R. C. Bast, Jr., M. Brewer, C. Zou, M. A. Hernandez, M. Daley, R. Ozols, K. Lu, Z. Lu, D. Badgwell, G. B. Mills, S. Skates, Z. Zhang, D. Chan, A. Lokshin, and Y. Yu, "Prevention and early detection of ovarian cancer: mission impossible?," Recent Results Cancer Res, vol. 174, pp. 91-100, 2007.

[5] W. Jiang, R. Huang, C. Duan, L. Fu, Y. Xi, Y. Yang, W.-M. Yang, D. Yang, D.-H. Yang, and R.-P. Huang, "Identification of Five Serum Protein Markers for Detection of Ovarian Cancer by Antibody Arrays," PLoS ONE, vol. 8, p. e76795, 2013. doi: 10.1371/journal.pone.0076795

[6] L. A. Torre, F. Bray, R. L. Siegel, J. Ferlay, J. Lortet-Tieulent, and A. Jemal, "Global cancer statistics, 2012," CA. Cancer J. Clin., vol. 65, pp. 87-108, 2015. doi: 10.3322/caac.21262

[7] N. S. Larsen, "Invasive Cervical Cancer Rising in Young White Females," J. Natl. Cancer Inst., vol. 86, pp. 6-7, January 5, 1994 1994. doi: 10.1093/jnci/86.1.6

[8] L. G. Koss, "The Papanicolaou test for cervical cancer detection. A triumph and a tragedy," JAMA, vol. 261, pp. 737-43, Feb 3 1989.

[9] C. J. L. M. Meijer, T. J. M. Helmerhorst, L. Rozendaal, J. C. van der Linden, F. J. Voorhorst, and J. M. M. Walboomers, "HPV typing and testing in gynaecological pathology: has the time come?," Histopathology, vol. 33, pp. 83-86, 1998. doi: 10.1046/j.1365-2559.1998.00436.x

[10] J. Li, J. Y. Lee, and E. S. Yeung, "Quantitative screening of single copies of human papilloma viral DNA without amplification," Anal. Chem., vol. 78, pp. 6490-6, Sep 15 2006. doi: 10.1021/ac060864o

[11] G. Wu and M. H. Zaman, "Low-cost tools for diagnosing and monitoring HIV infection in low-resource settings," Bull. World Health Organ., vol. 90, pp. 914-920, 2012.

[12] BiotechMichael. „Anti human IgG“ Double Antibody Sandwich ELISA. Available: https://commons.wikimedia.org/wiki/File:ELISA.jpg

[13] Y. Farhat. Sandwich ELISA Protocol. Available: http://protocol-place.com/assays/elisa/sandwich-elisa-protocol/

[14] F. Brunner, N. Schofer, M. Schlueter, F. Ojeda, T. Zeller, C. Bickel, T. Muenzel, T. Keller, S. Blankenberg, and B. Goldmann, "Diagnosis of acute myocardial infarction: super-sensitivity vs. high-sensitivity cardiac troponin I assay," Eur. Heart J., vol. 34, 2015. doi: 10.1093/eurheartj/eht310.P5534

[15] M. E. Benford, M. Wang, J. Kameoka, and G. L. Coté, "Detection of cardiac biomarkers exploiting surface enhanced Raman scattering (SERS) using a nanofluidic channel based biosensor towards coronary point-of-care diagnostics," in SPIE BiOS: Biomedical Optics, 2009, pp. 719203-719203-6. doi: 10.1117/12.809661

[16] K. De Vos, J. Girones, T. Claes, Y. De Koninck, S. Popelka, E. Schacht, R. Baets, and P. Bienstman, "Multiplexed antibody detection with an array of silicon-on-insulator microring resonators," IEEE Photonics Journal, vol. 1, pp. 225-235, 2009.

[17] P. Daukantas, "Air-Quality Monitoring in the Mid-Infrared," Optics and Photonics News, vol. 26, pp. 26-33, 2015. doi: 10.1364/OPN.26.11.000026

[18] Q. Quan, D. L. Floyd, I. B. Burgess, P. B. Deotare, I. W. Frank, S. K. Y. Tang, R. Ilic, and M. Loncar, "Single particle detection in CMOS compatible photonic crystal nanobeam cavities," Opt. Express, vol. 21, pp. 32225-32233, 2013/12/30 2013. doi: 10.1364/oe.21.032225

[19] G. T. Reed and A. P. Knights, Silicon photonics: an introduction: John Wiley & Sons, 2004.

[20] E. Optics. Optics 101: Level 1 Theoretical Foundations. Available: https://www.edmundoptics.com/resources/application-notes/optics/optics-101-level-1-theoretical-foundations/

[21] K. Okamoto, Fundamentals of optical waveguides: Academic press, 2010.

[22] J. Brownson. (31/07/2017). The "Life" of a Photon. Available: https://www.e-education.psu.edu/eme810/sites/www.e-education.psu.edu.eme810/files/images/Lesson_03/radiationfates.png

[23] Pdcook. (2012, 31/07/2017). BioTek microplate reader. Available: https://commons.wikimedia.org/w/index.php?curid=19191924

[24] S. C. Terry, J. H. Jerman, and J. B. Angell, "A gas chromatographic air analyzer fabricated on a silicon wafer," IEEE Trans. Electron Devices, vol. 26, pp. 1880-1886, 1979.

[25] A. Manz, N. Graber, and H. M. Widmer, "Miniaturized total chemical analysis systems: A novel concept for chemical sensing," Sens. Actuators, B, vol. 1, pp. 244-248, 1990/01/01 1990. doi: http://dx.doi.org/10.1016/0925-4005(90)80209-I

[26] D. Kverno. Oscillations and Resonance in a Carbon Dioxide Laser. Available: http://www.phy.davidson.edu/StuHome/derekk/Resonance/pages/co2.htm

[27] I. Coblentz Society, "Evaluated Infrared Reference Spectra," in NIST Chemistry WebBook, NIST Standard Reference Database Number 69, P. J. L. a. W. G. Mallard, Ed., ed Gaithersburg MD, 20899: National Institute of Standards and Technology.

[28] O. Optical. Raman Spectroscopy. Available: http://www.omegafilters.com/applications/raman-spectroscopy/

[29] E. C. Le Ru, E. Blackie, M. Meyer, and P. G. Etchegoin, "Surface Enhanced Raman Scattering Enhancement Factors: A Comprehensive Study," The Journal of Physical Chemistry C, vol. 111, pp. 13794-13803, 2007/09/01 2007. doi: 10.1021/jp0687908

[30] U. Leonhardt, "Optical metamaterials: Invisibility cup," Nat. Photonics, vol. 1, pp. 207-208, 2007.

[31] J. A. Dionne, L. A. Sweatlock, H. A. Atwater, and A. Polman, "Plasmon slot waveguides: Towards chip-scale propagation with subwavelength-scale localization," Physical Review B, vol. 73, 2006. doi: 10.1103/PhysRevB.73.035407

[32] K. Tanaka and M. Tanaka, "Simulations of nanometric optical circuits based on surface plasmon polariton gap waveguide," Appl. Phys. Lett., vol. 82, p. 1158, 2003. doi: 10.1063/1.1557323

[33] D. F. P. Pile, T. Ogawa, D. K. Gramotnev, Y. Matsuzaki, K. C. Vernon, K. Yamaguchi, T. Okamoto, M. Haraguchi, and M. Fukui, "Two-dimensionally localized modes of a nanoscale gap plasmon waveguide," Appl. Phys. Lett., vol. 87, p. 261114, 2005. doi: 10.1063/1.2149971

[34] S. A. Maier, P. G. Kik, H. A. Atwater, S. Meltzer, E. Harel, B. E. Koel, and A. A. Requicha, "Local detection of electromagnetic energy transport below the diffraction limit in metal nanoparticle plasmon waveguides," Nat. Mater., vol. 2, p. 229, 2003.

[35] J. M. Steele, C. E. Moran, A. Lee, C. M. Aguirre, and N. J. Halas, "Metallodielectric gratings with subwavelength slots: Optical properties," Physical Review B, vol. 68, p. 205103, 2003.

[36] S. A. Maier and H. A. Atwater, "Plasmonics: Localization and guiding of electromagnetic energy in metal/dielectric structures," J. Appl. Phys., vol. 98, p. 10, 2005.

[37] K. M. Mayer and J. H. Hafner, "Localized surface plasmon resonance sensors," Chem. Rev., vol. 111, pp. 3828-57, Jun 8 2011. doi: 10.1021/cr100313v

[38] S. A. Maier, Plasmonics: fundamentals and applications: Springer US, 2007. doi: 10.1007/0-387-37825-1

[39] M. G. Albrecht and J. A. Creighton, "Anomalously intense Raman spectra of pyridine at a silver electrode," J. Am. Chem. Soc., vol. 99, pp. 5215-5217, 1977/06/01 1977. doi: 10.1021/ja00457a071

[40] U. Wenning, B. Pettinger, and H. Wetzel, "Anguler-resolved raman spectroscopy of pyridine on copper and gold electrodes," Chem. Phys. Lett., vol. 70, pp. 49-54, 1980/02/15 1980. doi: http://dx.doi.org/10.1016/0009-2614(80)80058-3

[41] H. Wetzel and H. Gerischer, "Surface enhanced Raman scattering from pyridine and halide ions adsorbed on silver and gold sol particles," Chem. Phys. Lett., vol. 76, pp. 460-464, 1980/12/15 1980. doi: http://dx.doi.org/10.1016/0009-2614(80)80647-6

[42] Z. Yang, Y. Li, Z. Li, D. Wu, J. Kang, H. Xu, and M. Sun, "Surface enhanced Raman scattering of pyridine adsorbed on Au@Pd core/shell nanoparticles," The Journal of Chemical Physics, vol. 130, p. 234705, 2009. doi: doi:http://dx.doi.org/10.1063/1.3153917

[43] F. Toderas, M. Baia, L. Baia, and S. Astilean, "Controlling gold nanoparticle assemblies for efficient surface-enhanced Raman scattering and localized surface plasmon resonance sensors," Nanotechnology, vol. 18, p. 255702, 2007.

[44] F. Bai, M. Li, P. Fu, R. Li, T. Gu, R. Huang, Z. Chen, B. Jiang, and Y. Li, "Silicon nanowire arrays coated with electroless Ag for increased surface-enhanced Raman scattering," APL Materials, vol. 3, p. 056101, 2015.

[45] M. S. Schmidt, J. Hübner, and A. Boisen, "Large area fabrication of leaning silicon nanopillars for surface enhanced Raman spectroscopy," Adv. Mater., vol. 24, 2012.

[46] L. Cao, B. Nabet, and J. E. Spanier, "Enhanced Raman scattering from individual semiconductor nanocones and nanowires," Phys. Rev. Lett., vol. 96, p. 157402, 2006.

[47] S. Christiansen, M. Becker, S. Fahlbusch, J. Michler, V. Sivakov, G. Andrä, and R. Geiger, "Signal enhancement in nano-Raman spectroscopy by gold caps on silicon nanowires obtained by vapour–liquid–solid growth," Nanotechnology, vol. 18, p. 035503, 2007.

[48] Q. Hao, B. Wang, J. A. Bossard, B. Kiraly, Y. Zeng, I. K. Chiang, L. Jensen, D. H. Werner, and T. J. Huang, "Surface-Enhanced Raman Scattering Study on Graphene-Coated Metallic Nanostructure Substrates," The Journal of Physical Chemistry C, vol. 116, pp. 7249-7254, 2012/04/05 2012. doi: 10.1021/jp209821g

[49] M. Khorasaninejad, S. Raeis-Zadeh, S. Jafarlou, M. Wesolowski, C. Daley, J. Flannery, J. Forrest, S. Safavi-Naeini, and S. Saini, "Highly enhanced Raman scattering of graphene using plasmonic nano-structure," Sci. Rep., vol. 3, 2013.

[50] M. Li, S. K. Cushing, J. Zhang, J. Lankford, Z. P. Aguilar, D. Ma, and N. Wu, "Shape-dependent surface-enhanced Raman scattering in gold–Raman-probe–silica sandwiched nanoparticles for biocompatible applications," Nanotechnology, vol. 23, p. 115501, 2012. doi: 10.1088/0957-4484/23/11/115501

[51] F. De Angelis, F. Gentile, F. Mecarini, G. Das, M. Moretti, P. Candeloro, M. Coluccio, G. Cojoc, A. Accardo, and C. Liberale, "Breaking the diffusion limit with super-hydrophobic delivery of molecules to plasmonic nanofocusing SERS structures," Nat. Photonics, vol. 5, pp. 682-687, 2011. doi: 10.1038/nphoton.2011.222

[52] A. Erik, K. Magnus, A. R. Chraplyvy, J. R. David, M. K. Peter, W. Peter, R. Kim, F. Johannes Karl, J. S. Seb, J. E. Benjamin, S. Marco, R. K. Frank, L. Andrew, P. Josep, T. Ioannis, E. B. John, S. Sudha, B.-P. Maïté, and G. Nicolas, "Roadmap of optical communications," Journal of Optics, vol. 18, p. 063002, 2016. doi: 10.1088/2040-8978/18/6/063002

[53] P. Tien, "Integrated optics," Sci Am, vol. 230, pp. 28-35, 1974.

[54] R. Ulrich, "Self imaging system using a waveguide," ed: Google Patents, 1978.

[55] R. Nagarajan, M. Kato, J. Pleumeekers, P. Evans, S. Corzine, S. Hurtt, A. Dentai, S. Murthy, M. Missey, and R. Muthiah, "InP photonic integrated circuits," IEEE J. Sel. Top. Quantum Electron., vol. 16, pp. 1113-1125, 2010.

[56] M. K. Smit, X. Leijtens, E. Bente, J. van der Tol, H. Ambrosius, D. Robbins, M. J. Wale, N. Grote, and M. Schell, "A generic foundry model for InP-based photonic ICs," in Optical Fiber Communication Conference, 2012, p. OM3E. 3.

[57] D. A. B. Miller, "Rationale and challenges for optical interconnects to electronic chips," Proceedings of the IEEE, vol. 88, pp. 728-749, 2000. doi: 10.1109/5.867687

[58] D. Normile, "The End--Not Here Yet, But Coming Soon," Science, vol. 293, pp. 787-787, 2001-08-03 00:00:00 2001. doi: 10.1126/science.293.5531.787

[59] R. Ho, K. W. Mai, and M. A. Horowitz, "The future of wires," Proceedings of the IEEE, vol. 89, pp. 490-504, 2001. doi: 10.1109/5.920580

[60] R. Ho, M. Ken, and M. Horowitz, "Managing wire scaling: a circuit perspective," in Interconnect Technology Conference, 2003. Proceedings of the IEEE 2003 International, 2003, pp. 177-179. doi: 10.1109/iitc.2003.1219747

[61] A. Karkar, T. Mak, K. F. Tong, and A. Yakovlev, "A Survey of Emerging Interconnects for On-Chip Efficient Multicast and Broadcast in Many-Cores," IEEE Circuits and Systems Magazine, vol. 16, pp. 58-72, 2016. doi: 10.1109/mcas.2015.2510199

[62] M. Haurylau, C. Guoqing, C. Hui, Z. Jidong, N. A. Nelson, D. H. Albonesi, E. G. Friedman, and P. M. Fauchet, "On-Chip Optical Interconnect Roadmap: Challenges and Critical Directions," Selected Topics in Quantum Electronics, IEEE Journal of, vol. 12, pp. 1699-1705, 2006. doi: 10.1109/jstqe.2006.880615

[63] G. T. Reed and A. P. Knights, "Silicon-On-Insulator (SOI) Photonics," in Silicon Photonics, ed: John Wiley & Sons, Ltd, 2005, pp. 57-110. doi: 10.1002/0470014180.ch4

[64] C. Gunn, "CMOS Photonics for High-Speed Interconnects," IEEE Micro, vol. 26, pp. 58-66, 2006. doi: 10.1109/mm.2006.32

[65] R. Soref, "The Past, Present, and Future of Silicon Photonics," IEEE J. Sel. Top. Quantum Electron., vol. 12, pp. 1678-1687, 2006. doi: 10.1109/jstqe.2006.883151

[66] T. Barwicz, H. Byun, F. Gan, C. Holzwarth, M. Popovic, P. Rakich, M. Watts, E. Ippen, F. Kärtner, and H. Smith, "Silicon photonics for compact, energy-efficient interconnects [Invited]," Journal of Optical Networking, vol. 6, pp. 63-73, 2007.

[67] J. P. S. Lorenzo, R. A., "1.3 μm electro-optic silicon switch," Appl. Phys. Lett., vol. 51, p. 3, 1987.

[68] R. Soref, Bennett, B., "Electrooptical effects in silicon," EEE J. Quant. Electron, vol. 23, p. 7, 1987.

[69] G. R. Cocorullo, I., "Thermo-optical modulation at 1.5 μm in silicon etalon," Electron. Lett., vol. 28, p. 3, 1992.

[70] L. Friedman, Soref, R. A., Lorenzo, J. P., "Silicon double-injection electrooptic modulator with junction gate control," J. Appl. Phys., vol. 63, p. 9, 1988.

[71] G. V. Treyz, "Silicon Mach–Zehnder waveguide interferometers operating at 1.3 μm," Electron. Lett., vol. 27, p. 3, 1991.

[72] U. Fischer, Schuppert, B., Petermann, K., "Integrated optical switches in silicon based on SiGe-waveguides," IEEE Photon. Tech. Lett., vol. 5, p. 3, 1993.

[73] P. D. Hewitt, Reed, G. T., "Multi micron dimension optical p-i-n modulators in silicon-on-insulator," in SPIE, 1999, pp. 237-243.

[74] C. Sun, M. T. Wade, Y. Lee, J. S. Orcutt, L. Alloatti, M. S. Georgas, A. S. Waterman, J. M. Shainline, R. R. Avizienis, S. Lin, B. R. Moss, R. Kumar, F. Pavanello, A. H. Atabaki, H. M. Cook, A. J. Ou, J. C. Leu, Y.-H. Chen, K. Asanović, R. J. Ram, M. A. Popović, and V. M. Stojanović, "Single-chip microprocessor that communicates directly using light," Nature, vol. 528, pp. 534-538, 2015. doi: 10.1038/nature16454

http://www.nature.com/nature/journal/v528/n7583/abs/nature16454.html#supplementary-information

[75] J. E. Bowers, T. Komljenovic, M. Davenport, J. Hulme, A. Y. Liu, C. T. Santis, A. Spott, S. Srinivasan, E. J. Stanton, and C. Zhang, "Recent advances in silicon photonic integrated circuits," 2016, pp. 977402-977402-18.

[76] T. David, Z. Aaron, E. B. John, K. Tin, T. R. Graham, V. Laurent, M.-M. Delphine, C. Eric, V. Léopold, F. Jean-Marc, H. Jean-Michel, H. S. Jens, X. Dan-Xia, B. Frédéric, O. B. Peter, Z. M. Goran, and M. Nedeljkovic, "Roadmap on silicon photonics," Journal of Optics, vol. 18, p. 073003, 2016. doi: 10.1088/2040-8978/18/7/073003

[77] R. G. Beausoleil, P. J. Kuekes, G. S. Snider, S. Y. Wang, and R. S. Williams, "Nanoelectronic and Nanophotonic Interconnect," Proceedings of the IEEE, vol. 96, pp. 230-247, 2008. doi: 10.1109/jproc.2007.911057

[78] C. H. C. R. Wu, T. C. Huang, K. T. Cheng, R. Beausoleil, "20 Gb/s carrier-injection silicon microring modulator with SPICE-compatible dynamic model," presented at the Photonics in Switching, 2015.

[79] C. Zhang, D. Liang, C. Li, G. Kurczveil, J. E. Bowers, and R. G. Beausoleil, "High-speed Hybrid Silicon Microring Lasers," in Circuits and Systems (MWSCAS), 2015 IEEE 58th International Midwest Symposium on, 2015, pp. 1-4.

[80] J. E. Cunningham, I. Shubin, H. D. Thacker, J.-H. Lee, G. Li, X. Zheng, J. Lexau, R. Ho, J. G. Mitchell, and Y. Luo, "Scaling hybrid-integration of silicon photonics in freescale 130nm to TSMC 40nm-CMOS VLSI drivers for low power communications," in 2012 IEEE 62nd Electronic Components and Technology Conference, 2012, pp. 1518-1525.

[81] Z. X. Li G, Thacker H, Yao J, Loo Y, Shubin I, Raj K, Cunningham JE, Krishnamoorthy AV., "40Gb/s Thermally Tunable CMOS ring Modulator," in Group IV photonics, San Diego, USA, 2012.

[82] X. Zheng, F. Liu, J. Lexau, D. Patil, G. Li, Y. Luo, H. Thacker, I. Shubin, J. Yao, K. Raj, R. Ho, J. E. Cunningham, and A. Krishnamoorthy, "Ultra-Low Power Arrayed CMOS Silicon Photonic Transceivers for an 80 Gbps WDM Optical Link," in Optical Fiber Communication Conference/National Fiber Optic Engineers Conference 2011, Los Angeles, California, 2011, p. PDPA1. doi: 10.1364/nfoec.2011.pdpa1

[83] F. Liu, D. Patil, J. Lexau, P. Amberg, M. Dayringer, J. Gainsley, H. F. Moghadam, X. Zheng, J. Cunningham, and A. Krishnamoorthy, "10 Gbps, 530 fJ/b optical transceiver circuits in 40 nm CMOS," in IEEE Symp. VLSI circuits Dig. Tech. Papers, 2011, pp. 290-291.

[84] X. Zheng, F. Liu, D. Patil, H. Thacker, Y. Luo, T. Pinguet, A. Mekis, J. Yao, G. Li, J. Shi, K. Raj, J. Lexau, E. Alon, R. Ho, J. E. Cunningham, and A. V. Krishnamoorthy, "A sub-picojoule-per-bit CMOS photonic receiver for densely integrated systems," Opt. Express, vol. 18, pp. 204-211, 2010/01/04 2010. doi: 10.1364/oe.18.000204

[85] X. Z. A. V. Krishnamoorthy, D. Feng, J. Lexau, J. F. Buckwalter, H. D. Thacker, F. Liu, Y. Luo, E. Chang, P. Amberg, I. Shubin, S. S. Djordjevic, J. H. Lee, S. Lin, H. Liang, A. Abed, R. Shafiiha, K. Raj, R. Ho, M. Asghari, and J. E. Cunningham, "A low-power, high-speed, 9-channel germanium-silicon electro-absorption modulator array integrated with digital CMOS driver and wavelength multiplexer," Opt. Express, vol. Vol. 22, p. 7, 2014.

[86] N. Dupuis, B. G. Lee, J. E. Proesel, A. Rylyakov, R. Rimolo-Donadio, C. W. Baks, C. L. Schow, A. Ramaswamy, J. E. Roth, R. S. Guzzon, B. Koch, D. K. Sparacin, and G. A. Fish, "30Gbps optical link utilizing heterogeneously integrated III-V/Si photonics and CMOS circuits," in Optical Fiber Communications Conference and Exhibition (OFC), 2014, 2014, pp. 1-3. doi: 10.1364/OFC.2014.Th5A.6

[87] P. W. Coteus, J. U. Knickerbocker, C. H. Lam, and Y. A. Vlasov, "Technologies for exascale systems," IBM Journal of Research and Development, vol. 55, pp. 14:1-14:12, 2011. doi: 10.1147/jrd.2011.2163967

[88] Y. Vlasov, "Silicon photonics for next generation computing systems," in 34th European Conf. Optical Communications, 2008.

[89] cnet. (2016, 17 July 2017). Intel: Our laser chips will make sites like Google and Facebook faster. Available: https://www.cnet.com/news/intel-our-laser-chips-will-make-sites-like-google-and-facebook-faster/

[90] L. Chrostowski and M. Hochberg, Silicon photonics design: from devices to systems: Cambridge University Press, 2015.

[91] S. Law, V. Podolskiy, and D. Wasserman, "Towards nano-scale photonics with micro-scale photons: the opportunities and challenges of mid-infrared plasmonics," Nanophotonics, vol. 2, 2013. doi: 10.1515/nanoph-2012-0027

[92] D. K. Gramotnev and S. I. Bozhevolnyi, "Plasmonics beyond the diffraction limit," Nat Photon, vol. 4, pp. 83-91, 2010.

[93] B. Lau, M. A. Swillam, and A. S. Helmy, "Hybrid orthogonal junctions: wideband plasmonic slot-silicon waveguide couplers," Opt. Express, vol. 18, pp. 27048-27059, 2010/12/20 2010. doi: 10.1364/oe.18.027048

[94] M. A. Swillam and A. S. Helmy, "Feedback effects in plasmonic slot waveguides examined using a closed form model," IEEE Photonics Technology Letters, vol. 24, p. 497, 2012.

[95] M. A. Swillam and A. S. Helmy, "Analysis and applications of 3D rectangular metallic waveguides," Opt. Express, vol. 18, pp. 19831-19843, 2010/09/13 2010. doi: 10.1364/oe.18.019831

[96] M. H. El Sherif, O. S. Ahmed, M. H. Bakr, and M. A. Swillam, "Polarization-controlled excitation of multilevel plasmonic nano-circuits using single silicon nanowire," Opt. Express, vol. 20, pp. 12473-12486, 2012/05/21 2012. doi: 10.1364/oe.20.012473

[97] S. Law, L. Yu, and D. Wasserman, "Epitaxial growth of engineered metals for mid-infrared plasmonics," Journal of Vacuum Science & Technology B: Microelectronics and Nanometer Structures, vol. 31, p. 03C121, 2013. doi: 10.1116/1.4797487

[98] S. Law, D. C. Adams, A. M. Taylor, and D. Wasserman, "Mid-infrared designer metals," Opt Express, vol. 20, pp. 12155-65, May 21 2012. doi: 10.1364/oe.20.012155

[99] Rafaelgarcia. (22 July 2017). Electrona in crystallo fluentia. Available: https://commons.wikimedia.org/w/index.php?curid=11926841

[100] F. B. Myers and L. P. Lee, "Innovations in optical microfluidic technologies for point-of-care diagnostics," Lab Chip, vol. 8, pp. 2015-2031, 2008.

[101] L. Malic, M. G. Sandros, and M. Tabrizian, "Designed Biointerface Using Near-Infrared Quantum Dots for Ultrasensitive Surface Plasmon Resonance Imaging Biosensors," Anal. Chem., vol. 83, pp. 5222-5229, 2011/07/01 2011. doi: 10.1021/ac200465m

[102] Y. Guo, H. Li, K. Reddy, H. S. Shelar, V. R. Nittoor, and X. Fan, "Optofluidic Fabry–Pérot cavity biosensor with integrated flow-through micro-/nanochannels," Appl. Phys. Lett., vol. 98, p. 041104, 2011.

[103] J. Teng, P. Dumon, W. Bogaerts, H. Zhang, X. Jian, X. Han, M. Zhao, G. Morthier, and R. Baets, "Athermal Silicon-on-insulator ring resonators by overlaying a polymer cladding on narrowed waveguides," Opt. Express, vol. 17, pp. 14627-14633, 2009.

[104] A. Densmore, M. Vachon, D.-X. Xu, S. Janz, R. Ma, Y.-H. Li, G. Lopinski, A. Delâge, J. Lapointe, and C. Luebbert, "Silicon photonic wire biosensor array for multiplexed real-time and label-free molecular detection," Opt. Lett., vol. 34, pp. 3598-3600, 2009.

[105] J. Zhou, Y. Wang, C. Liao, B. Sun, J. He, G. Yin, S. Liu, Z. Li, G. Wang, X. Zhong, and J. Zhao, "Intensity modulated refractive index sensor based on optical fiber Michelson interferometer," Sens. Actuators, B, vol. 208, pp. 315-319, 2015. doi: http://dx.doi.org/10.1016/j.snb.2014.11.014

[106] F. Hideki, A. Tomohiro, and T. Shuji, "High-sensitivity fiber-optic refractive index sensor based on multimode interference using small-core single-mode fiber for biosensing," Japanese Journal of Applied Physics, vol. 53, p. 04EL08, 2014.

[107] R. A. Rodriguez, R. Dominguez-Cruz, D. A. May-Arrioja, I. Matias-Maestro, F. Arregui, and C. Ruiz-Zamarreno, "Fiber optic refractometer based in multimode interference effects (MMI) using Indium Tin Oxide (ITO) coating," in SENSORS, 2015 IEEE, 2015, pp. 1-3. doi: 10.1109/icsens.2015.7370600

[108] A. Irace and G. Breglio, "All-silicon optical temperature sensor based on Multi-Mode Interference," Opt. Express, vol. 11, pp. 2807-2812, 2003/11/03 2003. doi: 10.1364/oe.11.002807

[109] M. A. Swillam and A. S. Helmy, "Characteristics and applications of rectangular waveguide in sensing, slow light, and negative refraction," in SPIE OPTO, 2011, p. 794110.

[110] X. Wang, N. Lu, J. Zhu, and G. Jin, "An ultracompact refractive index gas-sensor based on photonic crystal microcavity," 2007, p. 68310D.

[111] R. Gamal, Y. Ismail, and M. A. Swillam, "Optical biosensor based on a silicon nanowire ridge waveguide for lab on chip applications," Journal of Optics, vol. 17, p. 045802, 2015.

[112] A. B. Ayoub, Q. Gan, and M. Swillam, "Silicon plasmonic-integrated sensor," 2016, p. 97540W.

[113] J. A. Dionne, L. A. Sweatlock, H. A. Atwater, and A. Polman, "Plasmon slot waveguides: Towards chip-scale propagation with subwavelength-scale localization," Physical Review B, vol. 73, p. 035407, 2006.

[114] A. Raman and S. Fan, "Perturbation theory for plasmonic modulation and sensing," Physical Review B, vol. 83, 2011. doi: 10.1103/PhysRevB.83.205131

[115] B. Schwarz, P. Reininger, D. Ristanic, H. Detz, A. M. Andrews, W. Schrenk, and G. Strasser, "Monolithically integrated mid-infrared lab-on-a-chip using plasmonics and quantum cascade structures," Nat Commun, vol. 5, p. 4085, 2014. doi: 10.1038/ncomms5085

[116] L. Guo, J. A. Jackman, H.-H. Yang, P. Chen, N.-J. Cho, and D.-H. Kim, "Strategies for enhancing the sensitivity of plasmonic nanosensors," Nano Today, vol. 10, pp. 213-239, 2015. doi: 10.1016/j.nantod.2015.02.007

[117] M. Y. Elsayed, Y. Ismail, and M. A. Swillam, "Semiconductor plasmonic gas sensor using on-chip infrared spectroscopy," Applied Physics A, vol. 123, p. 113, 2017. doi: 10.1007/s00339-016-0707-2

[118] S. M. Sherif and M. A. Swillam, "Metal-less silicon plasmonic mid-infrared gas sensor," Journal of Nanophotonics, vol. 10, pp. 026025-026025, 2016. doi: 10.1117/1.jnp.10.026025

[119] S. M. Sherif, D. C. Zografopoulos, L. A. Shahada, R. Beccherelli, and M. Swillam, "Integrated plasmonic refractometric sensor using Fano resonance," J. Phys. D: Appl. Phys., vol. 50, p. 055104, 2017.

[120] S. E. El-Zohary, A. Azzazi, H. Okamoto, T. Okamoto, M. Haraguchi, and M. A. Swillam, "Design optimization and fabrication of plasmonic nano sensor," in Photonic and Phononic Properties of Engineered Nanostructures IV, 2014, p. 89940V. doi: 10.1117/12.2038858

[121] R. Kotb, Y. Ismail, and M. A. Swillam, "Integrated coupled multi-stage plasmonic resonator for on-chip sensing," in Proc. SPIE 9126, Nanophotonics V, 2014, p. 91263M. doi: 10.1117/12.2057541

[122] R. Kotb, Y. Ismail, and M. A. Swillam, "Integrated metal-insulator-metal plasmonic nano resonator: an analytical approach," Progress In Electromagnetics Research Letters, vol. 43, pp. 83-94, 2013.

[123] A. Zaki, K. Kirah, and M. Swillam, "High Sensitivity Hybrid Plasmonic Rectangular Resonator for Gas Sensing Applications," in Frontiers in Optics 2015, San Jose, California, 2015, p. JW2A.2. doi: 10.1364/fio.2015.jw2a.2

[124] F. Kong, B.-I. Wu, H. Chen, and J. A. Kong, "Surface plasmon mode analysis of nanoscale metallic rectangular waveguide," Opt. Express, vol. 15, pp. 12331-12337, 2007/09/17 2007. doi: 10.1364/oe.15.012331

[125] A. O. Zaki, K. Kirah, and M. A. Swillam, "Integrated optical sensor using hybrid plasmonics for lab on chip applications," Journal of Optics, vol. 18, p. 085803, 2016.

[126] A. S. Abdeen, A. B. Ayoub, A. M. Attiya, and M. A. Swillam, "High efficiency compact Bragg sensor," in Photonics North (PN), 2016, 2016, pp. 1-1.

[127] L. B. Soldano and E. C. Pennings, "Optical multi-mode interference devices based on self-imaging: principles and applications," J. Lightwave Technol., vol. 13, pp. 615-627, 1995.

[128] C. Gouveia, G. Chesini, C. M. Cordeiro, J. Baptista, and P. A. Jorge, "Simultaneous measurement of refractive index and temperature using multimode interference inside a high birefringence fiber loop mirror," Sens. Actuators, B, vol. 177, pp. 717-723, 2013.

[129] J. S. M. Rusby, "Measurements of the refractive index of sea water relative to copenhagen standard sea water," Deep Sea Research and Oceanographic Abstracts, vol. 14, pp. 427-IN14, 1967/08/01 1967. doi: http://dx.doi.org/10.1016/0011-7471(67)90050-2

[130] S. E. El-Zohary, A. Azzazi, H. Okamoto, T. Okamoto, M. Haraguchi, and M. A. Swillam, "Design optimization and fabrication of plasmonic nano sensor," 2014, pp. 89940V-89940V-6.

[131] A. Bideau-Mehu, Y. Guern, R. Abjean, and A. Johannin-Gilles, "Interferometric determination of the refractive index of carbon dioxide in the ultraviolet region," Opt. Commun., vol. 9, pp. 432-434, 1973/12/01 1973. doi: http://dx.doi.org/10.1016/0030-4018(73)90289-7

[132] R. Rollefson and R. Havens, "Index of Refraction of Methane in the Infra-Red and the Dipole Moment of the CH Bond," Physical Review, vol. 57, pp. 710-717, 1940.

[133] X. Liu, S. Cheng, H. Liu, S. Hu, D. Zhang, and H. Ning, "A survey on gas sensing technology," Sensors (Basel), vol. 12, pp. 9635-65, 2012. doi: 10.3390/s120709635

[134] N. A. Yebo, S. P. Sree, E. Levrau, C. Detavernier, Z. Hens, J. A. Martens, and R. Baets, "Selective and reversible ammonia gas detection with nanoporous film functionalized silicon photonic micro-ring resonator," Opt. Express, vol. 20, pp. 11855-11862, 2012/05/21 2012. doi: 10.1364/oe.20.011855

[135] S. Law, L. Yu, A. Rosenberg, and D. Wasserman, "All-Semiconductor Plasmonic Nanoantennas for Infrared Sensing," Nano Lett., vol. 13, pp. 4569-4574, 2013/09/11 2013. doi: 10.1021/nl402766t

[136] A. G. Milnes and A. Y. Polyakov, "Indium arsenide: a semiconductor for high speed and electro-optical devices," Mater. Sci. Eng., B, vol. 18, pp. 237-259, 1993/04/15 1993. doi: http://dx.doi.org/10.1016/0921-5107(93)90140-I

[137] R. Gamal, Y. Ismail, and M. A. Swillam, "Silicon Waveguides at the Mid-Infrared Range," Journal of Lightwave Technology, vol. 33, pp. 3207 - 3214, 2015. doi: 10.1109/jlt.2015.2410493

[138] T. R. Harris, "Optical properties of Si, Ge, GaAs, GaSb, InAs, and InP at elevated temperatures," Master, Air Force Institute of Technology, 2010.

[139] D. Li and C. Z. Ning, "All-semiconductor active plasmonic system in mid-infrared wavelengths," Opt. Express, vol. 19, pp. 14594-14603, 2011/07/18 2011. doi: 10.1364/oe.19.014594

[140] N. V. Zotova, N. D. Il'inskaya, S. A. Karandashev, B. A. Matveev, M. A. Remennyi, and N. M. Stus', "Sources of spontaneous emission based on indium arsenide," Semiconductors, vol. 42, pp. 625-641, 2008. doi: 10.1134/s1063782608060018

[141] S. C. Jain, J. M. McGregor, and D. J. Roulston, "Band-gap narrowing in novel III-V semiconductors," J. Appl. Phys., vol. 68, pp. 3747-3749, 1990. doi: doi:http://dx.doi.org/10.1063/1.346291

[142] M. Sotoodeh, A. H. Khalid, and A. A. Rezazadeh, "Empirical low-field mobility model for III–V compounds applicable in device simulation codes," J. Appl. Phys., vol. 87, pp. 2890-2900, 2000. doi: doi:http://dx.doi.org/10.1063/1.372274

[143] R. S. Popovic, Hall Effect Devices, Second Edition: CRC Press, 2003.

[144] G. M. Hale and M. R. Querry, "Optical Constants of Water in the 200-nm to 200-µm Wavelength Region," Appl. Opt., vol. 12, pp. 555-563, 1973/03/01 1973. doi: 10.1364/ao.12.000555

[145] J. J. S. V. Lucarini, K.-E. Peiponen, E.M. Vartiainen, Kramers-Kronig Relations in Optical Materials Research vol. 110. Berlin, Germany: Springer, 2005.

[146] A. Campion and P. Kambhampati, "Surface-enhanced Raman scattering," Chem. Soc. Rev., vol. 27, pp. 241-250, 1998.

[147] A. Brolo, D. Irish, and J. Lipkowski, "Surface-enhanced Raman spectra of pyridine and pyrazine adsorbed on a Au (210) single-crystal electrode," The Journal of Physical Chemistry B, vol. 101, pp. 3906-3909, 1997.

[148] A. Fojtik and A. Henglein, "Laser ablation of films and suspended particles in a solvent: formation of cluster and colloid solutions," Berichte der Bunsen-Gesellschaft, vol. 97, pp. 252-254, 1993.

[149] S. Chen and D. L. Carroll, "Synthesis and characterization of truncated triangular silver nanoplates," Nano Lett., vol. 2, pp. 1003-1007, 2002. doi: 10.1021/nl025674h

[150] C. J. Orendorff, A. Gole, T. K. Sau, and C. J. Murphy, "Surface-enhanced Raman spectroscopy of self-assembled monolayers: sandwich architecture and nanoparticle shape dependence," Anal. Chem., vol. 77, pp. 3261-3266, 2005. doi: 10.1021/ac048176x

[151] Y. Sun and Y. Xia, "Shape-controlled synthesis of gold and silver nanoparticles," Science, vol. 298, pp. 2176-2179, 2002.

[152] P. S. Kumar, I. Pastoriza-Santos, B. Rodríguez-González, F. J. G. De Abajo, and L. M. Liz-Marzan, "High-yield synthesis and optical response of gold nanostars," Nanotechnology, vol. 19, p. 015606, 2007. doi: 10.1088/0957-4484/19/01/015606

[153] M. Procházka, Surface-Enhanced Raman Spectroscopy: Bioanalytical, Biomolecular and Medical Applications: Springer, 2015.

[154] L. G. Olson, Y.-S. Lo, T. P. Beebe Jr, and J. M. Harris, "Characterization of silane-modified immobilized gold colloids as a substrate for surface-enhanced Raman spectroscopy," Anal. Chem., vol. 73, pp. 4268-4276, 2001.

[155] M. Procházka, P. Šimáková, and N. Hajduková-Šmídová, "SE (R) RS microspectroscopy of porphyrins on immobilized Au nanoparticles: Testing spectral sensitivity and reproducibility," Colloids Surf., A, vol. 402, pp. 24-28, 2012.

[156] M. Fan, G. F. S. Andrade, and A. G. Brolo, "A review on the fabrication of substrates for surface enhanced Raman spectroscopy and their applications in analytical chemistry," Anal. Chim. Acta, vol. 693, pp. 7-25, 2011. doi: http://dx.doi.org/10.1016/j.aca.2011.03.002

[157] G. Das, M. Chirumamilla, A. Toma, A. Gopalakrishnan, R. P. Zaccaria, A. Alabastri, M. Leoncini, and E. Di Fabrizio, "Plasmon based biosensor for distinguishing different peptides mutation states," Sci. Rep., vol. 3, p. 1792, 2013.

[158] D. Weitz, M. Lin, and C. Sandroff, "Colloidal aggregation revisited: new insights based on fractal structure and surface-enhanced Raman scattering," Surf. Sci., vol. 158, pp. 147-164, 1985.

[159] E. Le Ru and P. Etchegoin, Principles of Surface-Enhanced Raman Spectroscopy: and related plasmonic effects: Elsevier, 2008.

[160] M. Becker, V. Sivakov, U. Gösele, T. Stelzner, G. Andrä, H. J. Reich, S. Hoffmann, J. Michler, and S. H. Christiansen, "Nanowires Enabling Signal-Enhanced Nanoscale Raman Spectroscopy," Small, vol. 4, pp. 398-404, 2008.

[161] J. Yang, J. Li, Q. Gong, J. Teng, and M. Hong, "High aspect ratio SiNW arrays with Ag nanoparticles decoration for strong SERS detection," Nanotechnology, vol. 25, p. 465707, 2014.

[162] F. M. Hassan, A. R. Elsayed, V. Chabot, R. Batmaz, X. Xiao, and Z. Chen, "Subeutectic Growth of Single-Crystal Silicon Nanowires Grown on and Wrapped with Graphene Nanosheets: High-Performance Anode Material for Lithium-Ion Battery," Acs Applied Materials & Interfaces, vol. 6, pp. 13757-13764, 2014/08/27 2014. doi: 10.1021/am5032067

[163] L. J. Chen, "Silicon nanowires: the key building block for future electronic devices," J. Mater. Chem., vol. 17, pp. 4639-4643, 2007.

[164] B. Tian, X. Zheng, T. J. Kempa, Y. Fang, N. Yu, G. Yu, J. Huang, and C. M. Lieber, "Coaxial silicon nanowires as solar cells and nanoelectronic power sources," Nature, vol. 449, pp. 885-889, 2007.

[165] L. Latu-Romain, C. Mouchet, C. Cayron, E. Rouviere, and J.-P. Simonato, "Growth parameters and shape specific synthesis of silicon nanowires by the VLS method," Journal of Nanoparticle Research, vol. 10, pp. 1287-1291, 2008.

[166] R. Wagner and W. Ellis, "Vapor-liquid-solid mechanism of single crystal growth," Appl. Phys. Lett., vol. 4, pp. 89-90, 1964.

[167] B. Fuhrmann, H. S. Leipner, H.-R. Höche, L. Schubert, P. Werner, and U. Gösele, "Ordered arrays of silicon nanowires produced by nanosphere lithography and molecular beam epitaxy," Nano Lett., vol. 5, pp. 2524-2527, 2005.

[168] Y.-H. Yang, S.-J. Wu, H.-S. Chiu, P.-I. Lin, and Y.-T. Chen, "Catalytic growth of silicon nanowires assisted by laser ablation," The Journal of Physical Chemistry B, vol. 108, pp. 846-852, 2004.

[169] H. Pan, S. Lim, C. Poh, H. Sun, X. Wu, Y. Feng, and J. Lin, "Growth of Si nanowires by thermal evaporation," Nanotechnology, vol. 16, p. 417, 2005.

[170] Y. Fu, A. Colli, A. Fasoli, J. Luo, A. Flewitt, A. Ferrari, and W. Milne, "Deep reactive ion etching as a tool for nanostructure fabrication," Journal of Vacuum Science & Technology B, vol. 27, pp. 1520-1526, 2009.

[171] R. Das, S. S. Nath, D. Chakdar, G. Gope, and R. Bhattacharjee, "Synthesis of silver nanoparticles and their optical properties," Journal of Experimental Nanoscience, vol. 5, pp. 357-362, 2010.

[172] A. M. Gouda, M. Elsayed, N. K. Allam, and M. A. Swillam, "Black silicon based on simple fabrication of mesoporous silicon nanowires for solar energy harvesting," in 2016 IEEE 43rd Photovoltaic Specialists Conference (PVSC), 2016, pp. 2893-2895. doi: 10.1109/pvsc.2016.7750185

[173] S. K. Srivastava, D. Kumar, S. Schmitt, K. Sood, S. Christiansen, and P. Singh, "Large area fabrication of vertical silicon nanowire arrays by silver-assisted single-step chemical etching and their formation kinetics," Nanotechnology, vol. 25, p. 175601, 2014.

[174] H. Han, Z. Huang, and W. Lee, "Metal-assisted chemical etching of silicon and nanotechnology applications," Nano Today, vol. 9, pp. 271-304, 2014.

[175] S. A. Razek, M. A. Swillam, and N. K. Allam, "Vertically aligned crystalline silicon nanowires with controlled diameters for energy conversion applications: Experimental and theoretical insights," J. Appl. Phys., vol. 115, p. 194305, 2014. doi: doi:http://dx.doi.org/10.1063/1.4876477

[176] D. Kumar, S. K. Srivastava, P. Singh, K. Sood, V. Singh, N. Dilawar, and M. Husain, "Room temperature growth of wafer-scale silicon nanowire arrays and their Raman characteristics," Journal of Nanoparticle Research, vol. 12, pp. 2267-2276, 2010.

[177] A. G. Nassiopoulou, V. Gianneta, and C. Katsogridakis, "Si nanowires by a single-step metal-assisted chemical etching process on lithographically defined areas: formation kinetics," Nanoscale Research Letters, vol. 6, pp. 1-8, 2011.

[178] K. Peng, J. Hu, Y. Yan, Y. Wu, H. Fang, Y. Xu, S. Lee, and J. Zhu, "Fabrication of single-crystalline silicon nanowires by scratching a silicon surface with catalytic metal particles," Adv. Funct. Mater., vol. 16, pp. 387-394, 2006.

[179] A. M. Gouda, M. Y. Elsayed, C. Tharwat, and M. A. Swillam, "Silicon-based nanostructures as surface enhanced Raman scattering substrates," in 2016 Photonics North (PN), 2016, pp. 1-1. doi: 10.1109/pn.2016.7537981

[180] Lumerical Solutions Inc. Available: http://www.lumerical.com/tcad-products/fdtd/

[181] E. D. Palik, Handbook of Optical Constants of Solids: Elsevier Science, 2012.

[182] P. B. Johnson and R.-W. Christy, "Optical constants of the noble metals," Physical Review B, vol. 6, p. 4370, 1972.

[183] A. M. Gouda, N. K. Allam, and M. A. Swillam, "Facile omnidirectional black silicon based on porous and nonporous silicon nanowires for energy applications," in 2016 Photonics North (PN), 2016, pp. 1-1. doi: 10.1109/pn.2016.7537973

[184] Y. Li, L. Zhou, L. Tang, M. Li, and J. J. He, "Improved Surface Enhanced Raman Scattering Based on Hybrid Au Nanostructures for Biomolecule Detection," IEEE Photonics Journal, vol. 8, pp. 1-7, 2016. doi: 10.1109/jphot.2016.2619063

[185] Y. Wang, M. Huang, K. Wang, X. Liu, Y. Zou, B. Song, and J. Chen, "Raman Enhancement in Metal-Cladding Waveguide and the Influence of the Metal Film Surface Roughness," J. Lightwave Technol., vol. 34, pp. 3616-3621, 2016. doi: 10.1109/jlt.2016.2571618

[186] S. Jiang, J. Guo, C. Zhang, C. Li, M. Wang, Z. Li, S. Gao, P. Chen, H. Si, and S. Xu, "A sensitive, uniform, reproducible and stable SERS substrate has been presented based on MoS2@Ag nanoparticles@pyramidal silicon," RSC Advances, vol. 7, pp. 5764-5773, 2017. doi: 10.1039/c6ra26879j

[187] C. Zhang, S. Z. Jiang, C. Yang, C. H. Li, Y. Y. Huo, X. Y. Liu, A. H. Liu, Q. Wei, S. S. Gao, X. G. Gao, and B. Y. Man, "Gold@silver bimetal nanoparticles/pyramidal silicon 3D substrate with high reproducibility for high-performance SERS," Sci. Rep., vol. 6, p. 25243, 2016. doi: 10.1038/srep25243

http://www.nature.com/articles/srep25243#supplementary-information

[188] L. He, C. Ai, W. Wang, N. Gao, X. Yao, C. Tian, and K. Zhang, "An effective three-dimensional surface-enhanced Raman scattering substrate based on oblique Si nanowire arrays decorated with Ag nanoparticles," J. Mater. Sci., vol. 51, pp. 3854-3860, 2016. doi: 10.1007/s10853-015-9704-7